

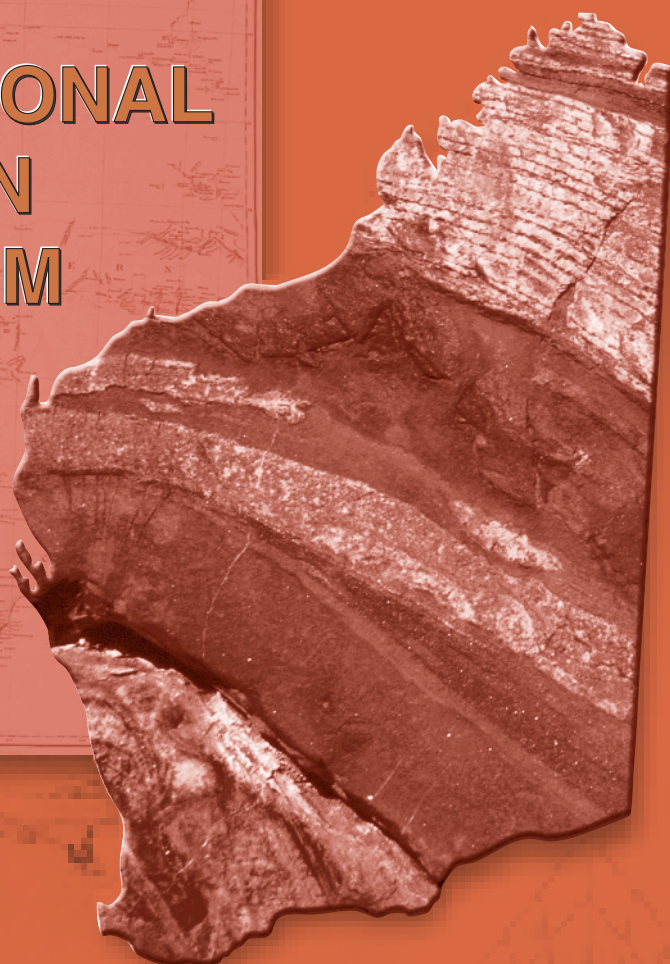
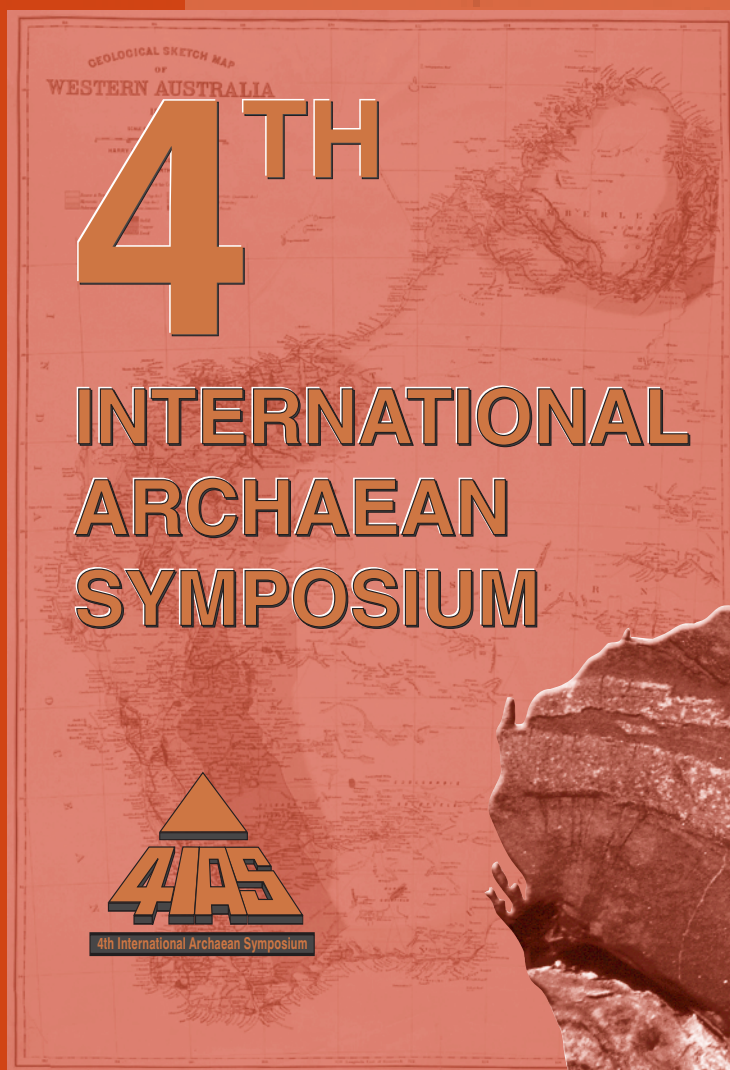


Department of Mineral and  
Petroleum Resources

**RECORD  
2001/14**

# **ARCHAEAN GRANITE–GREENSTONES OF THE CENTRAL YILGARN CRATON WESTERN AUSTRALIA — A FIELD GUIDE**

**compiled by S. F. Chen and S. Wyche**



Geological Survey of Western Australia



**GEOLOGICAL SURVEY OF WESTERN AUSTRALIA**

**Record 2001/14**

# **ARCHAEAN GRANITE–GREENSTONES OF THE CENTRAL YILGARN CRATON, WESTERN AUSTRALIA — A FIELD GUIDE**

**compiled by**

**S. F. Chen<sup>1</sup> and S. Wyche<sup>1</sup>**

**with contributions from**

**S. F. Chen<sup>1</sup>, A. Riganti<sup>1</sup>, S. Wyche<sup>1</sup>, J. E. Greenfield<sup>1</sup>, P. Baudry<sup>2</sup>,  
J. Whitelock<sup>2</sup>, and J. Withall<sup>3</sup>**

<sup>1</sup> Geological Survey of Western Australia

<sup>2</sup> Sons of Gwalia Ltd

<sup>3</sup> Vanadium Australia Pty Ltd

**Perth 2001**

**MINISTER FOR STATE DEVELOPMENT**  
**Hon. Clive Brown MLA**

**DIRECTOR GENERAL**  
**DEPARTMENT OF MINERAL AND PETROLEUM RESOURCES**  
**Jim Limerick**

**DIRECTOR, GEOLOGICAL SURVEY OF WESTERN AUSTRALIA**  
**Tim Griffin**

**Notice to users of this guide:**

This field guide is one of a series published by the Geological Survey of Western Australia (GSWA) for excursions conducted as part of the 4th International Archaean Symposium, held in Perth on 24–28 September 2001. Authorship of these guides included contributors from AGSO, CSIRO, tertiary academic institutions, and mineral exploration companies, as well as GSWA. Editing of manuscripts was restricted to bringing them into GSWA house style. The scientific content of each guide, and the drafting of the figures, was the responsibility of the authors.

**REFERENCE**

**The recommended reference for this publication is:**

CHEN, S. F., and WYCHE, S., (compilers), 2001, Archaean granite–greenstones of the central Yilgarn Craton, Western Australia — a field guide: Western Australia Geological Survey, Record 2001/14, 76p.

**National Library of Australia Card Number and ISBN 0 7307 5702 1**

**Grid references in this publication refer to the Geocentric Datum of Australia 1994 (GDA94). Locations mentioned in the text are referenced using Map Grid Australia (MGA) coordinates, Zone 50. All locations are quoted to at least the nearest 100 m.**

Printed by Image Source, Perth, Western Australia

**Published 2001 by Geological Survey of Western Australia**

**Copies available from:**

Information Centre  
Department of Mineral and Petroleum Resources  
100 Plain Street  
EAST PERTH, WESTERN AUSTRALIA 6004  
Telephone: (08) 9222 3459 Facsimile: (08) 9222 3444

**This and other publications of the Geological Survey of Western Australia are available online through dme.bookshop at [www.dme.wa.gov.au](http://www.dme.wa.gov.au)**

# Contents

Preface .....	1
Part I: An overview of Archaean geology in the central Yilgarn Craton .....	4
Introduction .....	4
Lower greenstone succession .....	6
Diemals area .....	6
Bungalbin–Marda area .....	8
Die Hardy Range area .....	8
Lithostratigraphic correlation .....	9
Upper greenstone succession .....	9
Marda Complex .....	9
Diemals Formation .....	11
Granite and granitoid gneiss .....	13
Structural geology .....	14
North–south compression ( $D_1$ ) .....	14
East–west orogenic shortening ( $D_2$ ) .....	16
Progressive, inhomogeneous east–west shortening ( $D_3$ ) .....	16
Post- $D_3$ deformation .....	20
Metamorphism .....	20
Tectonic evolution of late Archaean greenstone basins .....	22
Early extensional basins .....	22
Late compressional basins .....	23
Economic geology .....	24
Gold and silver .....	24
Nickel .....	24
Iron oxides .....	25
Other commodities .....	25
Summary .....	25
Part II: Excursion localities .....	26
Locality 1: Marvel Loch gold mine .....	26
Introduction .....	26
Regional geology .....	26
Deposit geology .....	27
Stratigraphy .....	27
Structure .....	27
Alteration .....	28
Vein types .....	28
Mineralization .....	28
Locality 2: Koolyanobbing Shear Zone .....	30
Locality 3: Deformation of granitoid gneiss within the Koolyanobbing Shear Zone .....	32
Locality 4: Millars Monzogranite .....	32
Locality 5: Granitoid gneiss at Yacke Yackine Dam .....	33
Locality 6: Quartzite at Victoria Hill .....	36
Locality 7: Marda Complex conglomerate at Allens Find .....	37
Locality 8: Marda Complex fragmental ignimbrite west of Marda airstrip .....	40
Locality 9: Marda Complex rheoignimbrite .....	41
Locality 10: Marda Complex volcanic rocks — igneous and tectonic fabrics .....	46
Locality 11: Butcher Bird Monzogranite .....	47
Locality 12: Red Legs gold prospect .....	48
Locality 13: Pigeon Rocks Monzogranite .....	50
Locality 14: Diemals Formation conglomerate .....	51
Locality 15: Deception Hill Porphyry .....	52
Locality 16: Refolded BIF, Evanston .....	54
Locality 17: Asymmetric feldspar porphyroclasts in the Evanston Shear Zone .....	57
Locality 18: Overprinting deformation and metamorphic relationships around a fold hinge .....	58
Locality 19: Unconformity at the base of the Diemals Formation south of Kim Bore .....	59
Locality 20: Mafic tuff south of Diemals Homestead .....	60
Locality 21: Altered volcanic rocks at Pincher Well .....	62
Locality 22: Yuinmery Shear Zone near Yuinmery Homestead .....	62
Locality 22a: Eastern part of the Yuinmery Shear Zone .....	63
Locality 22b: Western part of the Yuinmery Shear Zone .....	63

Locality 23: Youanmi Shear Zone in the Bell Chambers Well area .....	65
Locality 23a: Centre of the Youanmi Shear Zone .....	65
Locality 23b: Eastern part of the Youanmi Shear Zone .....	66
Locality 23c: Eastern part of the Youanmi Shear Zone .....	66
Locality 24: Windimurra vanadium mine .....	67
Regional geology .....	68
Windimurra vanadium deposit and the Shephards Discordant Zone (SDZ) .....	68
Geological summary .....	68
Mineralization .....	71
Mine production .....	72
References .....	73

## Appendix

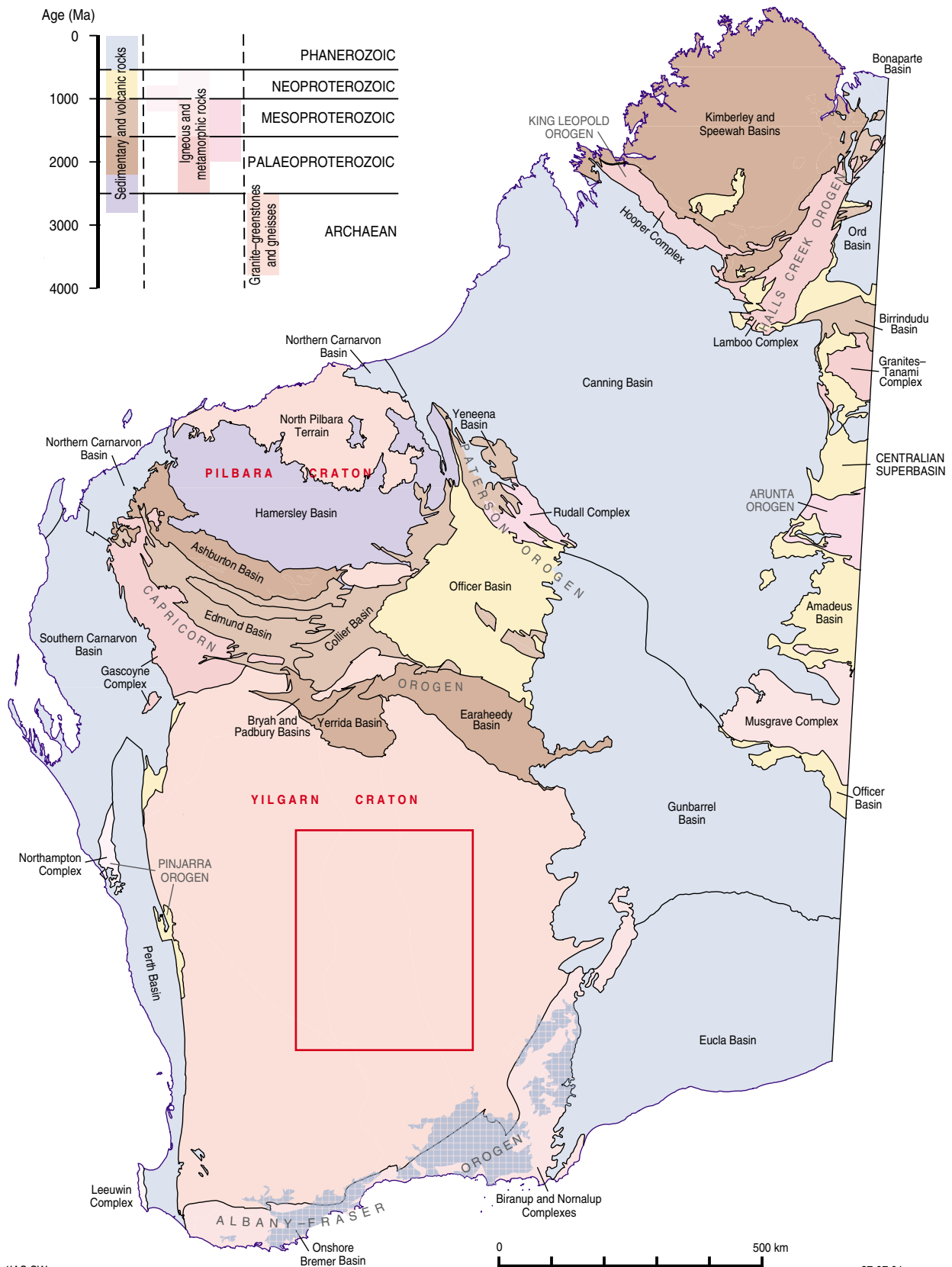
1. Selected whole-rock geochemical data .....	76
---	----

## Figures

1. Main components of the Archaean Yilgarn Craton .....	2
2. Central Yilgarn region showing excursion localities .....	3
3. Generalized solid geological map of the Marda–Diemals area .....	5
4. Generalized lithostratigraphic columns of the Marda–Diemals greenstone belt .....	7
5. Geology of the Marda Complex .....	10
6. Geological map of the Diemals Formation .....	12
7. First vertical derivative aeromagnetic image of the YOUANMI, BARLEE, and JACKSON 1:250 000 map sheets .....	15
8. D <sub>1</sub> and D <sub>2</sub> structures .....	17
9. Simplified geological map of the Youanmi region .....	18
10. Schematic diagram, showing the origin of arcuate structures .....	19
11. Metamorphic map of the Southern Cross Terrane .....	21
12. Marvel Loch gold deposit .....	29
13. Compositional banding in granitoid gneiss .....	31
14. A small-scale sinistral shear zone marked by a narrow zone of ultramylonite .....	33
15. Outcrop geology of central–western JACKSON .....	34
16. Pavement of northerly trending granitoid gneiss west of the Yacke Yackine Dam .....	35
17. Geological map of the western part of the Marda Complex .....	38
18. Clast-supported conglomerate bed near the base of the Marda Complex .....	39
19. Rhyolitic ignimbrite near Marda .....	40
20. Photomicrographs of fragmental rhyolitic ignimbrite .....	42
21. Flow foliation in rhyolitic ignimbrite .....	43
22. Devitrification textures in spherulitic rhyolite .....	45
23. Textural characteristics of the Butcher Bird Monzogranite .....	48
24. Die Hardy Range and Pigeon Rocks area .....	49
25. Polymictic conglomerate of the Diemals Formation .....	53
26. Deception Hill Porphyry under crossed nicols showing abundant albitized plagioclase phenocrysts .....	54
27. Interpreted geology of the Evanston area .....	55
28. Schematic illustration of the refolding geometry seen at Locality 16 .....	56
29. Rotated and stretched asymmetric porphyroclasts of feldspar and quartz .....	58
30. Sillimanite porphyroblasts grown on S <sub>1</sub> surface are parallel to F <sub>2</sub> fold hinge .....	59
31. Geology of the Diemals – Kim Bore area .....	61
32. Basal conglomerate in the Diemals Formation .....	61
33. Shear sense indicators from the Yuinmery Shear Zone .....	64
34. Asymmetric porphyroclasts of feldspar showing a dextral shear sense on the Youanmi Shear Zone .....	67
35. Geological map of the Windimurra Complex .....	69
36. Schematic section, and range and composition of the cumulus minerals of the Layered Series of the Windimurra Complex .....	70



# Record 2001/14 Central Yilgarn Excursion



# **Archaean granite–greenstones of the central Yilgarn Craton, Western Australia — a field guide**

**compiled by**

**S. F. Chen<sup>1</sup> and S. Wyche<sup>1</sup>**

**with contributions from**

**S. F. Chen<sup>1</sup>, A. Riganti<sup>1</sup>, S. Wyche<sup>1</sup>, J. E. Greenfield<sup>1</sup>, P. Baudry<sup>2</sup>,  
J. Whitelock<sup>2</sup>, and J. Withall<sup>3</sup>**

## **Preface**

This excursion guide examines the Archaean granite–greenstone geology in the Southern Cross Terrane, central Yilgarn Craton, Western Australia (Fig. 1). The excursion traverses greenstone belts (particularly the largest, Marda–Diemals greenstone belt), adjacent granite and granitoid gneiss, regional-scale ductile shear zones, and recently recognized, large-scale arcuate structures formed by impingement of rigid granitoids into greenstone belts (Chen et al., 2001). The guide is based on recent 1:100 000-scale geological mapping by the Geological Survey of Western Australia (Wyche et al., 2000; Riganti and Chen, 2000; Greenfield, 2001; Chen and Wyche, 2001; Chen and Greenfield, 2001; Riganti, 2001), and more regional stratigraphic and structural studies (Greenfield and Chen, 1999; Riganti et al., 2000; Chen et al., 2001).

The first part of the guide provides a geological overview that outlines the lithostratigraphy, structure, tectonic history, and economic geology of the central Yilgarn Craton, whereas the second part contains detailed descriptions of individual excursion localities. Figure 2 shows the central Yilgarn region with the various localities described in this guide indicated.

---

<sup>1</sup> Geological Survey of Western Australia

<sup>2</sup> Sons of Gwalia Ltd

<sup>3</sup> Vanadium Australia Pty Ltd

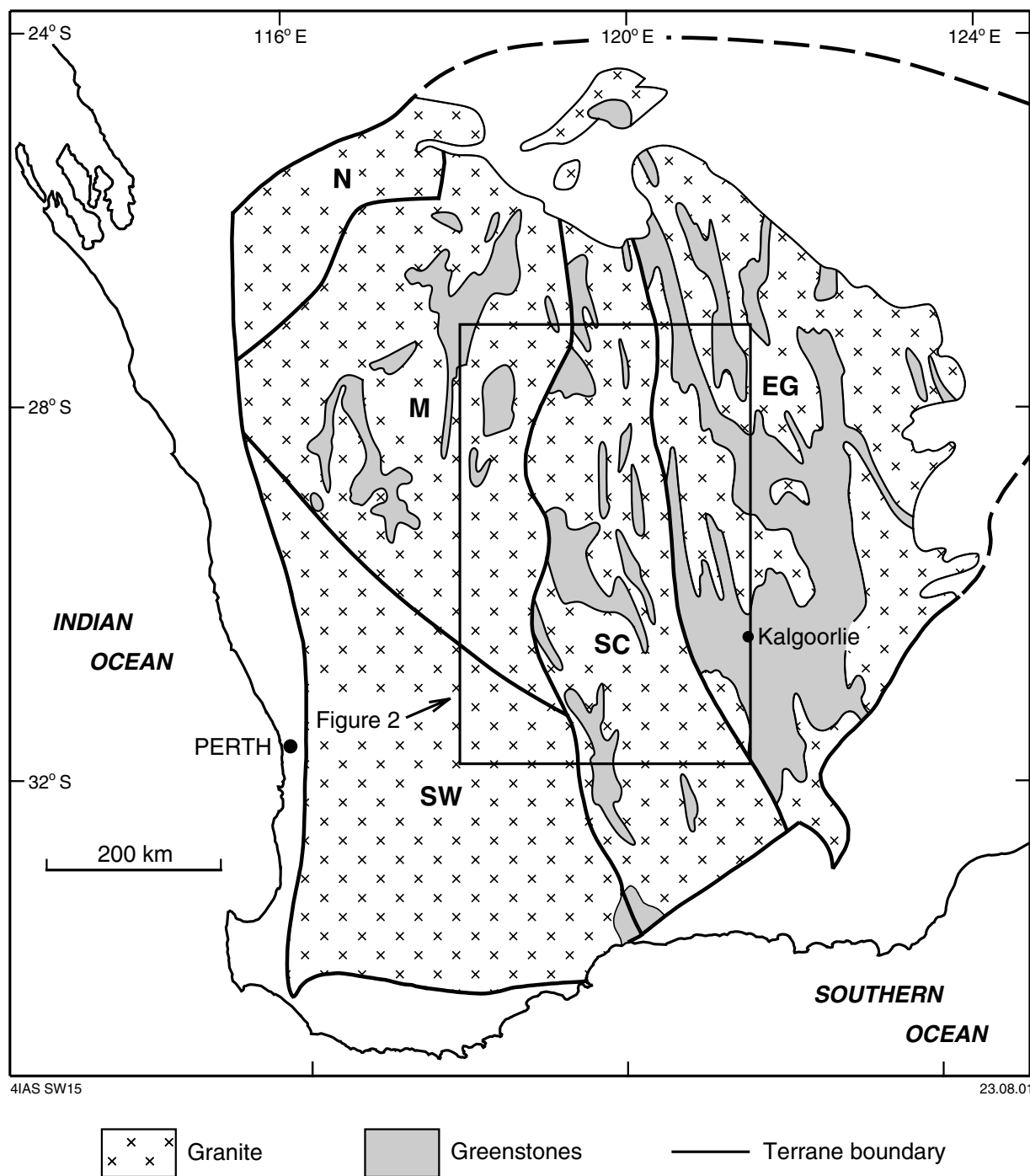


Figure 1. Main components of the Archaean Yilgarn Craton (modified from Myers, 1997), showing subdivision of major tectonic units, and the area covered by this excursion guide. EG — Eastern Goldfields Terrane; SC — Southern Cross Terrane; M — Murchison Terrane; N — Narryer Terrane; SW — South West Terrane

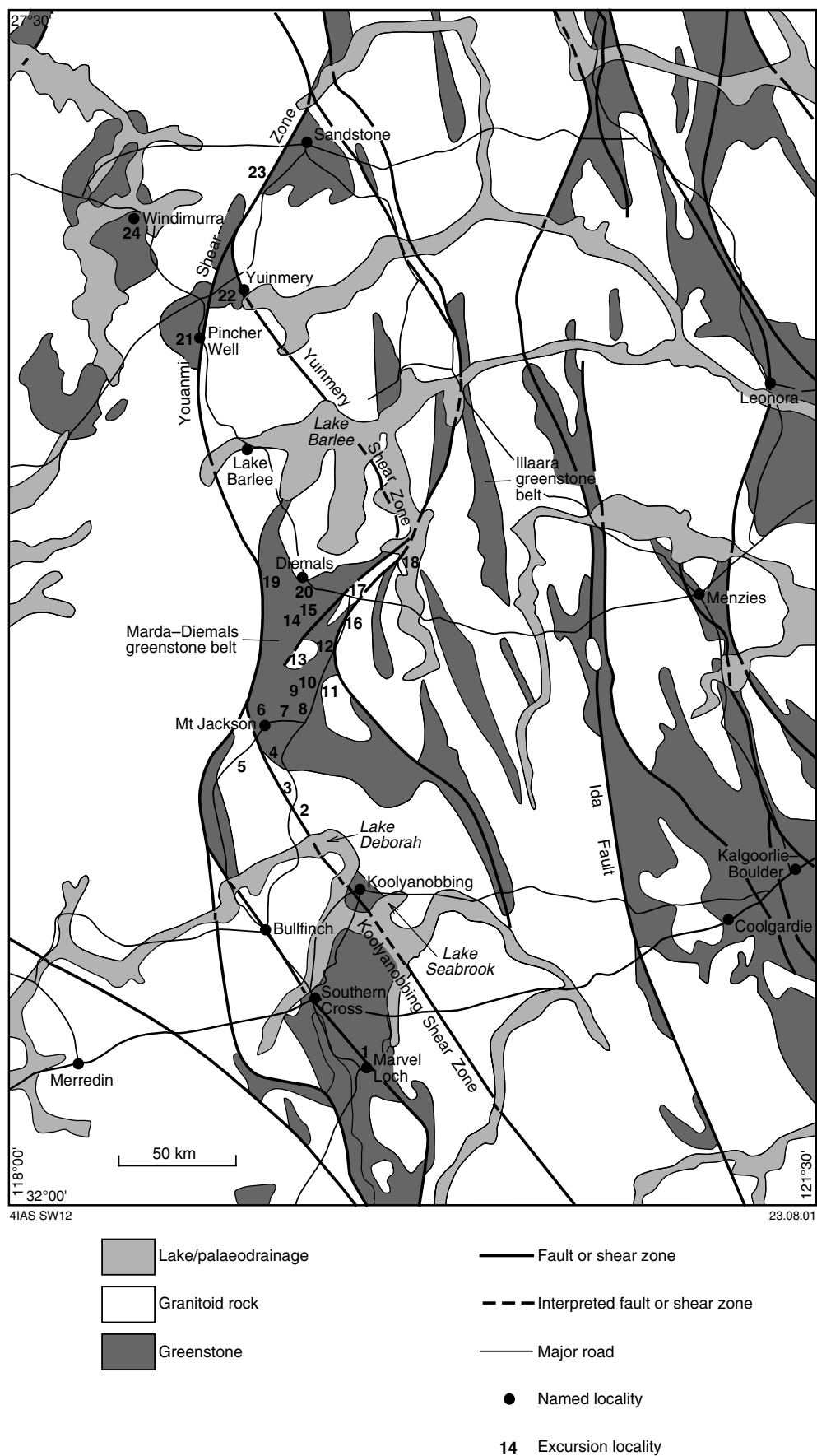


Figure 2. Central Yilgarn region showing excursion localities (adapted from Myers and Hocking, 1998)

## Part I: An overview of Archaean geology in the central Yilgarn Craton

by S. F. Chen, S. Wyche, J. E. Greenfield, and A. Riganti

### Introduction

The Yilgarn Craton consists of extensive tracts of variously deformed granite and granitoid gneiss that separate multiply deformed, generally older greenstone belts. Gee et al. (1981) divided the Yilgarn Craton into four components — the Western Gneiss Terrain, and the Murchison, Southern Cross, and Eastern Goldfields Provinces. Various changes and amendments have been proposed since that time (e.g. Myers, 1990; Myers and Hocking, 1998), and the term ‘Province’ has now been discarded in favour of the term ‘Granite–Greenstone Terrane’ so that, for example, the Southern Cross Province is now the Southern Cross Granite–Greenstone Terrane (Tyler and Hocking, 2001; Fig. 1). Greenstones and granitoids in the Murchison and Southern Cross Terranes are typically older than those in the Eastern Goldfields Terrane (Barley and Groves, 1990; Pidgeon and Wilde, 1990; Pidgeon and Hallberg, 2000; Nelson, 1997, 2001). The structural grain trends northeast in the Murchison Terrane, and north-northwest in the Eastern Goldfields Terrane, whereas both northeast and northwest structural grains are present in the Southern Cross Terrane.

Compared with the extensive Eastern Goldfields literature, there is relatively little published work on the central Southern Cross Terrane. The first regional geological studies were the mapping programs by the Geological Survey of Western Australia (GSWA) and the Bureau of Mineral Resources, Geology and Geophysics (BMR), now the Australian Geological Survey Organisation (AGSO – Geoscience Australia), that resulted in the publication of first-edition, 1:250 000-scale geological maps (Chin and Smith, 1983; Walker and Blight, 1983; Stewart et al., 1983).

Greenstones in the Marda–Diemals greenstone belt of the central Southern Cross Terrane (Fig. 2) comprise a widespread, mafic-dominated, c. 3.0 Ga lower succession, unconformably overlain by a c. 2.73 Ga upper succession. Both were intruded by monzogranite, predominantly between c. 2.74 and c. 2.65 Ga (Fig. 3; Fletcher et al., 1984; Pidgeon and Wilde, 1990; Wang et al., 1996; Dalstra et al., 1998; Qiu et al., 1999; Nelson, 1999, 2000, 2001). The lower succession is characterized by abundant banded iron-formation (BIF) at some stratigraphic levels, and rare komatiite. The upper succession consists of felsic volcanic rocks (Marda Complex; Hallberg et al., 1976; Chin and Smith, 1983), and clastic sedimentary rocks (Diemals Formation; Walker and Blight, 1983). Dalstra et al. (1999) recognized five deformation events in the central Southern Cross Terrane:

- north–south compression ( $D_1$ ) that produced regional detachment and localized recumbent folds;
- east–west compression ( $D_2$ ) that resulted in regional-scale upright to inclined folds;
- further east–west compression ( $D_3$  and  $D_4$ ) that produced regional-scale ductile shear zones and conjugate ductile–brittle faults respectively;
- relaxation and north–south compression ( $D_5$ ) that resulted in localized brittle reactivation and thrusting.

Libby et al. (1991), Libby (1992), and Eisenlohr et al. (1993) recognized that northeasterly trending dextral and northwesterly trending sinistral shear zones change into northerly trending flattening zones along strike. The regional metamorphic pattern has been described by Ahmat (1986a) and Dalstra et al. (1999).

Previous work in the central part of the Southern Cross Terrane did not resolve many of the fundamental geological issues, such as the lithostratigraphy of greenstones, the

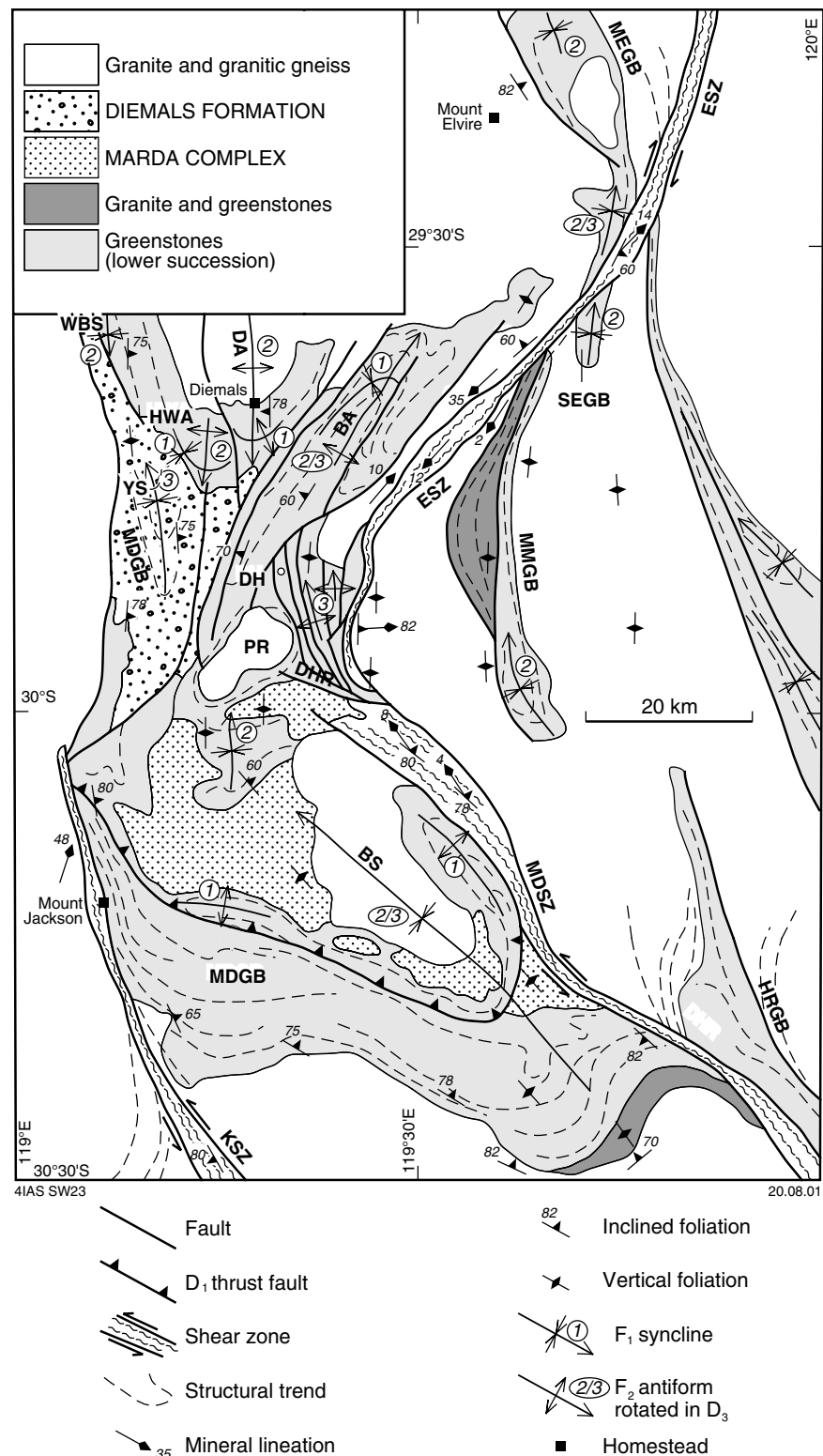


**Figure 3.** Simplified solid geological map of the Marda-Diemals area, showing distribution of the lower and upper greenstone successions and major structural elements. Greenstone belts: HRGB — Hunt Range greenstone belt; MDGB — Marda-Diemals greenstone belt; MEGB — Mount Elvire greenstone belt; SEGB — South Elvire greenstone belt; MMGB—Mount Manning greenstone belt. Shear zones: ESZ — Evanston Shear Zone; KSZ — Koolyanobbing Shear Zone; MDSZ — Mount Dimer Shear Zone. Folds: BA — Broadbents Antiform; BS — Bungalbin Syncline; DA — Diemals Anticline; HWA — Horse Well Anticline; WBS — Watch Bore Syncline; YS — Yarbu Syncline. Locality names: DH — Deception Hill; DHR — Die Hardy Range; PR — Pigeon Rocks

depositional and tectonic environments of greenstone basins, and the origin of regional-scale structures.

The recent mapping by GSWA has shown that the marine-facies lower greenstone succession contains three major associations that were deposited in an extensional setting, whereas the younger, terrestrial Marda Complex and Diemals Formation of the upper succession were deposited in a compressional regime. Greenstones and granitoid rocks have been deformed in three principal deformation episodes:

- north–south compression ( $D_1$ ) produced low-angle thrusts, isoclinal and sheath folds, and a bedding-parallel foliation;
- east–west regional shortening ( $D_2$ ) produced north-trending upright folds with an axial-planar foliation that overprinted  $D_1$  structures;
- protracted, inhomogeneous east–west shortening during  $D_3$  reoriented  $F_2$  folds and produced northeasterly trending dextral and northwesterly trending sinistral shear zones.

The northeast- and northwest-trending shear zones are subparallel to macroscopic folds, and both the shear zones and folds are joined by northerly trending contractional zones, forming regional-scale arcuate structures. The arcuate structures were formed by impingement of rigid granitoids into greenstone belts during  $D_3$  progressive shortening.

## Lower greenstone succession

The Marda–Diemals greenstone belt (Fig. 3) is the largest greenstone belt in the Southern Cross Terrane. Locally well exposed greenstones, relatively simple structures, and lower metamorphic grades make it one of the key areas for the investigation of the stratigraphy of Archaean greenstone belts in the Yilgarn Craton. The lithostratigraphy of this greenstone belt is based on detailed geological mapping, various way-up indicators (such as pillow-lava structures in basalt and cross-bedding in quartzite), an understanding of the regional structure, and geochronological data. Mineral-exploration drillhole data and aeromagnetic images assisted in the geological interpretation in poorly exposed areas.

## Diemals area

The lithostratigraphy of well-exposed greenstones in the Diemals area comprises three major associations (Fig. 4a). The lower association is exposed in the core of the Diemals and Horse Well Anticlines (Fig. 3), where ultramafic rocks are structurally underlain and intruded by granitoids, and stratigraphically overlain by high-Mg basalt and tholeiitic basalt (Appendix 1). The high-Mg basalt is underlain, at least locally, by tremolite–chlorite(–talc) schist. This stratigraphic relationship is exposed both in surface outcrops and in old gold-mining shafts. However, massive to weakly foliated tholeiitic basalt is the dominant rock type within the lower association. It is locally deformed and metamorphosed into amphibolite and basaltic schist adjacent to the granite–greenstone contact, and its upper part is intercalated with several well-bedded mafic tuffs which range from 5 to 30 m in thickness.

The middle association is exposed in the limbs of the Diemals and Horse Well Anticlines, and the Watch Bore Syncline (Fig. 3). It consists of BIF and chert, with minor shale and siltstone, that are extensively intruded by gabbro sills (Fig. 4a). Thick BIF units in the eastern limb of the Diemals Anticline gradually change along strike into thin layers of chert and BIF in the western limb of the Horse Well Anticline. Medium- to coarse-grained, massive gabbro sills that intruded into the BIF and chert horizons are typically concordant with bedding, but discontinuous along strike.

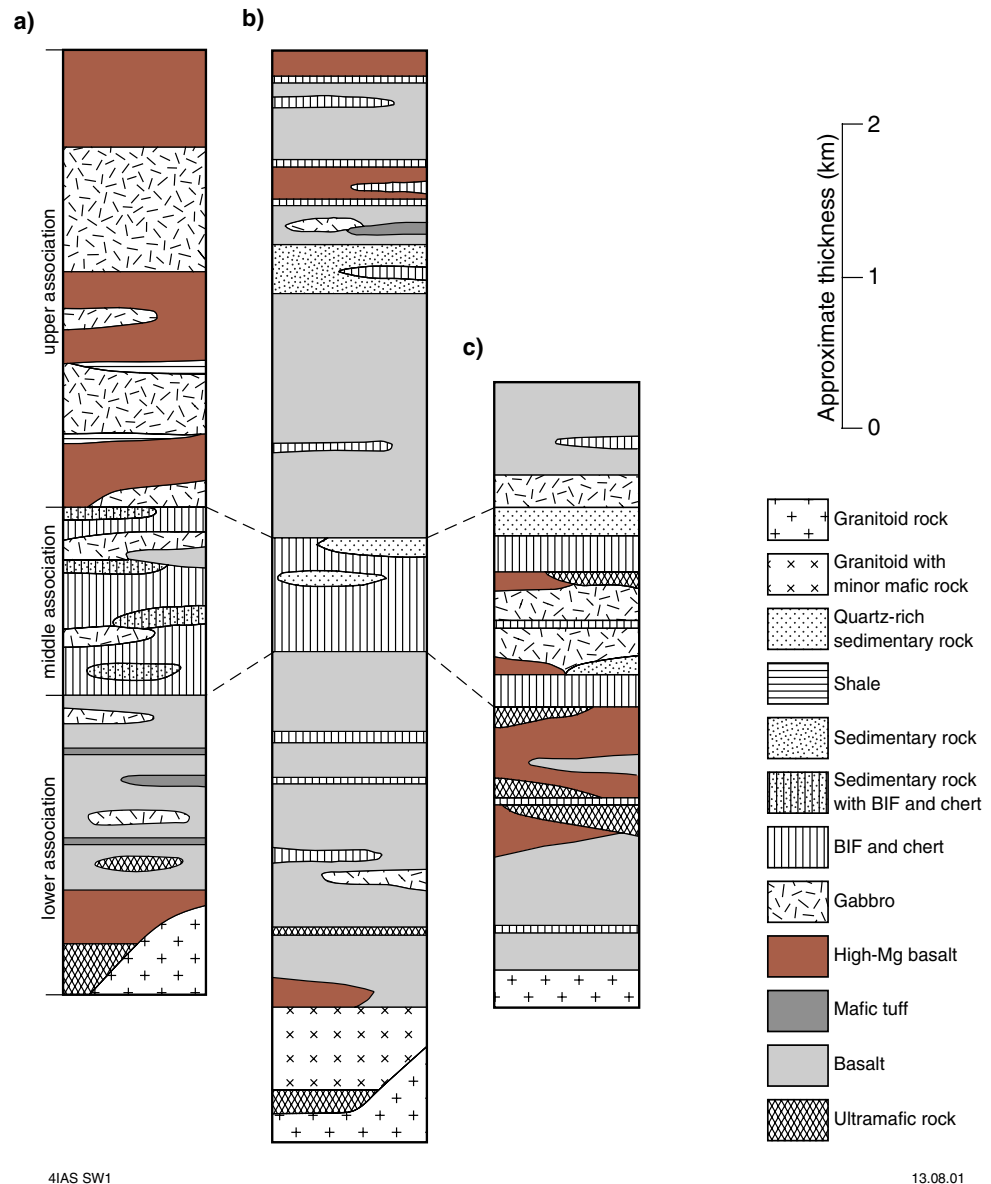


**Figure 4. Simplified lithostratigraphic columns of the Marda–Diemals greenstone belt: a) Diemals area; b) Bungalbin Hill area; c) Die Hardy Range area**

The upper association is well exposed in the Watch Bore Syncline, and contains seven lithological units (Fig. 4a):

1. tremolite–chlorite schist and high-Mg basalt (200–500 m) at the base of the association; some of the tremolite–chlorite schist is probably derived from strongly foliated high-Mg basalt and contains relict pyroxene-spinifex texture;
2. shale (3–15 m thick), locally with cherty bands; bedding in both limbs dips steeply towards the core of the syncline;
3. differentiated gabbro sill (500–1000 m thick), typically containing acicular clinopyroxene crystals up to 20 cm long in a medium- to coarse-grained matrix; igneous layering is concordant with the shale underneath;
4. black shale (5–20 m thick) with local copper mineralization, exposed in the eastern limb but absent from the western limb;
5. high-Mg basalt (600–1500 m thick), fine grained, with pyroxene-spinifex texture;
6. medium- to coarse-grained gabbro sill (~1000 m thick);

7. poorly exposed high-Mg basalt at the top of the association, with pyroxene-spinifex texture.

### **Bungalbin–Marda area**

In the Bungalbin–Marda area, where exposure is not as good as in the Diemals area, the lithostratigraphy of the lower greenstone succession is exposed in the well-defined Bungalbin Syncline (Fig. 3) and mineral-exploration drillholes (Riganti and Chen, 2000; Chen and Wyche, 2001). Here the succession can also be subdivided into three associations (Fig. 4b). At the base, a poorly exposed ultramafic unit is structurally underlain by granitoid rocks and stratigraphically overlain by interleaved mafic and granitoid rocks. The majority of the lower association consists of a thick unit of dominantly tholeiitic basalt (Fig. 4b). However, the lower part contains foliated high-Mg basalt and basaltic schist intercalated with thin units of ultramafic rock, and the upper part contains BIF and chert layers, and is locally intruded by feldspar porphyry.

The middle association consists of a major BIF and chert unit, up to 800 m thick, that forms prominent ridges up to 180 m above the surrounding areas. In the Bungalbin Hill area, BIF is dominant in the south, and chert with intercalated lenticular quartzite layers is dominant in the north. The finely laminated BIF and chert dips steeply, predominantly to the north and northwest. Cross-bedding in the quartzite indicates a consistent younging direction towards the core of the Bungalbin Syncline. In the Mount Jackson area to the west, the same unit is mainly composed of BIF and jaspilite (Riganti and Chen, 2000).

The upper association is best preserved in a large-scale anticline within the northeastern limb of the Bungalbin Syncline where it consists of six units (Fig. 4b):

1. poorly exposed basaltic rocks at the base of the association;
2. clastic sedimentary rocks dominated by shale and siltstone in the core of the anticline that are intercalated with and overlain by BIF and chert layers;
3. fine-grained, massive tholeiitic basalt and minor gabbro, intercalated with BIF and, locally, well bedded mafic tuff;
4. high-Mg basalt with thin BIF intercalations;
5. tholeiitic basalt with minor BIF and chert;
6. fine-grained, massive, high-Mg basalt with pyroxene-spinifex texture at the top of the association; locally well preserved pillow-lava structures in the high-Mg basalt indicate younging upwards.

### **Die Hardy Range area**

Greenstones in the Die Hardy Range area (Fig. 3) are locally well exposed, but structurally complex. Only the lower two of the regional associations are widely preserved in this area (Fig. 4c). The lower association is best exposed east of the Die Hardy Range, and the middle association forms the prominent ridges of BIF in the Die Hardy Range. These BIF units extend to the north and west around the Pigeon Rocks Monzogranite in low ridges that dip away from the pluton.

The lowest exposed part of the lower association is an interval of fine- to medium-grained mafic rocks containing a thin chert horizon. Limited outcrop suggests that this part of the succession is dominated by tholeiitic basalt. A thin BIF unit towards the top of the lower association lies within ultramafic schist and high-Mg basalt.

The middle association in the Die Hardy Range consists of two prominent units of ridge-forming BIF and chert separated by a unit of gabbro which is commonly clinopyroxene-rich and contains a thin, disrupted horizon of BIF. The major BIF and

chert units become thinner along strike to the north and west. The top of the middle association in the Die Hardy area contains a widely distributed clastic sedimentary unit that is dominated by quartzite with cross-bedding and graded bedding and is, at least locally, overlain by gabbro (Wyche et al., 2001). Local BIF and mafic rocks west of Pigeon Rocks and east of Deception Hill may represent parts of the upper association, but stratigraphic relationships are not clear (see **Locality 12**).

## Lithostratigraphic correlation

Although they differ in detail, the lithostratigraphic associations of the lower greenstone succession described above can be broadly correlated by using the BIF-rich middle association as a marker unit. A composite lithostratigraphy of the lower greenstone succession in the Marda–Diemals greenstone belt can be generalized as follows:

1. a lower association dominated by tholeiitic basalt, with minor ultramafic rocks and high-Mg basalt near the base;
2. a middle association characterized by major ridge-forming BIF and chert units;
3. an upper association that contains diverse lithological units in different areas, but is dominated by mafic rocks (high-Mg and tholeiitic basalts, and gabbro sills) that are intercalated with thin units of clastic sedimentary rocks; BIF and chert form part of this association in some areas.

Only parts of these lithostratigraphic associations are recognized in other, narrow greenstone belts of the central Southern Cross Terrane. For instance, the Hunt Range greenstone belt (Fig. 3) to the east comprises high-Mg basalt and tholeiitic basalt, with intercalated mafic tuff, that is overlain by a major unit of chert, BIF, and lenticular quartzite (Chen and Wyche, 2001). This succession is broadly comparable to the lower and middle associations of the Marda–Diemals greenstone belt.

The age of the lower greenstone succession is poorly constrained in the Marda–Diemals greenstone belt. A large body of feldspar porphyry at Deception Hill (see **Locality 15**) has yielded a SHRIMP (sensitive high-resolution ion microprobe) U–Pb zircon age of  $3023 \pm 10$  Ma (Nelson, 1999). However, the stratigraphic position of this porphyry with respect to the lower greenstone succession is unknown. Fletcher et al. (1984) used Sm–Nd model ages to constrain the age of lower greenstone succession basalts from Diemals to  $3050 \pm 100$  Ma. The only other constraint on the age of the lower greenstone succession is a maximum depositional age, based on SHRIMP ages of detrital zircons, of c. 3.3 Ga for quartzites at the base of the exposed greenstone succession in the Illaara greenstone belt 70 km to the east-northeast (Fig. 2; Nelson, 2000). However, the stratigraphy of the Illaara greenstone belt is significantly different from that of the Marda–Diemals greenstone belt (Wyche, 1999). Limited SHRIMP U–Pb zircon geochronology on similar greenstone successions from the southern part of the Southern Cross Terrane and the Murchison Terrane also supports a c. 3.0 Ga age for the lower greenstone succession (e.g. Wang et al. 1996; Pidgeon and Wilde, 1990), although no terrane- or craton-wide correlations have yet been established.

## Upper greenstone succession

### Marda Complex

The Marda Complex (Chin and Smith, 1983) comprises interfingering andesitic and rhyolitic lava flows, and pyroclastic and associated volcanoclastic rocks that were erupted in a mainly subaerial environment (Hallberg et al., 1976; Riganti et al., 2000; see **Localities 7–10**). Rhyolitic ignimbrite within the complex has yielded a SHRIMP U–Pb zircon age of  $2732 \pm 3$  Ma (Nelson, 2001). The Marda Complex occupies a roughly elliptical area of about 600 km<sup>2</sup> that is surrounded by rocks of the lower

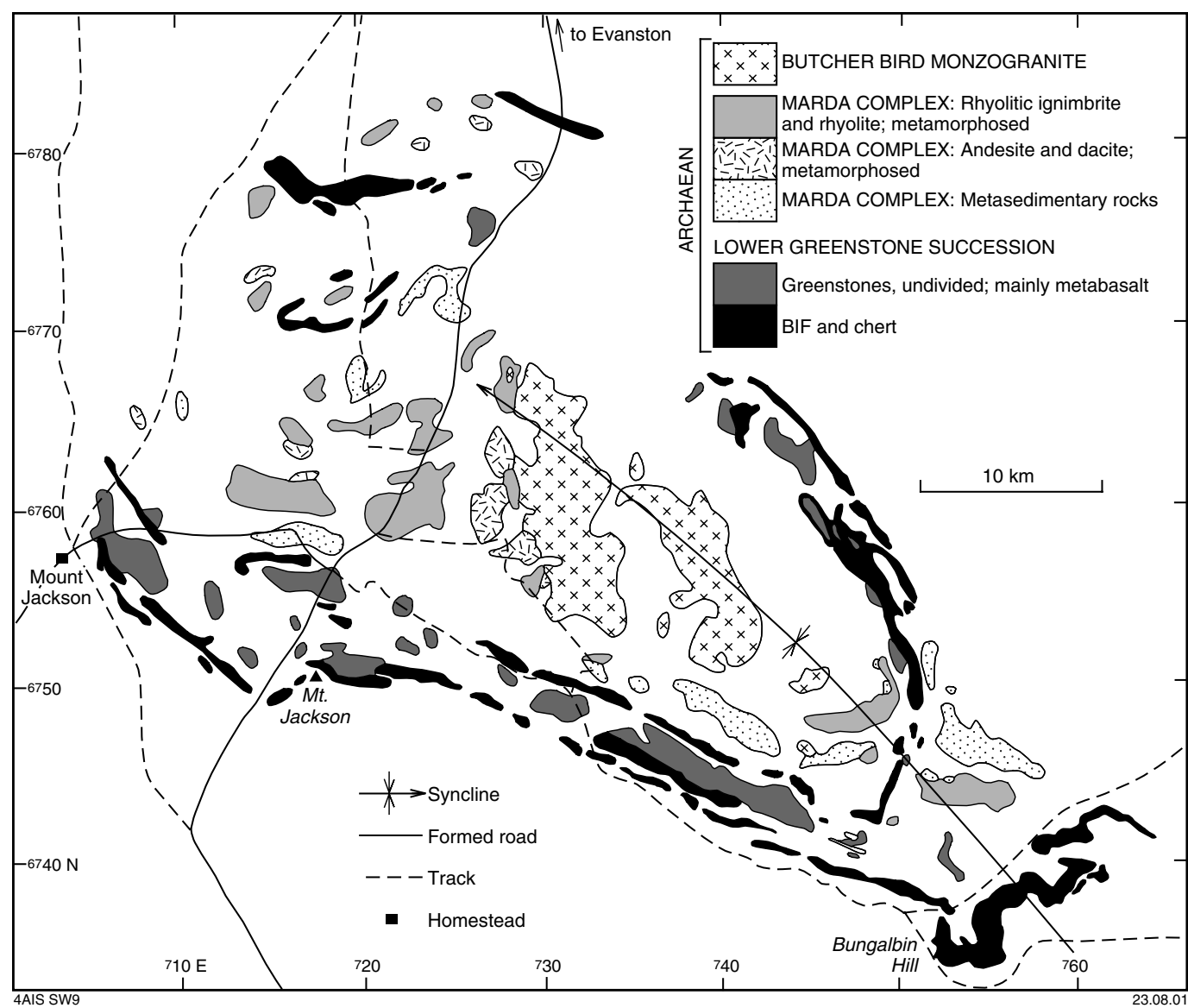


Figure 5. Geology of the Marda Complex, showing the outcrop distribution of the main lithotypes and the adjacent lower greenstone succession

greenstone succession in the core of the Bungalbin Syncline (Fig. 5; Hallberg et al., 1976; Riganti and Chen, 2000; Chen and Wyche, 2001). It is intruded to the east by the Butcher Bird Monzogranite (Fig. 5; see **Locality 11**). The ubiquitous granophyric texture of this granitoid, and its chemical similarity to the Marda Complex rhyolite, suggest that it represents the high-level intrusion of the magma which was the source of the more acid component of the Marda felsic volcanic rocks (Hallberg et al., 1976; Riganti et al., 2000).

The lower part of the Marda Complex is dominated by thick flows of grey andesite and subordinate dacite that are typically porphyritic and commonly amygdaloidal (Riganti et al., 2000). Overlying the andesites are thick sheets of rhyolitic ignimbrites and subordinate rhyolite flows, with textures indicative of subaerial deposition. Pyroclastic rocks include rheomorphic ignimbrite in which eutaxitic banding is defined by alternating layers of quartz and feldspar that wrap around altered plagioclase phenocrysts and lithic fragments. Fragmental ignimbrite includes crystal and lithic lapilli tuffs, as well as minor ash tuffs and agglomerates (Riganti et al., 2000). Lapilli include rhyolite, devitrified glass, and minor dacite, andesite, and chert, typically set in a crystal-rich, welded and devitrified groundmass. In the crystal tuffs, plagioclase and resorbed quartz crystals are commonly surrounded by a matrix of welded shards. Rhyolite flows are massive to quartz- and plagioclase-phyric, with an aphanitic groundmass of devitrified glass; sericitization is common, and locally pronounced (Riganti et al., 2000).

Geochemical investigation of the Marda Complex has confirmed that volcanic rocks of the Marda Complex form a broadly continuous geochemical series with a distinctive calc-alkaline trend (cf. Hallberg et al., 1976). Differences in the rare-earth element (REE) geochemistry of andesites and rhyolites preclude a simple derivation of the more acid rocks from the andesites by a process of crystal fractionation. A crustal source for both lithotypes is indicated by the lack of significant heavy REE depletion, and is supported by high contents of Th and U (Taylor and Hallberg, 1977; Riganti et al., 2000). Selected geochemical analyses of rocks from the Marda Complex are presented in Appendix 1.

Sedimentary rocks in the Marda Complex include polymictic conglomerate, sandstone, and siltstone. They locally interfinger with andesitic and rhyolitic volcanic rocks, and commonly have a volcanoclastic component. Composition of the sedimentary clasts is strongly dependent on the adjacent rock types, with chert and BIF the most abundant clast varieties. Locally prominent felsic volcanic clasts are probably derived from contemporaneous volcanism within the Marda Complex (Hallberg et al., 1976; Chin and Smith, 1983). Angular to rounded clasts range from 2 to 50 cm in size, and are contained in a poorly sorted, lithic, sandy and silty matrix. Grain size fines broadly upward (Chin and Smith, 1983). Conglomerate is mainly concentrated in the lower part, and the rocks grade upward into lithic sandstone and siltstone. The clast composition and immaturity of these rocks suggest proximal deposition.

## Diemals Formation

The Diemals Formation (Walker and Blight, 1983; see **Locality 19**) is composed of polymictic conglomerate, pebbly sandstone, siltstone, argillite, and minor quartzite that are typically metamorphosed to lower greenschist facies, with higher grades adjacent to granite–greenstone contacts. The formation occupies a roughly triangular basin, approximately 45 km long and up to 17 km wide. It is bound mainly by faults, but is locally unconformable on the lower greenstone succession (Fig. 6). The unconformity is best exposed along the northern margin of the basin, where a moderately southerly to southwesterly dipping basal conglomerate overlies steeply west-southwesterly dipping black shale and mafic rocks. Poorly sorted clasts, typically 3–15 cm in size, in the basal

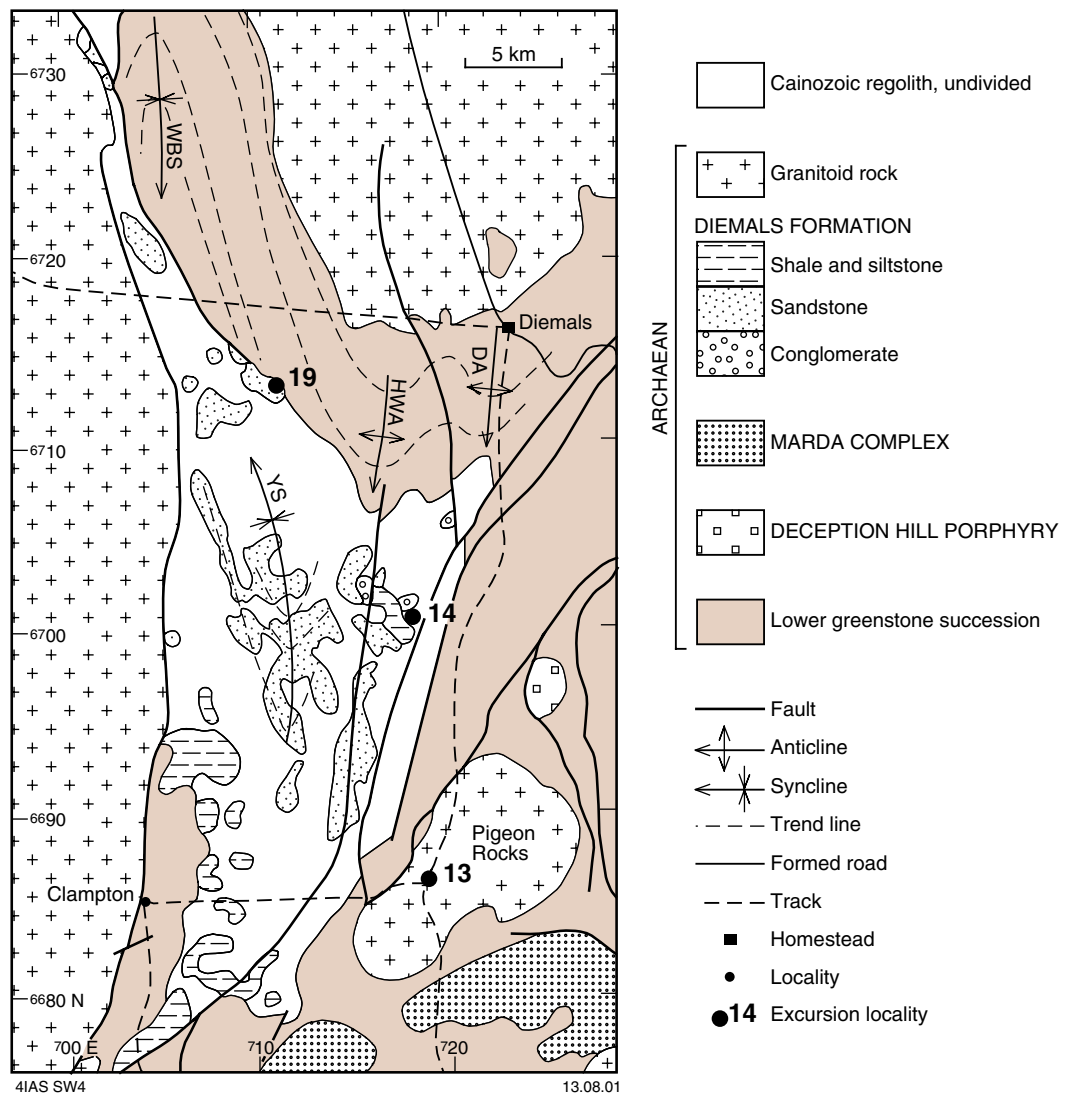


**Figure 6.** Geological map of the Diemals Formation, showing the outcrop distribution of the main lithotypes. Also shown are the relationships of the Diemals Formation with the lower greenstone succession and granitoid rocks, as interpreted from field and aeromagnetic data. Folds: DA — Diemals Anticline; HWA — Horse Well Anticline; WBS — Watch Bore Syncline; YS — Yarbu Syncline

conglomerate are identical in composition to the underlying rocks. The majority of the Diemals Formation is deformed into the regional-scale, west-verging Yarbu Syncline that plunges moderately to the north (Fig. 6). Graded bedding, cross-bedding, and scour troughs (Walker and Blight, 1983) indicate younging towards the core of the syncline. The total thickness of the Diemals Formation appears to be more than 2 km, but is difficult to determine due to the poor exposure and the complicated folding in the limbs of the Yarbu Syncline.

The lithostratigraphy of the Diemals Formation comprises a lower part, in the limbs of the syncline, and an upper part in the core (Fig. 6). The lower part, in the western limb, consists of silty argillite, with chloritic schist and graphitic shale near the base, and in the eastern limb consists of polymictic conglomerate, interbedded with pebbly sandstone, siltstone, and argillite. Clasts in the conglomerate (5–40 cm in size) are composed of chert, BIF, reworked sandstone, and deeply weathered mafic rocks, with minor granitoid and felsic-porphyry clasts, that are similar in composition to rocks exposed to the east. Some chert and BIF boulders contain tight to isoclinal folds

indicating a folding event in the BIF prior to the erosion and redeposition. Some clasts of reworked sandstone and mafic rocks are strongly flattened.

The upper part of the Diemals Formation, exposed in the core of the Yarbu Syncline, consists of sandstone and pebbly sandstone. Pebbles are dominantly chert and vein quartz, in a matrix of medium- to coarse-grained quartz, feldspar, and muscovite. A SHRIMP U–Pb zircon age of  $2729 \pm 9$  Ma (Nelson, 2000) has been obtained from detrital zircons in the sandstone, providing a maximum depositional age.

Field characteristics and facies relationships suggest that the Diemals Formation was deposited in a fluvial environment (Walker and Blight, 1983) over a deformed basement (lower greenstone succession). The asymmetric distribution of sedimentary facies and grain-size variation in the lower part of the formation suggest that the sediments were transported mainly from east to west, and that they were derived mainly from the uplifted and eroded lower greenstone succession to the east, with some contribution from granitoid sources, either from the east or the west. The presence of reworked sandstone clasts within the conglomerate also indicates a relatively active tectonic environment during the deposition. Sandstone and pebbly sandstone in the upper part of the Diemals Formation range from relatively mature, clean quartz arenite (locally quartzite) to lithic greywacke, indicating a variety of conditions of transport and deposition (Riganti et al., 2000).

## Granite and granitoid gneiss

There is little published material about the granitoid rocks of the Southern Cross Terrane. Granitoid rocks occupy a substantially larger proportion of the western two-thirds of the granite–greenstone terrain of the Yilgarn Craton than those in the Eastern Goldfields Terrane. Various classification schemes have been proposed for granitoid rocks of the Eastern Goldfields Terrane based on either their structural setting (e.g. Witt and Swager, 1989) or geochemistry (e.g. Wyborn, 1993; Champion and Sheraton, 1997), or both (e.g. Witt and Davy, 1997). Watkins and Hickman (1990) classified the granitoid rocks of the Murchison Terrane according to their field relationships with respect to greenstones and their chemical character. No regional-scale classification has been published for the granitoid rocks of the Southern Cross Terrane.

There is a substantial amount of published SHRIMP U–Pb zircon geochronology for the Eastern Goldfields Terrane (e.g. Nelson, 1997), but the dataset for the rest of the craton is limited. A complete synthesis of the granitoid rock data for the Yilgarn Craton, including a large amount of new geochemical and geochronological data, is currently being compiled through the AMIRA (Australian Mineral Industries Research Association Limited) Yilgarn granitoid project P482, but this material is not yet available for public release.

Granitoid rocks make up more than 60% of the granite–greenstone terrain in the north of the Southern Cross Terrane, but less than 20% outcrops, and much of the outcrop is deeply weathered. Aeromagnetic images (e.g. Fig. 7) suggest that some non-outcropping areas, away from known greenstone belts, may be underlain by patches of greenstone, or gneissic granitoid rock that may contain greenstone enclaves. Granitoid rocks have a broad range of compositions from syenogranite to tonalite, but most fall in the range from monzogranite to granodiorite (Wyborn, 1993; Dalstra et al., 1998). Wyborn (1993) suggested that the available geochemical data for the eastern Southern Cross Terrane and western Eastern Goldfields Terrane indicated that most granitoid rocks belong to the I-type (igneous) of Chappell and White (1974), and that they have had a substantial crustal prehistory. Selected geochemical analyses of rocks in the Marda–Diemals region are presented in Appendix 1.

The granitoid rocks of the central Yilgarn include a range of textural types from massive, undeformed (see **Locality 4**) to strongly deformed varieties with locally developed gneissic or compositional banding (see **Locality 5**). However, the degree of deformation is not an indicator of relative age, as all of the granitoid rocks for which SHRIMP zircon ages have been determined have been shown to be substantially younger than the greenstones of the lower succession (Nelson, 1999, 2000, 2001).

The oldest granitoid rocks that have been dated in the area are the Butcher Bird Monzogranite ( $2730 \pm 4$  Ma; Nelson, 2001 — see **Locality 11**) and the Pigeon Rocks Monzogranite ( $2729 \pm 4$  Ma; Nelson, 1999 — see **Locality 13**), which form distinct plutons that are apparently related to the emplacement of the nearby Marda Complex. Both these bodies are weakly deformed, but with substantially less evident strain than much younger granitoid rocks that are external to, or at the margins of, greenstone belts. Examples of younger, deformed granitoid rocks include the granitoid gneiss at Yacke Yackine ( $2711 \pm 4$  Ma; Nelson, 2001) and mylonitized monzogranite within the Evanston Shear Zone ( $2654 \pm 6$  Ma; Nelson, 2001 — see **Locality 17**). Most of the granitoid rocks from areas between greenstone belts that have been dated using SHRIMP U–Pb zircon geochronology range from c. 2700 to c. 2650 Ma, although granitoid rocks as young as c. 2635 Ma have been identified (Qiu et al., 1999; Nelson, 2001).

Granite–greenstone contacts are rarely well exposed. A clear cross-cutting relationship is evident between the Millars Monzogranite and the adjacent greenstones, but elsewhere contacts are typically sheared. Chen et al. (2001) explained the nature of the sheared contacts by invoking a model whereby large, relatively rigid granitoid masses impinged upon less competent greenstones in an east–west compressional regime (see **Structural geology**).

Dalstra et al. (1998) argued for diapiric emplacement of granitoid rocks in the Ghooli Dome to the south of the Marda–Diemals greenstone belt (Fig. 3), based on mapping of concentric foliations and radiating lineations in the granitoid rocks and adjacent greenstones, and regional metamorphic patterns. Concentric foliation and radiating lineation patterns are not commonly evident in the extensive granitoid bodies of the Marda–Diemals area. In this area, only the Pigeon Rocks Monzogranite contains fabrics that suggest possible diapiric emplacement.

Because of the deep weathering and lack of continuous outcrop, relationships between different phases in granitoid rocks are unclear, and patterns may only be seen in aeromagnetic images. Where such patterns are not easily discerned, these relationships remain unresolved.

## Structural geology

The deformation history of the Southern Cross Terrane, particularly its southern part, has been described by Bloem et al. (1994) and Dalstra et al. (1999). The current mapping program has recognized three main phases of deformation in the central Southern Cross Terrane on the basis of overprinting relationships, deformation styles, and structural orientations.

### North–south compression ( $D_1$ )

North–south compression,  $D_1$  (Dalstra et al., 1999; Greenfield and Chen, 1999), produced originally easterly trending, tight to isoclinal folds, low-angle thrusts, and a gently dipping foliation with a locally pronounced down-dip mineral lineation in the lower greenstone succession. Overprinting relationships are best seen in the prominent BIF ridges. For example, there are large-scale, east-trending  $F_1$  folds in the hinge zone



**Figure 7. First vertical derivative aeromagnetic image of the Youanmi, Barlee, and Jackson 1:250 000 sheets**

of the north-trending  $F_2$  Diemals Anticline (Fig. 3); and a kilometre-scale  $F_1$  anticline is truncated by a  $D_1$  thrust fault subparallel to the bedding, with both structures folded around the hinge of the Bungalbin Syncline (Fig. 3). At the local scale, examples include tight  $F_1$  folds in BIF refolded into northerly trending  $F_2$  open folds (Fig. 8a);  $F_1$  sheath folds with curved hinges in the hinge zone of a large-scale  $F_2$  fold indicate probable south-directed thrusting (see **Locality 16**); and a  $D_1$  thrust surface parallel to the bedding of BIF contains gently northerly plunging slickenlines and is deformed into a  $F_2$  upright fold whose hinge is parallel to the slickenlines and crenulation hinge lineations (Fig. 8b). The  $S_1$  bedding-parallel foliation is preferentially developed in shale, siltstone, and ultramafic and mafic schists, particularly where they are intercalated with BIF, chert, and gabbro sills, and is most readily recognized in  $F_2$  fold hinge zones (see **Locality 18**). Although most of the  $D_1$  structures can be explained by north–south compression, the significance of  $D_1$  is unclear, and it does not appear to have disrupted the overall lithostratigraphy of the lower greenstone succession.

### East–west orogenic shortening ( $D_2$ )

In the Marda–Diemals greenstone belt, east–west shortening,  $D_2$  (Dalstra et al., 1999), produced originally northerly trending upright folds (e.g. the Watch Bore Syncline and Diemals Anticline in Fig. 3) and an axial-planar foliation in greenstones. The regional-scale Diemals Anticline, which is superimposed on  $D_1$  structures and truncated by a northerly trending fault, contains small-scale, S- and Z-asymmetric folds in the western and eastern limbs respectively. Northerly trending, macroscopic  $F_2$  folds are widely developed in other, smaller greenstone belts, particularly in the northern part of the Mount Elvire greenstone belt. In most cases, the axial-planar foliation to  $F_2$  folds is not pervasive, and has not transposed the bedding and igneous layering of greenstones. The northeast- and northwest-trending, regional-scale folds (e.g. the Bulgalbin Syncline and Broadbents Antiform in Fig. 3) were probably initiated during  $D_2$ , and then re-oriented during  $D_3$  (see below).

In granitoid rocks,  $D_2$  strain is markedly inhomogeneous, with the most intense deformation partitioned into granitic gneiss and along granite–greenstone contacts, where northerly trending gneissic banding and foliation are well developed. Elsewhere, granitoid rocks are mainly massive, although narrow  $D_2$  high-strain zones (typically 1–50 m wide) are developed locally. The granitic gneiss along the Koolyanobbing Shear Zone is up to 15 km wide and contains northerly trending  $S_2$  gneissic banding and foliation that are overprinted by a northwest-trending  $S_3$  foliation. A steeply easterly dipping, pervasive  $S_2$  foliation in the granitoid rocks adjacent to the western margin of the Mount Elvire greenstone belt (Figs 3 and 9) contains a steeply plunging mineral lineation. Here, the effects of  $D_2$  deformation are most pronounced near granite–greenstone contacts, with granitoid rocks massive to only weakly deformed more than about 1.5 km away from contacts.

### Progressive, inhomogeneous east–west shortening ( $D_3$ )

During  $D_3$  progressive east–west shortening, regional-scale arcuate structures were generated in the central part of the Southern Cross Terrane by impingement of competent granitoid blocks into the less competent greenstone belts (Chen et al., 2001). Sinistral shear zones (e.g. the Mount Dimer, Edale, and Yuinmery Shear Zones) developed along northwest-trending margins of the granitoid blocks, whereas dextral shear zones (e.g. the Evanston and Youanmi Shear Zones) developed along northeast-trending margins (Figs 3 and 9). In apex regions of the arcuate structures (e.g. the Die Hardy Range area on Fig. 3), these northeast- and northwest-trending shear zones are linked by north-trending contractional zones across which shortening was



4IAS SW26

06.07.01

**Figure 8.** D<sub>1</sub> and D<sub>2</sub> structures: (a) F<sub>1</sub> tight folds are refolded into a north-trending F<sub>2</sub> open fold in BIF (MGA 765300E 6738800N); (b) L<sub>1</sub> slickenlines (middle left) are parallel to F<sub>2</sub> fold hinge and L<sub>2</sub> crenulation lineation in BIF (MGA 728420E 6690600N)

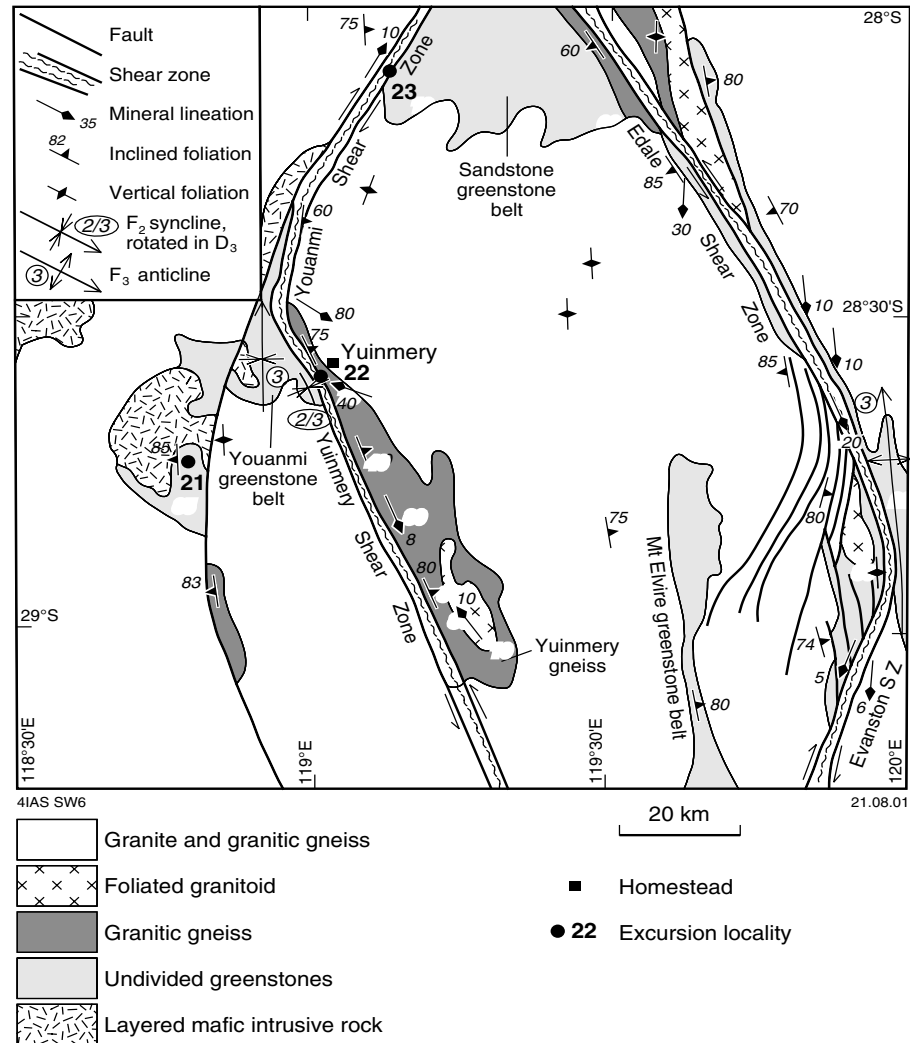


**Figure 9.** Simplified geological map of the Youanmi region, showing the Youanmi and Yuinmery Shear Zones, and the Youanmi–Yuinmery and Edale–Evanston arcuate structures. Locations of Stops 22A–B and 23A–B are also shown (adapted from Stewart et al., 1983, and Eisenlohr et al., 1993)

accommodated by the formation of folds and reverse faults in the greenstone belts, and a coaxial flattening fabric in granitoid rocks. Lateral escape of the greenstone belts is indicated by the progressive rotation of early macroscopic folds (e.g. the Bungalbin Syncline and Broadbents Antiform) into parallelism with the strike-slip shear zones during granitoid impingement.

The regional-scale arcuate structures share a number of common features:

1. They are convex towards greenstones and concave towards impinging granitoid rocks, a geometry reflecting control by the shape of the granitoid plutons.
2. Deformation in the northeast- and northwest-trending shear zones is non-coaxial, whereas it is coaxial in the north-trending contractional zones. Major shear zones commonly follow the granitoid margins but areas of strongest deformation are commonly in mylonitic granitoid rocks 0.5 – 2 km away from the granite–greenstone contacts.
3. The northeasterly and northwesterly trending shear zones do not mutually intersect each other (i.e. they do not have a conjugate geometry), but are subparallel to

macroscopic folds and are linked by northerly trending reverse faults, folds, and flattening fabrics.

4. Folding and reverse faulting in the greenstone belts are most intense within the northerly trending linking zones, to accommodate local shortening induced by horizontal displacements on the northeast- and northwest-trending shear zones during impingement of granitoid rocks into the greenstone belts.

Development of the regional-scale arcuate structures that dominate the structural architecture in the central Yilgarn Craton requires an east–west far-field maximum principal stress ( $\sigma_1$ ).  $D_2$  east–west regional shortening produced macroscopic, north-trending folds in greenstones, accompanied by intrusion of voluminous granitoid rocks (Fig. 10a). As the granitoid bodies cooled and became more rigid, they impinged into greenstone belts during  $D_3$  progressive, bulk, inhomogeneous east–west shortening, with movement accommodated along the northeasterly trending dextral and northwesterly trending sinistral shear zones (Fig. 10b). Adjacent to the shear zones, earlier ( $F_2$ ) folds rotated into parallelism with the shear zones, whereas in the contractional zone at the broad apex of the lozenge-shaped impinging granitoid bodies, earlier folds were tightened and new folds and flattening fabrics developed. The lozenge shapes of granitoid blocks, the competency differences between granitoid rocks and greenstone belts, and strain partitioning during horizontal shortening were the major factors that controlled the development of the arcuate structures. The centres of solid granitoid blocks were relatively resistant to deformation, compared with the adjacent hydrated greenstone belts. Thus, during progressive shortening, strain was partitioned along the granitoid margins. This resulted in the impingement of the rigid granitoid blocks into the greenstone belts along strike-slip shear zones with opposite movement senses (Fig. 10b), and the lateral escape of the greenstone belts along the granitoid margins.

A minimum age of  $D_3$  is suggested by the SHRIMP U–Pb zircon age of  $2656 \pm 3$  Ma (Qiu et al., 1999) for an undeformed porphyritic syenogranite that intruded into the  $D_3$  Koolyanobbing Shear Zone to the south, near Koolyanobbing. However, another

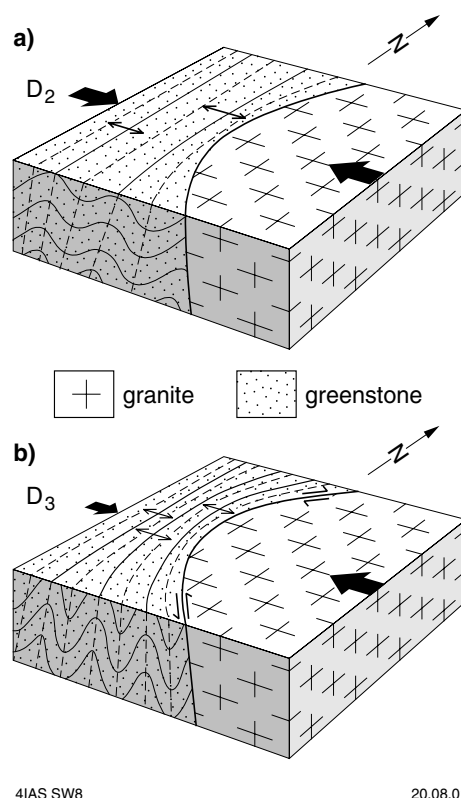


**Figure 10.** Schematic diagram, showing the origin of arcuate structures (after Chen et al., 2001): (a)  $D_2$  east–west orogenic shortening producing north-trending upright folds; (b)  $D_3$  progressive, bulk, inhomogeneous shortening reoriented  $D_2$  folds and generated northeasterly trending dextral and northwesterly trending sinistral shear zones to form arcuate structures

SHRIMP U–Pb zircon age, for strongly deformed monzogranite in the D<sub>3</sub> Evanston Shear Zone near Evanston, was  $2654 \pm 6$  Ma (Nelson, 2001).

### Post-D<sub>3</sub> deformation

Post-D<sub>3</sub> structures include east-trending, small-scale open folds, and foliation; variously oriented kink folds; and northeast-, east-, and northwest-trending, semi-ductile to brittle fractures, some of which are filled by quartz veins or Proterozoic mafic and ultramafic dykes. These later structures overprint and cross-cut all the earlier structures, but the timing of deformation is uncertain.

### Metamorphism

Ahmat (1986a) and Dalstra (1995) have undertaken regional metamorphic studies in the central part of the Yilgarn Craton, and the following summary is based on their work.

The central part of the Yilgarn Craton has been subjected to at least two episodes of metamorphism, with the effects particularly evident in the lower greenstone succession. Metamorphic grades range from very low grade, low-strain prehnite–pumpellyite facies to high-strain, upper amphibolite facies, with peak temperature conditions at lithostatic pressures between approximately 200 and 500 MPa (Dalstra et al., 1999). The distribution of isograds (Fig. 11) shows a consistent pattern of higher grade domains on the edges of the greenstone belts (particularly the eastern margins) gradational to lower grades in the cores of the belts.

Dalstra (1995) recognized an early, low strain metamorphic event preserved in the core of the Marda–Diemals greenstone belt. He attributed this event to sea-floor metamorphism that caused partial to complete spilitization of plagioclase in tholeiitic basalts. Pressure–temperature conditions for these rocks were estimated by Dalstra et al. (1999) at less than 180 MPa and 250 to 300°C. Ahmat (1986a) did not recognize sea-floor metamorphism, and attributed very low grade metamorphism in the core of the Marda–Diemals greenstone belt to elevated isotherms throughout the greenstones during peak metamorphism.

A locally preserved, layer-parallel, penetrative foliation in schistose rocks of the Marda–Diemals and South Elvire greenstone belts (Fig. 3), defined by chlorite and muscovite and crenulated by S<sub>2</sub>, has been ascribed to S<sub>1</sub> (Wyche et al., 2001; Greenfield, 2001). This foliation may be related to recrystallization during D<sub>1</sub>.

A high-strain event preserved on the greenstone margins is associated with a penetrative foliation that is parallel to the trend of F<sub>2</sub>–F<sub>3</sub> fold axes. Both Dalstra et al. (1999) and Ahmat (1986a) considered this event to be due to synmetamorphic uplift of higher grade greenstones adjacent to rising semi-solid granitoid rocks. Thus metamorphic isograds at the margins of the greenstone belts are considerably compressed, resulting in high metamorphic field gradients of approximately 80°C/km at greenstone margins. Peak P–T conditions during this event were estimated by Dalstra et al. (1999) at less than 400 MPa and 540°C. Most peak metamorphic minerals grew parallel to the dominant S<sub>2</sub>–S<sub>3</sub> foliation. However, porphyroblast–matrix relationships suggest that peak metamorphism postdated deformation on the western margin of the Marda–Diemals greenstone belt, and was broadly pre- to syn-deformation near the Evanston Shear Zone (Wyche et al., 2001; Greenfield et al., 2001). Two stages of garnet growth, pre- and syn-deformation, in pelites in the Clearwaters Bore area, along with the spatial distribution of metamorphic domains across the region, suggest that differential uplift of the eastern greenstone margins was more pronounced than in the west. This was probably due to the effects of differential compression during D<sub>3</sub>. All

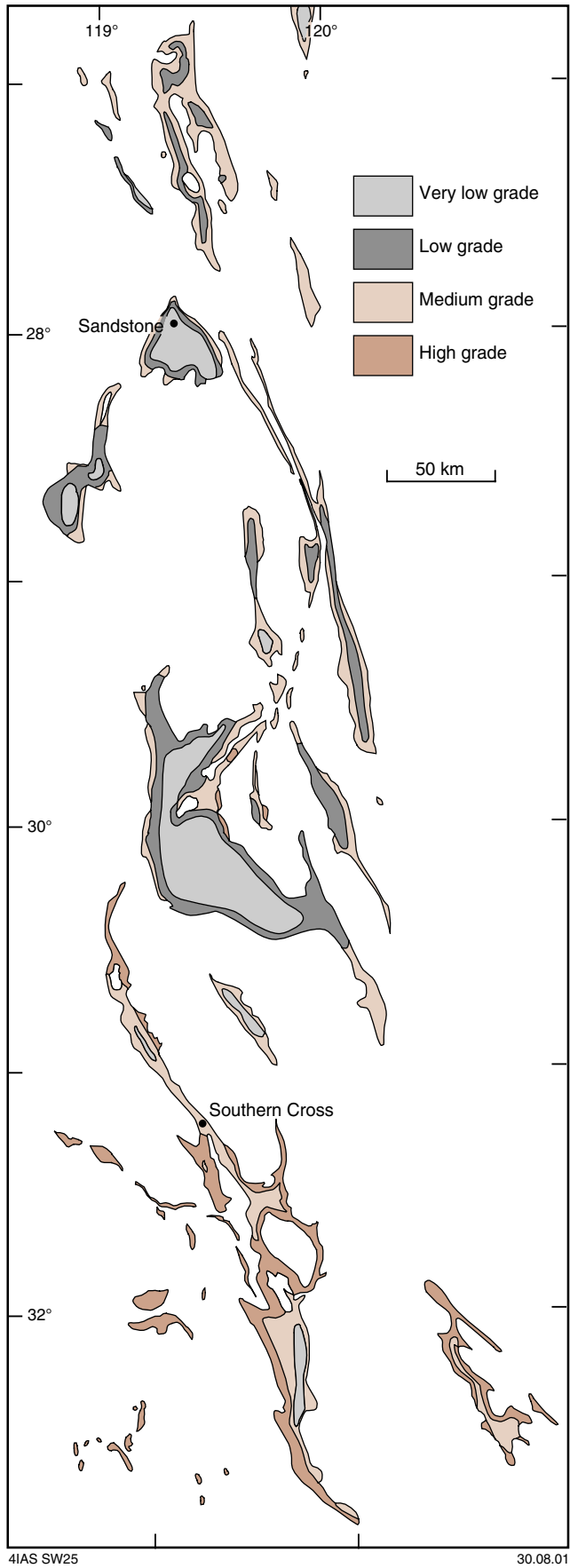


**Figure 11. Metamorphic map of greenstones of the Southern Cross Terrane (modified from Ahmat, 1986a)**

the evidence suggests that metamorphism on the greenstone margins took place over a prolonged period, and was mainly synchronous with an extended period of deformation and granitoid intrusion during  $D_2$ – $D_3$ .

Local calc-silicate alteration in the Mount Manning and South Elvire greenstone belts has a hornfelsic to granoblastic texture, and is interpreted to have a metasomatic origin associated with fluids released from the crystallizing granitoid rocks.

Late (post- $D_3$ ) passive retrogression is evident in most areas, especially on the greenstone margins. Effects include sericitization and saussuritization of feldspars, chloritization, and talc–carbonate alteration of ultramafic schists. Coarse-grained gedrite cuts across a biotite ( $S_2$ ) foliation in the northern part of the Marda–Diemals greenstone belt.

## **Tectonic evolution of late Archaean greenstone basins**

### **Early extensional basins**

The c. 3.0 Ga lower greenstone succession in the Marda–Diemals greenstone belt is characterized by dominant basalts, abundant BIF and associated clastic sedimentary rocks, and rare ultramafic extrusive and, possibly, intrusive rocks. It is similar in age and character to the Luke Creek Group, the lower part of the Murchison Terrane greenstone stratigraphy of Watkins and Hickman (1990). With respect to the Eastern Goldfields Terrane, the Marda–Diemals lower greenstone succession has aspects in common with the Laverton and Duketon areas of the northeastern Yilgarn Craton (e.g. abundant BIF), but is significantly different from greenstones in the Norseman–Wiluna belt that contain abundant komatiite and rare BIF (Williams, 1974; Gee et al., 1981; Barley et al., 1989).

Most greenstone belts in the Southern Cross Terrane contain a similar range of rock types in successions that are similar in character to the lower greenstone succession of the Marda–Diemals greenstone belt (Griffin, 1990). Future mapping may allow the correlation of these greenstone successions across the terrane. In the stratigraphy described above for the Marda–Diemals greenstone belt, the lower and middle associations can be broadly correlated throughout the belt, whereas the upper association varies significantly between different parts of the greenstone belt. The local preservation of pillow-lava structures in tholeiitic and high-Mg basalts in the lower and upper associations indicates that these rocks were deposited in a subaqueous environment. In the middle association, widely preserved ripple marks in BIF and chert, and cross-bedding in quartzite indicate a shallow-marine depositional environment. Circumstantial evidence, such as the presence of extensive, possibly very old (i.e. up to 3.3 Ga), quartzite units to the east (Wyche, 1999), and the widespread intrusion of granitoid rocks that appear to have had a substantial crustal prehistory (Wyborn, 1993), suggests that the lower greenstone succession was deposited on a sialic basement. However, no such basement has yet been identified.

The dominant basalts of the lower greenstone succession may have been deposited in extensional marine basins that were probably bound by syn-depositional normal faults. The exact nature of these faults is unknown because of subsequent deformation and lack of exposure. However, some may have been precursors to granite–greenstone contact faults or shear zones and could have acted as conduits for mafic magmas derived from the lower crust or mantle. The mafic magmas would have been extruded along these faults and deposited mainly in their hangingwalls, while their footwalls contained thinner greenstone intervals. The faults were subsequently intruded by voluminous monzogranite that was probably derived from remelting of older crust. Deposition of

BIF and chert in the middle association represented a period of relative quiescence. The upper association may have been deposited in separate sub-basins.

The first deformation event ( $D_1$ ) must have postdated deposition of the lower greenstone succession, as its upper association has been deformed by  $D_1$ . The widespread granitoid intrusion appears to have also postdated  $D_1$ .

### Late compressional basins

In the central Yilgarn Craton, the emplacement of the stratigraphically highest upper greenstone succession marked a major change in depositional and tectonic environments. The Marda Complex was erupted mainly in a subaerial environment (Hallberg et al., 1976; Riganti et al., 2000), and the Diemals Formation was deposited in a fluvial environment (Walker and Blight, 1983).

It is likely that the thick, clastic sedimentary rocks of the Diemals Formation were deposited as immature, molasse-style sediments, syn- to late- $D_2$ , in an overall compressional regime for the following reasons:

1.  $D_2$  resulted in folding and uplift of the lower greenstone succession, and coincided with a significant change from a marine to a terrestrial depositional environment. The process of folding and uplift of the lower greenstone succession was accompanied by subsidence and the associated deposition of the Diemals Formation. Similar tectonic processes have been documented in many younger orogenic belts (e.g. Busby and Ingersoll, 1995; Chen et al., 1994; Chen and Wilson, 1996).
2. The composition of conglomerate clasts within the Diemals Formation is comparable to the lithologies of the lower greenstone succession to the east. This indicates that the sediments were mainly derived from erosion of the uplifted lower greenstone succession to the east. Moreover, the grain size of the lower part in the formation fines towards the west, consistent with a westward sediment transport direction. An abundance of sandstone in the upper part of the formation reflects a greater contribution from granitoid sources.
3. The unconformity between the lower greenstone succession and the Diemals Formation truncates the fold-axial trace of the north-trending  $F_2$  Watch Bore Syncline (Fig. 3). Therefore, deposition of the Diemals Formation followed the main phase of folding during  $D_2$ .

The following observations suggest that extrusion of the Marda Complex felsic volcanic rocks was broadly contemporaneous with deposition of the Diemals Formation during  $D_2$  east–west orogenic compression:

1. The polymictic conglomerate within the Marda Complex is similar to those in the Diemals Formation and locally contains felsic volcanic clasts that were derived from contemporaneous felsic volcanism of the Marda Complex (Chin and Smith, 1983).
2. The lower part of the Diemals Formation is equivalent to the clastic sedimentary rocks that underlie and interfinger with the Marda Complex felsic volcanic rocks (Hallberg et al., 1976; Chin and Smith, 1983; Dalstra, 1995). The SHRIMP U–Pb zircon maximum depositional age of  $2729 \pm 9$  Ma for the Diemals Formation is similar to the ages of Marda Complex felsic volcanic rocks, which have been dated at  $2732 \pm 3$  Ma and  $2734 \pm 3$  Ma (Nelson, 2001).

The felsic volcanic rocks in the Marda Complex are similar in age and composition to the comagmatic Butcher Bird Monzogranite (Hallberg et al., 1976; Riganti et al., 2000) that has a SHRIMP age of  $2730 \pm 4$  Ma (Nelson, 2001). A similar SHRIMP age of  $2729 \pm 4$  Ma has been obtained from the Pigeon Rocks Monzogranite (Nelson, 1999). These intrusions coincided with  $D_2$  orogenic movement that may have continued episodically, accompanied by further granitoid intrusion, until after c. 2680 Ma (Dalstra

et al., 1999; Nelson, 1999, 2000, 2001; Qiu et al., 1999). In the eastern Yilgarn Craton, granite plutons intruded predominantly between c. 2685 and c. 2660 Ma (e.g. Nelson, 1997). Some granites are intrusive equivalents of felsic volcanic rocks and granite intrusion peaked during D<sub>2</sub> regional shortening (Nelson, 1997; Witt and Davy, 1997). Similarly, in the Superior Terrane of Canada, peak granitoid intrusion also took place during the main phase of greenstone deformation (Corfu and Davis, 1991).

## Economic geology

The central Yilgarn Craton contains a relatively low number of economic mineral deposits when compared to the adjacent Eastern Goldfields Terrane to the east and the Southern Cross Terrane to the south, which contain major gold and nickel deposits; and the Murchison Terrane to the west, which contains substantial gold and base metal deposits. This apparent lack of mineral wealth in the central Yilgarn Craton is more remarkable considering that exploration targets contain similar affinities to proven deposits in the richer parts of the Yilgarn Craton. The large volume of greenstone in the Marda–Diemals area contains significant BIF and ultramafic units that are transected by major shear zones, as well as second- and third-order faults. These lithologies and their structural setting are considered favourable to gold, iron, and nickel mineralization in the Yilgarn Craton (Groves et al., 1990; Marston, 1984).

Prospecting for gold and silver in the east Yilgarn Craton began in the late 1880s, and exploration in the central Yilgarn Craton extended north from initial finds at Southern Cross. Most gold production and exploration diminished considerably after 1945. Following the discovery of komatiite-hosted nickel deposits at Kambalda in the Eastern Goldfields Terrane in 1966, there was a period of intense nickel exploration in the Yilgarn Craton, assisted by a boom in world nickel prices. Despite no significant mineralization being reported in the northern part of the Southern Cross Terrane, extensive track networks established throughout the greenstones are still used today to facilitate mapping and exploration. Recent exploration in the region has been mainly for gold.

## Gold and silver

Total gold produced in the Marda–Diemals area before 1986 was approximately 2481 kg (Townsend et al., 2000). Although there were a number of historical mining centres (Matheson and Miles, 1947; Chin and Smith, 1983; Walker and Blight, 1983), Evanston is the only one that is still active.

Gold deposits are epigenetic, structurally controlled, and commonly associated with quartz veining. Host lithologies range from mafic igneous to metasedimentary to felsic volcanic, with BIF a common host rock. Most deposits are associated with the lower greenstone succession, with the exception of the Marda mining centre, where gold mineralization is hosted by felsic volcanic and volcanoclastic rocks of the Marda Complex. Common alteration styles include carbonation and sulfidation.

Silver has been produced in the central Yilgarn Craton as a byproduct of gold mining. Total recorded silver production in the Marda–Diemals area is 102 kg since 1903 (Townsend et al., 2000).

## Nickel

Despite locally abundant ultramafic rocks in the central Yilgarn Craton, and extensive exploration, no nickel production has been recorded. Exploration has focused on disseminated sulfide mineralization using percussion and diamond drilling to investigate

targets. Anomalous concentrations of nickel sulfides have been found at basal ultramafic contacts, especially at contacts with BIF (Marston, 1984).

### Iron oxides

Iron-ore reserves of 170 million tonnes (t) at 60% iron have been estimated for a number of small- to medium-sized deposits in the central Yilgarn Craton, most notably at Koolyanobbing and Mount Jackson (Fig. 2). The host rocks to these deposits are tectonically thickened and supergene-enriched BIFs of the lower greenstone succession. The host rocks are also carbonate- and sulfide-rich, suggesting that hydrothermal alteration also played a role in concentrating the iron ore. Only the Koolyanobbing deposit has been mined, and recorded iron production prior to 1995 was 53.7 Mt (Townsend et al., 2000). A feasibility study is currently being undertaken with a view to mining some deposits in the Marda–Diemals greenstone belt.

### Other commodities

Copper mineralization is recorded in small, isolated deposits. However, the only recorded production is 0.82 t from the Mount Jackson prospect (Matheson and Miles, 1947). Copper is in an azurite–malachite–carbonate association in quartz veins. Host rocks include shale and peridotite. Possible volcanic-hosted base metal mineralization has been identified at Pincher Hill and Freddie Well (see **Locality 21**).

Lake Seabrook and Lake Deborah (Fig. 2) have been exploited for alunite, gypsum, and halite (Townsend et al., 2000). Minor sedimentary uranium mineralization has been identified in saline and gypsiferous clay deposits associated with Lake Barlee (Fig. 2; Walker and Blight, 1983).

## Summary

In the central Yilgarn Craton, syn-depositional extension and syn-orogenic compression were responsible for the late Archaean crustal evolution from mafic-dominated volcanism to felsic magmatism and clastic sedimentation. The c. 3.0 Ga, mafic-dominated lower greenstone succession was probably deposited in an extensional marine basin or sub-basins bound by syn-depositional normal faults. The c. 2.73 Ga upper greenstone succession, comprising felsic volcanic and volcanoclastic rocks (Marda Complex) and thick clastic sedimentary rocks (Diemals Formation), was deposited in compressional, probably terrestrial, basins coeval with D<sub>2</sub> orogenic folding and major granitoid activity between c. 2.73 and c. 2.68 Ga.

In addition to the D<sub>2</sub> east–west orogenic shortening event, D<sub>1</sub> north–south compression produced low-angle thrusts, isoclinal folds, and a gently dipping foliation that were restricted to the lower greenstone succession. D<sub>3</sub> progressive east–west shortening deformed the upper greenstone succession and produced regional-scale arcuate structures as a result of impingement of competent granitoid rocks into less competent greenstone belts.

## Part II: Excursion localities

### Locality 1: Marvel Loch gold mine

by P. Baudry and J. Whitelock

*The Marvel Loch gold mine is about 350 km east of Perth and 220 km west of Kalgoorlie at the township of Marvel Loch, approximately 30 km south of Southern Cross.*

#### Introduction

The Marvel Loch gold mine is hosted in the greenschist- to amphibolite-facies Southern Cross greenstone belt that extends about 300 km from near Mount Jackson in the north to south of Marvel Loch (Fig. 2). Although the belt is characterized by a large number of relatively small mines, it hosts four known deposits with more than one million ounces of contained gold.

The Marvel Loch gold deposits were discovered in 1905, and produced ore from underground workings between 1905 and 1939. Since the Second World War, mining has continued intermittently until the present day. Openpit operations in the weathered zone commenced in 1984 over the southern lodes (now the South pit), and separate openpit operations were developed in the weathered zones over the Exhibition–Firelight (now the Centre pit) and Undaunted (now the North pit) leases to the north in 1986. Underground operations ceased in late 1989. Recorded production pre-1987 is 923 840 t at a grade of 6.1 g/t Au for 181 593 oz of gold.

Sons of Gwalia Ltd acquired 100% ownership of the Marvel Loch mine leases in 1996. At that time, cutbacks were underway in both the South and North pits. Much larger cutbacks of all three pits were commissioned in 1997 to produce what is now the Marvel Loch pit, with projected production in the order of 10 Mt of ore (700 000 oz Au).

The openpit cutbacks are progressing from north to south with the North pit completed to a depth of 230 m. The Centre pit will be completed to a similar depth in 2002, and the South pit has approximately 3.5 years mining left, to a final depth of 275 m.

#### Regional geology

The north-northwesterly trending Southern Cross greenstone belt is approximately 7–10 km wide, and forms a narrow and sinuous, tight to isoclinally folded greenstone succession between massive granite and granitoid gneiss terrains. The succession in the Marvel Loch district (Gee, 1982) consists of psammitic metasedimentary rocks at the base overlain by a unit of ultramafic intrusive rocks, which is in turn overlain by a 3–5 km-thick unit of mafic and ultramafic volcanic rocks, and interflow sedimentary rocks including BIF. Above the BIF-bearing interval, there are felsic volcanic rocks and a 3–5 km-thick unit of pelitic rocks marking the top of the preserved succession.

The mafic–ultramafic–BIF unit in the middle of the succession is the major host to gold mineralization in the belt. Local mineral assemblages such as garnet–biotite–andalusite in metasedimentary rocks and anthophyllite–tremolite in mafic–ultramafic rocks indicate amphibolite-facies metamorphism, and there is evidence of retrograde metamorphism to greenschist facies. The deformation history of the belt is long and complex (Bloem et al., 1997), but is broadly similar to that described above for the Marda–Diemals region.

## Deposit geology

### Stratigraphy

The deposit lies within a westerly dipping succession of interlayered basalts and metasedimentary rocks, between hangingwall ultramafic rocks and footwall mafic rocks (Fig. 12). The succession is cut by a dextral shear zone oriented  $20^\circ$  to layering, and recognizable over at least 5 km strike length. The shear zone is 80–100 m wide, and is approximately 1 km west of the Ghooli Dome. The relative ages of the various rock types have been determined from crosscutting relationships in the pit.

The oldest rocks exposed in the pit are metasedimentary rocks, including graphitic and non-graphitic shales in the north wall, bound to the east by gabbro and to the west by high-Mg basalt. Alternate bands of light and dark (biotite-rich) material define bedding laminations that range in thickness from 2 to 3 cm. The best exposure in the pit is a thick metaquartzite unit that is overlain by a metamorphosed shale, now biotite schist with garnet porphyroblasts. A thin band of graphitic shale forms the footwall contact with the basalt to the west, and the other metasedimentary rocks to the east.

Metamorphosed high-Mg basalt in the west wall of the North pit is bound to the east by pelitic rocks and to the west by olivine-rich serpentinized komatiite. A thick unit of layered tholeiitic metabasalt, also in the North pit, is bound to the east by the graphitic shale unit and to the west by olivine-rich serpentinized komatiite. In the Centre pit, komatiite overlies the tholeiitic basalt to the east and contains local, thin interbeds of tholeiitic basalt. The komatiite has been strongly serpentinized, and later silicified. Unaltered olivine, observed in thin section, appears to postdate the serpentinization, suggesting a metamorphic origin. The komatiite unit extends into the South pit where it comprises more than 60% of the exposure.

A large metamorphosed gabbro dyke comprises more than 70% of the outcrop in the North pit, but is less prominent in the Centre and South pits. The gabbro is commonly strongly sheared, with schistosity defined by metamorphic biotite and hornblende.

Three ultramafic dykes in the Marvel Loch pit are strongly serpentinized and probably postdate mineralization, as they appear to have truncated mineralization in both the Centre and South pits. Three major pegmatite bodies probably pre-date the main shearing.

### Structure

The main structural element associated with mineralization in the Marvel Loch deposit is a ductile, sinistral shear. This wide (50–100 m), steeply dipping, northwesterly trending shear appears to control the broad alteration and mineralization of all rocks in the pit. The strong foliation in the host rocks is associated with the shear, and was probably the conduit for ore-fluid movement. This is indicated by the development of a strong biotite lineation with a plunge of  $70^\circ$  to the south, which mirrors the overall plunge of the orebody. The shear zone cuts all units in the deposit, and is accompanied by development of delimiting shears, Riedel shears, and thrust shears (Rolley and Baxter, 1990). Mineralization is interpreted to be concentrated in dilatant portions of delimiting shears in the Undaunted, Firelight, and Exhibition lodes (Fig. 12). The mineralized zones plunge steeply south at the intersection of delimiting and Riedel shears. Later cross fractures are barren and crosscut the mineralized lodes with minor dislocation (Rolley and Baxter, 1990). The juxtaposition of lithological contacts with the main shear was probably the focus for dilation and lode development. A broad range of lithology–shear intersection styles have resulted in the wide variety of lode types across the deposit.

### **Alteration**

Alteration within the Marvel Loch pit is highly varied in both style and intensity.

Potassic alteration affects ultramafic, basaltic, and gabbroic rock types. It is most intense in the Contact and Exhibition lode areas, where all amphiboles have been replaced by biotite grains with a distinct ductile deformation fabric. Lode rocks commonly contain quartz–diopside–tremolite veining approximately parallel to the main shear. Potassic calc-silicate alteration is transitional between potassic and calc-silicate alteration, and the typical mineral assemblage includes plagioclase, biotite, and hornblende. Here, gold is associated with quartz–diopside veining. Calc-silicate alteration is broadly distributed within the ore lodes that are hosted by gabbro. A typical mineral assemblage includes plagioclase and diopside, developed in a medium-grained rock.

Plagioclase alteration is well developed in the Sherwood lode (Fig. 12), where it is up to 10 m wide. A typical mineral assemblage includes plagioclase, quartz, hornblende, minor sericite, and altered diopside.

Talc alteration has been observed as a distal alteration type to all ultramafic-hosted lodes within the pit.

### **Vein types**

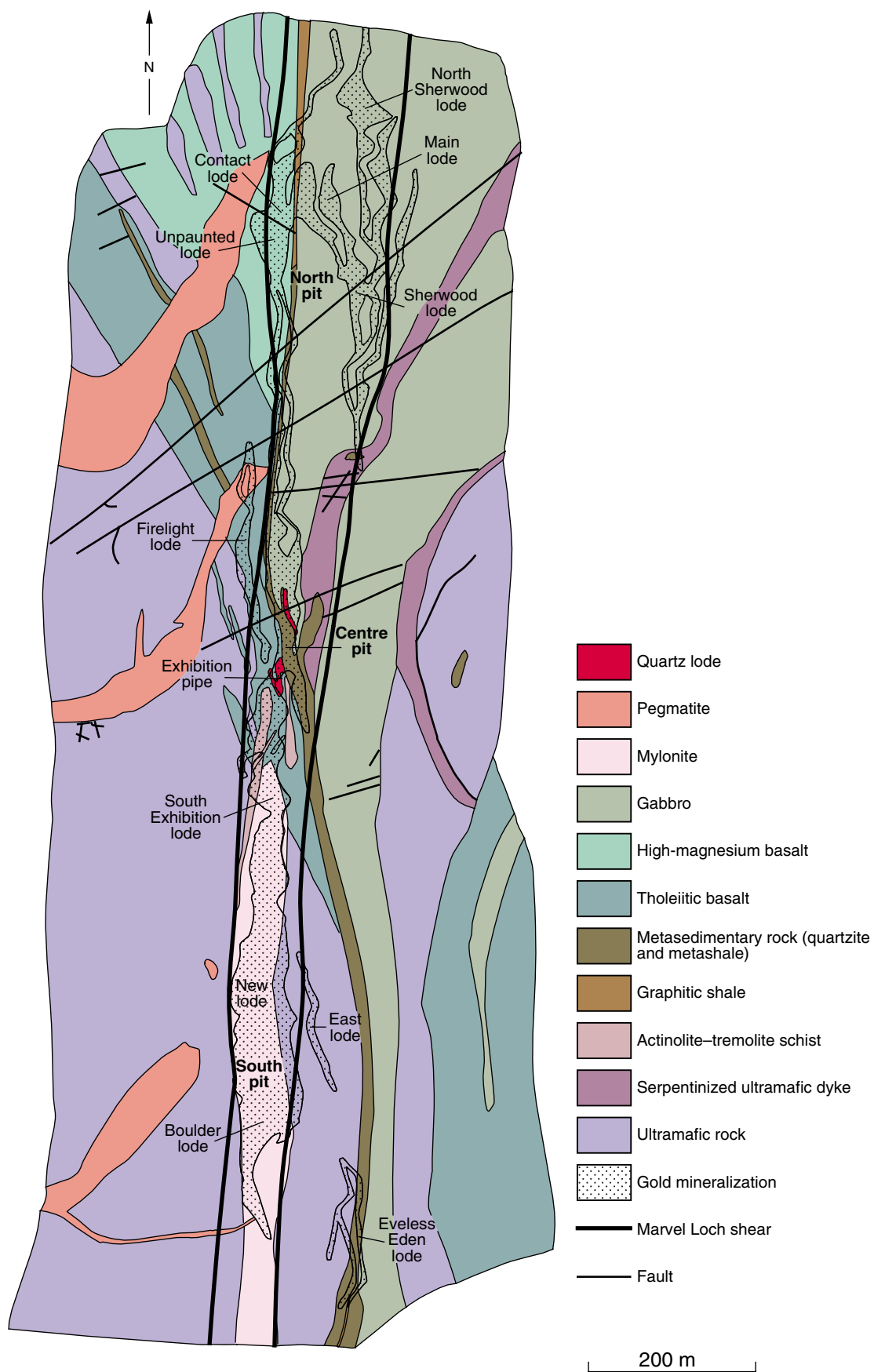
Five vein types have been recognized in the Marvel Loch deposit:

1. Quartz–diopside veins cut all lithologies and are often associated with pyrrhotite and arsenopyrite mineralization and can grade from 1 to 10 g/t Au.
2. Quartz–tremolite–actinolite veins are found in tholeiitic basalt, commonly around quartz–diopside veins.
3. Quartz–sulfide veins may contain pyrrhotite, arsenopyrite, galena, sphalerite, and pyrite, commonly together with native gold. Gold grade within these veins is highly variable and can reach 200–300 g/t.
4. Quartz–diopside–amphibole–sulfide veins contain altered slivers of wallrock, and are found within the main Exhibition pipe and Undaunted lodes. Sulfides including arsenopyrite and pyrrhotite may be present with native gold. Gold grade within these veins reaches up to 40–50 g/t.
5. Large quartz–pyrite veins intrude throughout the deposit. They do not carry gold and probably represent a late-stage, post-mineralization, veining event.

### **Mineralization**

The Marvel Loch pit contains a wide variety of lode styles. The following description proceeds from north to south (see Fig. 12 for lode locations). The lodes typically plunge to the south at around 60–70° and dip subvertically. Sherwood lode differs from the others in that it dips to the west at around 70–80°. The Marvel Loch deposit, with an approximate 0.73 g/t Au lower cutoff grade, boasts around 70 000 tvm (tonnes per vertical metre) at about 2.4 g/t Au across the three subpits.

In the North pit, the Sherwood lode, hosted by gabbro, is marked by plagioclase alteration, significant quartz veining, and minor diopside. The high-grade (i.e. >3 g/t Au) core manifests as an easily identifiable bleached unit grading into unmineralized potassic calc-silicate-altered gabbro. A halo of lower grades to the east of the lode appears to be associated with strong potassic alteration. Sulfides within the lode include pyrrhotite, arsenopyrite, and some pyrite, and are associated with late-stage veining. Both arsenopyrite and pyrrhotite contain fine-grained gold within the sulfide crystal lattice. Fine-grained free gold within the silicates associated with ilmenite was most likely sweated out of the sulfides (Eilu et al., 1999). The North Sherwood lode is also



4IAS SW24

13.08.01

**Figure 12. Marvel Loch gold deposit showing distribution of major rock types and the North, Centre, and South pits**

hosted by the North pit gabbro, but here gold appears to be concentrated within disseminated arsenopyrite, with a broad potassic calc-silicate alteration zone encompassing most of the gabbro in this part of the pit.

Also in the North pit, the Contact lode is hosted by the high-Mg basalt in the hangingwall of the metasediment–basalt contact. This lode contains strong potassic alteration with quartz–diopside veining. Pyrrhotite and arsenopyrite are the major sulfide phases, with gold both free and lattice-bound within pyrrhotite. The Undaunted lode is interpreted as a dilatation vein, with gold mostly as free gold in the quartz.

In the Centre pit, the northern part of the Exhibition pipe is hosted by pelitic rocks, metagabbro, and tholeiitic metabasalt. Quartzite is also mineralized, and forms small blocks to the east of the main orebody. Alteration within this lode is varied, with the high-grade zones defined by a strong plagioclase alteration with associated quartz-veining and bleaching, and the lower grade zones potassic altered, with strong quartz–diopside–tremolite veining, and common silicification. Sulfides are mainly pyrrhotite, arsenopyrite, and loellingite, with gold both as free gold in quartz–galena veins, and lattice-bound gold within the sulfides. The Exhibition pipe is a dilatation vein with a strike length of 50 m, and a width of 15 m. High grades within the quartz lode are associated with slivers of wallrock which have been strongly mineralized. Arsenopyrite is the dominant sulfide in the lode, and gold is both in free and lattice-bound forms. The South Exhibition lode is similar to the northern part of the Exhibition pipe, but is hosted entirely by tholeiitic metabasalt. The basalt is potassic calc-silicate-altered, with large quartz–diopside–tremolite veins. The main sulfides are arsenopyrite and pyrrhotite, and the rock is invariably silicified. The Firelight lode is a long, narrow, medium-grade lode on the western side of the Centre pit. It is parallel to the stratigraphy, outside the main shear, and hosted by a metabasalt which has undergone strong potassic alteration. The alteration includes fine-grained biotite and diopside banding.

In the South pit, the Eveless Eden lode lies within a metasedimentary unit to the east of the locally strongly silicified main shear. The lode is terminated to the west by a graphitic shale unit that marks the contact between the metasedimentary rocks and the metamorphosed ultramafic rocks. The average strike length is 80 m, and width 10 m. As with the Firelight lode, this lode appears to be lithologically, not structurally, controlled. The East lode east of the main shear is hosted by biotite–hornblende–actinolite schist, with the high grades in areas of intense silicification. The Boulder and New lodes are hosted by metamorphosed komatiite in the western and central parts of the South pit, within the main shear. Metamorphosed komatiite in the ore shoots is strongly foliated, and partially silicified. Gold lies in large, laminated, antitaxial veins. The lodes are characterized by diopside–quartz wallrock alteration, with shoots up to 100 m long, with an average width of 10–25 m.

## **Locality 2: Koolyanobbing Shear Zone (MGA 719410E 6618280N)**

**by S. F. Chen and J. E. Greenfield**

*This locality consists of pavement and low whaleback outcrop around a stone-sided well, about 6 km along a track (the well is on the northern side of the track) that heads east from the Bullfinch–Evanston road, 92 km north of Southern Cross.*

The northwesterly trending Koolyanobbing Shear Zone (Fig. 2) is a 6–15 km-wide, high-strain zone that has been described in detail by Libby et al. (1991). In the north (north of Koolyanobbing), a more northerly trending gneissic banding and foliation (S-fabric) is sinistrally displaced by a northwesterly trending foliation (C-fabric),

forming S–C fabrics within the shear zone. In granitoid gneiss away from the shear zone, the C-fabric is generally absent. The northerly trending fabrics have also been sinistrally truncated by a series of northwesterly trending, discrete shear zones within the high-strain zone. Asymmetric porphyroclasts, S–C fabrics, and a shallowly plunging mineral lineation indicate a sinistral strike-slip movement on the Koolyanobbing Shear Zone. Granitic mylonite with various kinematic indicators is particularly well exposed along the north shore of Lake Deborah East, but access to this area is difficult. Towards its southern end near Lake Johnston, 250 km to the southeast, the Koolyanobbing Shear Zone is defined by a wide zone of strongly recrystallized mylonitic gneiss, and amphibolite, in which shear-sense indicators are typically obscured by recrystallization and syn-tectonic emplacement of granitoid rocks (Libby et al., 1991).

At this locality, we will examine fabrics in banded granitoid gneiss in the northwestern part of the Koolyanobbing Shear Zone (Fig. 2). The gneissic banding is defined by compositional variation of leucocratic and mesocratic granitoid rocks. Leucocratic granitoid rocks include monzogranite and pegmatite, whereas mesocratic granitoid rocks are dominated by granodiorite and biotite-bearing microgranitoid. A fold hook in a pegmatite vein has an axial-planar trace parallel to the gneissic banding (Fig. 13). Elongate feldspar and quartz grains are aligned along an S-fabric that trends  $330\text{--}345^\circ$ , and is typically parallel to the gneissic banding. The S-fabric is sinistrally displaced by a steep C-fabric that trends  $315\text{--}320^\circ$ . This fabric is defined by alignment of mica grains and deflection of the S-fabric into the C-fabric orientation.

Asymmetric feldspar porphyroclasts indicating sinistral shear are locally prominent. A sinistral shear sense is also indicated by the drag pattern of gneissic banding across northwesterly trending, narrow, discrete shear zones. Gently plunging mineral lineations are locally preserved on a northwesterly trending foliation. A geochronological sample taken from granitoid gneiss at this locality did not contain sufficient high-quality zircons to allow a SHRIMP age determination.

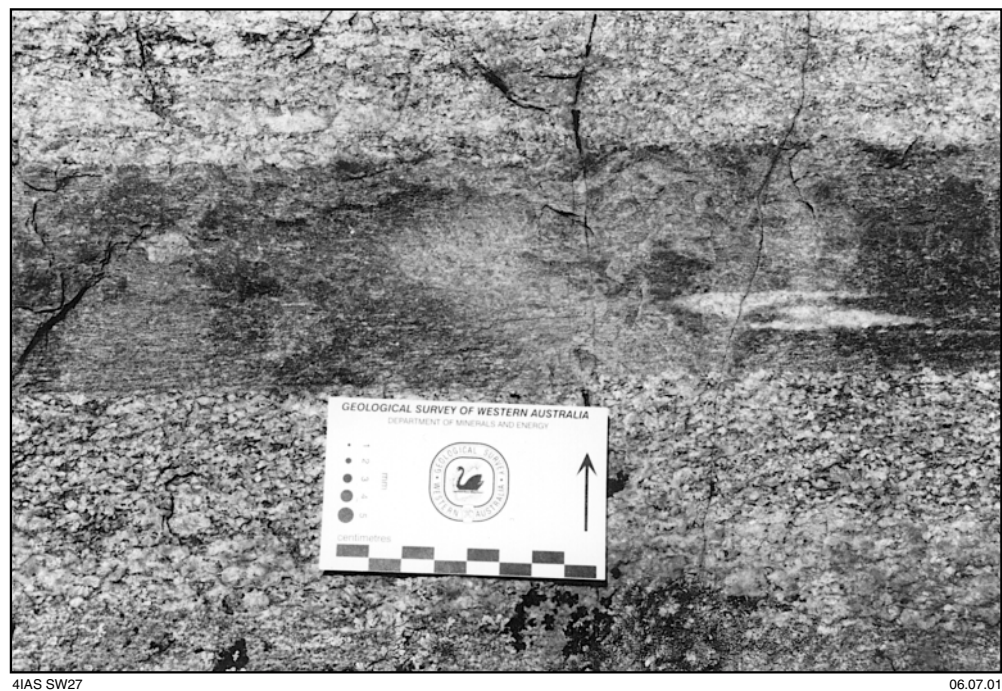


**Figure 13.** Compositional banding in granitoid gneiss, and a fold hook with axial planar trace parallel to the gneissic banding at Locality 2

In granitoid gneiss (MGA 726540E 6619210N) about 7 km to the east-northeast of Locality 2, deformation is characterized by north-northeasterly trending gneissic banding and weak foliation, and the northwesterly trending foliation (C-fabric) that is characteristic of the Koolyanobbing Shear Zone is absent. In addition, many pegmatite veins crosscut the banding at a high angle, whereas they are typically parallel to the banding within the shear zone. Libby et al. (1991) suggested that this granitoid gneiss lies outside the shear zone.

### **Locality 3: Deformation of granitoid gneiss within the Koolyanobbing Shear Zone (MGA 716930E 6625230N)**

**by S. F. Chen and A. Riganti**

*This locality is a large pavement of banded granitoid gneiss on the western side of the Bullfinch–Evanston road, about 23 km north of Lake Deborah East, and 7 km north of the turnoff to Locality 2.*

At this locality, northerly to north-northwesterly trending gneissic banding and foliation are sinistrally truncated by a series of small-scale, northwesterly trending discrete shear zones.

The banded granitoid gneiss is mainly monzogranitic in composition, with subordinate pegmatite and biotite-rich microgranitoid. It is compositionally banded, with most pegmatite veins parallel to the gneissic banding. Some discordant pegmatite veins are tightly folded, with fold-axial traces parallel to the gneissic banding. The subvertical gneissic banding trends north to north-northwest, and is parallel to a tectonic foliation.

Within the granitoid gneiss, discrete northwesterly trending shear zones range in width from 3 to 20 cm, but are typically less than 5 cm wide. Some are marked by narrow zones of fine-grained, dark-grey ultramylonite that have sinistrally displaced an earlier northerly to north-northwesterly trending gneissic banding or foliation (Fig. 14). Other discrete shear zones are indicated by the sinistral deflection of an early fabric. Some discrete, semi-ductile shear zones are intruded by pegmatite or quartz veins. Locally observed asymmetric porphyroclasts of feldspar and quartz also indicate a sinistral shear sense. Later structures include a small-scale dilational jog that is defined by north-northeasterly trending, right-stepping fractures with a dextral strike-slip component.

The discrete, northwesterly trending shear zones are always superimposed on the northerly to north-northwesterly trending gneissic banding and foliation. This overprinting relationship suggests that the shear zones and the gneissosity represent different deformation events. The gneissic banding in granitoid rocks was probably developed during D<sub>2</sub> regional shortening, and then overprinted by D<sub>3</sub> strike-slip shear zones. This interpretation implies that the formation of granitoid gneiss in this area is not necessarily related to any large-scale, strike-slip shear zones.

### **Locality 4: Millars Monzogranite (MGA 710310E 6642800N)**

**by A. Riganti**

*Bouldery outcrops near a gnamma hole beside the track leading to the Mount Jackson Homestead, about 1 km northwest from the Bullfinch–Evanston road intersection.*

The Millars Monzogranite (Fig. 15) is a leucocratic, pale-pink, medium- to coarse-grained, locally porphyritic monzogranite with K-feldspar (microcline) and quartz

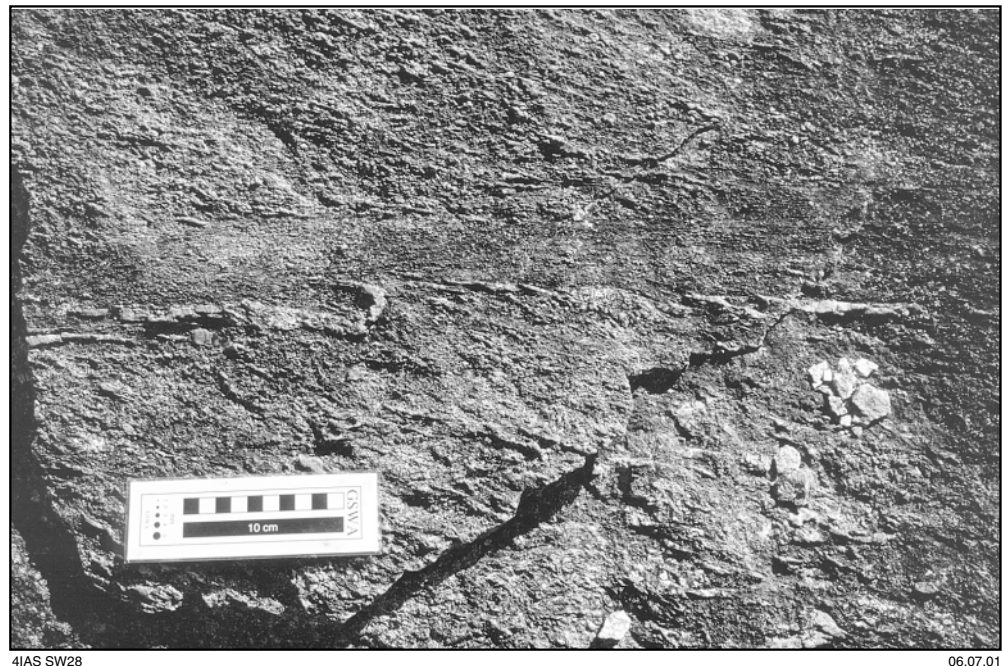


**Figure 14. A small-scale sinistral shear zone marked by a narrow zone of ultramylonite at Locality 3**

megacrysts, up to 2.5 and 1 cm long respectively, in a medium-grained granular host. Biotite, magnetite, apatite, and zircon are accessory phases.

To the northwest of the excursion locality, the Millars Monzogranite is in contact with strongly foliated granitic rocks deformed by the Koolyanobbing Shear Zone, whereas to the north and east it intrudes strongly foliated mafic rocks and crenulated tremolite schists of the lower greenstone succession. These relationships indicate that the Millars Monzogranite postdates deformation in the Koolyanobbing Shear Zone. Alteration of the zircons from the sample collected for SHRIMP dating at this locality resulted in an uninterpretable scatter of discordant analyses (Nelson, D. R., 2000, written comm.).

## **Locality 5: Granitoid gneiss at Yacke Yackine Dam (MGA 693630E 6644630N)**

**by A. Riganti**

*The Yacke Yackine locality is a large pavement west of the well at Yacke Yackine Dam, and east of the Bullfinch – Mount Jackson road. The dam is 1.2 km along a track that joins the Bullfinch – Mount Jackson road, about 15 km southwest of Mount Jackson Homestead.*

Heterogeneous granitoid gneiss and relatively undeformed monzogranite form extensive, undulating pavements near the Yacke Yackine Dam (Fig. 15). This granitoid gneiss is distinguished from other gneiss exposures in the region (see **Localities 2 and 3**) in that it has no obvious spatial relationship with any major regional shear zone.

At the excursion locality, sharp to diffuse gneissic banding trends northerly to north-northwesterly. Individual bands range in thickness from 1 to 30 cm (but typically less than 15 cm), and consist of alternating medium- to coarse-grained leucogranite and biotite-bearing granite, as well as granodiorite and minor tonalite (Fig. 16). A weak,

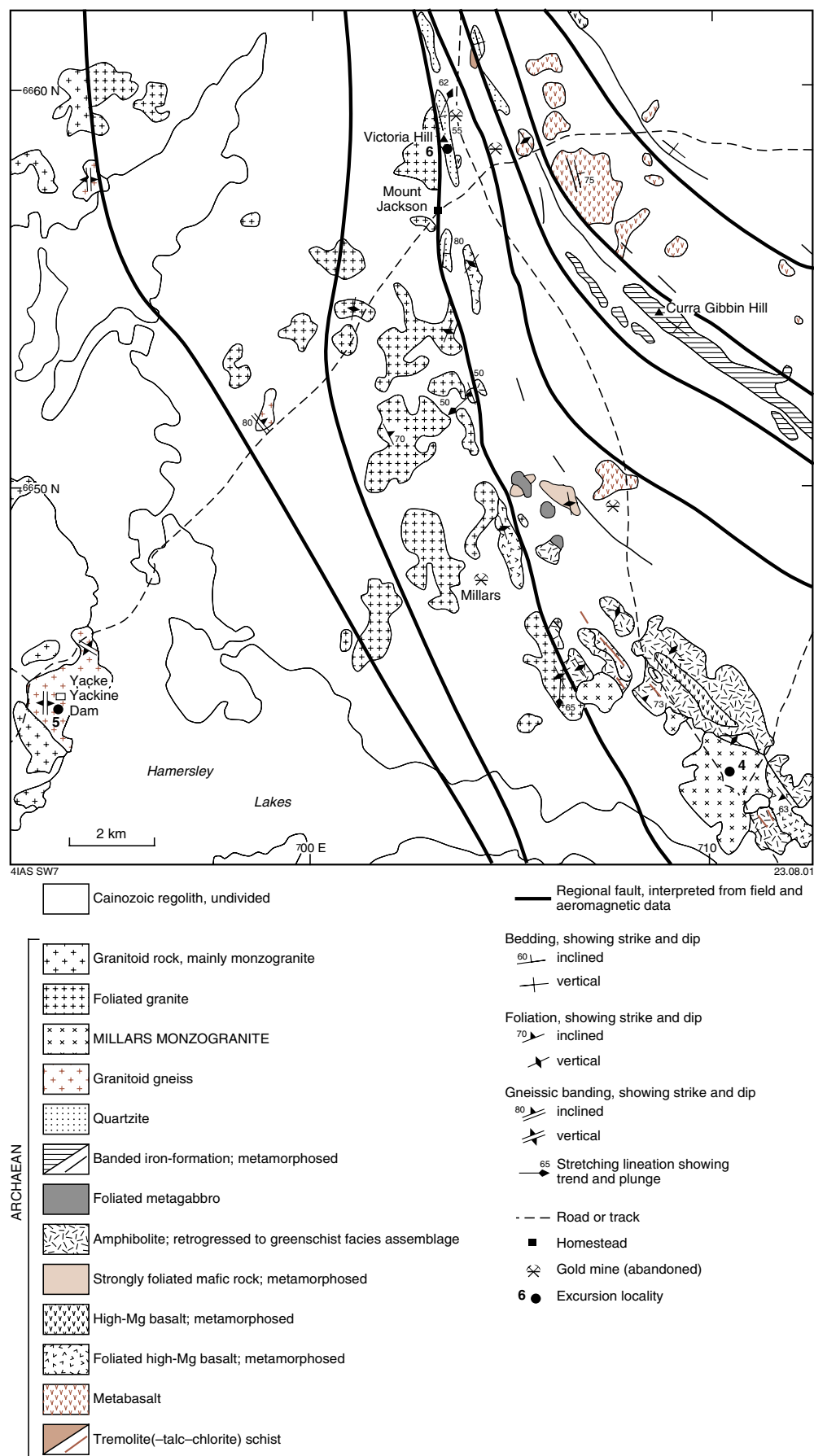


Figure 15. Outcrop geology of central–western JACKSON, showing Localities 4, 5, and 6



4IAS SW37

06.07.01

**Figure 16. Pavement of northerly trending granitoid gneiss west of the Yacke Yackine Dam**

steeply dipping to vertical foliation, approximately parallel to the gneissic banding, is defined by elongate grains of strained quartz and feldspar, and alignment of biotite grains. Asymmetric Z-shaped folds defined by the gneissic banding are locally preserved at the northern end of the pavement. The outcrop is extensively intruded by quartz, granite, and pegmatite veins. These veins typically cut across the foliation, and crosscutting relationships and a range of deformation intensity for the veins indicate that they represent several generations of intrusions.

A porphyritic biotite granodiorite phase from this locality yielded a SHRIMP U–Pb zircon igneous crystallization age of  $2711 \pm 4$  Ma (Nelson, 2001). The exposures at Yacke Yackine Dam form an isolated area of granitoid gneiss which is bound to the southwest by undeformed monzogranite. Similar but smaller gneiss outcrops are preserved 8 and 13 km to the northeast and north of the excursion locality, along the western margin of the Koolyanobbing Shear Zone. However, the Yacke Yackine Dam gneiss is located approximately 8 km away from this shear zone, and cannot be distinguished from the surrounding granite on aeromagnetic images. It may represent an enclave of gneiss, developed during the major regional  $D_2$ – $D_3$  deformation, that has been enveloped by subsequent granitoid intrusion. The adjacent, undeformed monzogranite is too weathered to sample for SHRIMP geochronology.

## **Locality 6: Quartzite at Victoria Hill (MGA 703370E 6658450N)**

**by A. Riganti**

*The locality lies about 1.5 km north of Mount Jackson Homestead, approximately 500 m west of the major track between the Mount Jackson mining centre and the Clampton mine.*

A well-bedded to massive quartzite unit outcrops discontinuously for about 6 km to the north and south of the abandoned Mount Jackson Homestead (Fig. 15). This is the ‘basal quartzite’ of Griffin (1990) and is generally regarded as the lowest exposed unit in the regional greenstone succession. The quartzite is in faulted contact with adjacent granitoid which is probably substantially younger than the quartzite. Griffin (1990) correlated this unit with similar but much thicker and more extensive quartzite units in the Illaara greenstone belt 70 km to the east-northeast (Wyche, 1999), but the current mapping has not yet established a sufficiently well constrained regional stratigraphy to support this correlation.

The best quartzite exposures are found just north of the Mount Jackson Homestead, and at Victoria Hill, where the quartzite forms a distinct, low ridge flanked by foliated, deeply weathered granitoid rocks to the west, and by poorly exposed, deformed mafic to ultramafic rocks to the east. The quartzite is typically white to pale grey, with common brown intercalations. Beds may be several centimetres thick, and dip moderately to steeply ( $55^\circ$ ) to the northeast. Some quartzite layers contain small concentrations of magnetite, and there are local quartz–muscovite schist and sillimanite-rich intercalations along the ridge. The formation of sillimanite is most likely related to contact metamorphism of more aluminous beds during the syn-tectonic intrusion of the adjacent granite. Chin and Smith (1983) described cross-bedding at this locality, defined by flaggy partings with consistent eastward younging. However, the rocks are strongly deformed and these flaggy partings are not unequivocally representative of cross-bedding. A fine-grained, laminated, strongly silicified, deformed unit that outcrops locally along the western side of the ridge may have been a shale band.

The quartzite typically has a well-developed granoblastic texture, with layers ranging in grain size from microgranular to coarse ( $>2$  mm). Scattered phyllosilicate flakes, including chlorite, are more common in the finer beds where they define a layer-parallel

schistosity. The quartzite unit has a well-defined bedding–cleavage intersection lineation, and a steep mineral lineation.

The quartzite at Victoria Hill lies adjacent to the eastern margin of the Koolyanobbing Shear Zone. The quartzite is strongly sheared and locally interleaved with tectonic slivers of amphibolite and granite. The contact with the foliated granite to the west is mainly covered by scree.

An attempt to date detrital zircons from the quartzite at Victoria Hill proved unsuccessful due to insufficient zircons being obtained from the sample. However, SHRIMP dating of detrital zircons from quartzites in the Illaara and Maynard Hills greenstone belts to the northeast found complex populations of grains, mainly older than 3.3 Ga (Froude et al., 1983; Nelson, 2000), indicating the presence of old sialic crust, on which the greenstones may have been deposited, in this region. No age data is available for the granitoid rocks adjacent to Victoria Hill, and the oldest SHRIMP U–Pb zircon ages obtained for granitoid rocks in the region are the 2.73 Ga ages of the Pigeon Rocks and Butcher Bird Monzogranites (see **Localities 11** and **13**).

## **Locality 7: Marda Complex conglomerate at Allens Find (MGA 716820E 6658670N)**

**by A. Riganti**

*The locality is at Allens Find, on the southern side of the road between Mount Jackson Homestead and the Bullfinch–Evanston road, 2.3 km west of the intersection of these roads.*

At Locality 7 (Fig. 17), a prominent unit of coarse clastic metasedimentary rocks is dominated by poorly outcropping conglomerate with minor sandstone and siltstone. Hallberg et al. (1976) inferred that these rocks were intruded by the 2.73 Ga Marda Complex. However, the presence of metamorphosed rhyolitic lavas and deeply weathered, possibly tuffaceous, fine-grained intercalations within the unit suggest that it should be regarded as part of the Marda Complex (Riganti and Chen, 2000).

At the excursion locality, a pale-grey, quartz- and feldspar-phyric rhyolite is poorly exposed around the old mining shafts, and immediately to the south of the road. Farther south, a deeply weathered conglomerate consists of poorly sorted, typically clast supported beds, with abundant tightly packed, angular to subrounded clasts of white and banded cherts, minor jaspilitic BIF, and subordinate quartz-vein fragments. The clasts range in size from a few millimetres up to 15 cm (typically only a few centimetres), but can be up to 30 cm. Some BIF clasts contain folds indicating deformation prior to erosion and redeposition as part of this unit. A ferruginous cement is typical, locally increasing in proportion to define some matrix-supported intervals. Intercalations of ferruginized, in places laminated, siltstones, as well as lenses of pebbly sandstone and weakly laminated sandstone, are relatively common, their overall distribution representing a fining of this sedimentary package towards the north. To the north and east of the excursion locality, conglomerate beds are less ferruginous, and contain highly polished, rounded to subangular, dominantly cherty clasts (Fig. 18). Outcrop is poor, and conglomerate exposures are commonly marked by low-lying mounds of loose chert pebbles.

The predominantly metasedimentary unit near Allens Find is delimited to the south by jaspilitic BIF of the lower greenstone succession. To the north, it dips steeply under the felsic volcanic rocks of the Marda Complex. Although contacts are not exposed in this area, the presence of rhyolitic intercalations within this metasedimentary unit, the

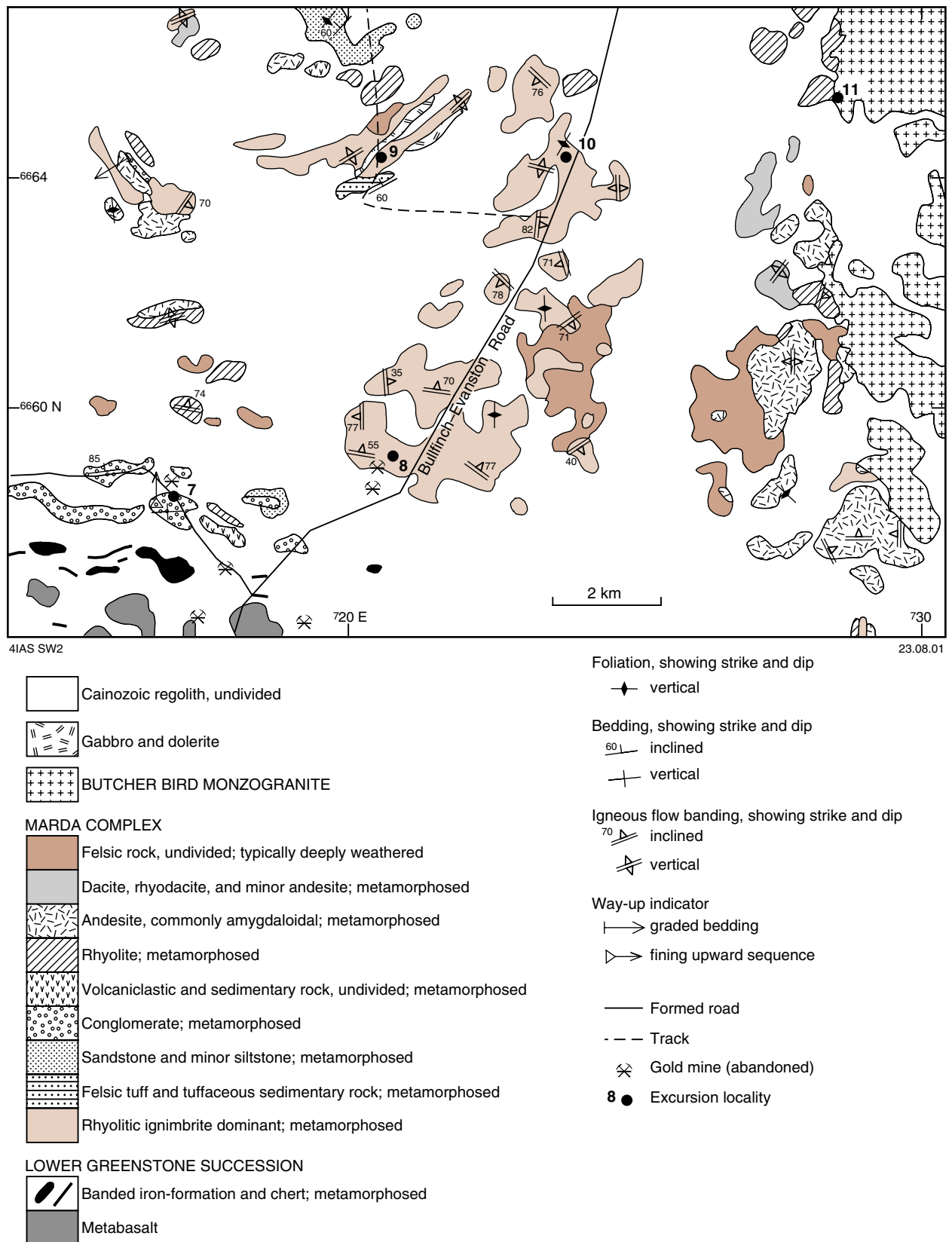
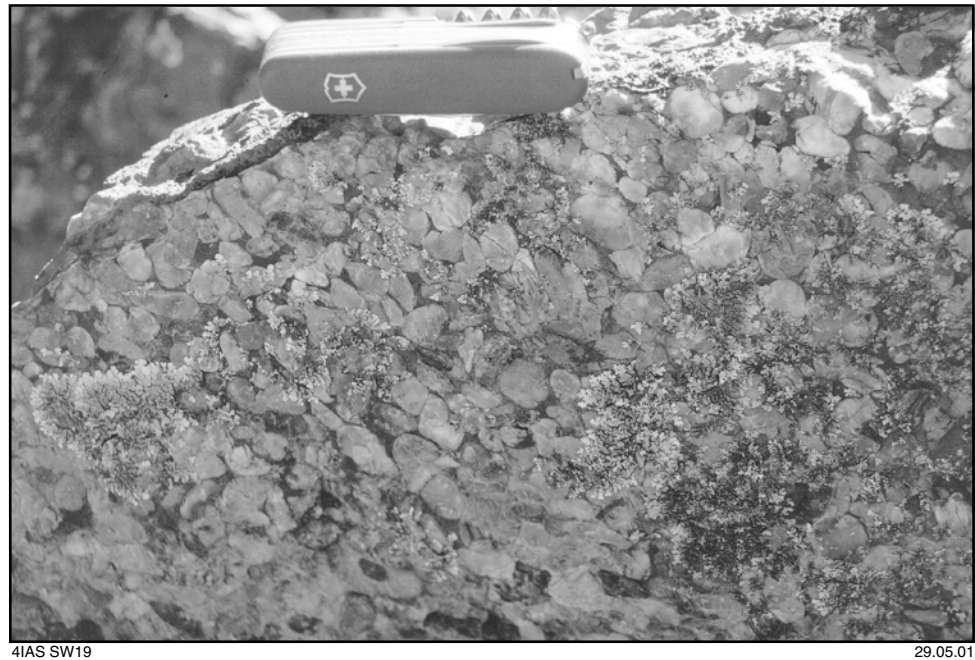


Figure 17. Geological map of the western part of the Marda Complex, showing Localities 7–11



**Figure 18. Clast-supported conglomerate bed near the base of the Marda Complex, 0.5 km west-northwest of Allens Find. The highly polished pebbles are predominantly white and grey chert. Pocket knife is 11 cm long**

clast lithology of the conglomerate, the broad northward-fining of the succession, and its relationships with adjacent rock types all suggest that these metasedimentary rocks were mainly sourced from, and deposited unconformably over, the lower greenstone succession at the onset of the Marda Complex volcanic activity. Metasedimentary rocks similar in character to, and occupying the same stratigraphic position as, those near Allens Find are patchily exposed farther to the east-southeast, and in the northern part of the Marda Complex.

A total of approximately 56 kg of gold was produced from the Allens Find mining operation in the first half of the twentieth century (Chin and Smith, 1983). The mineralization is hosted by a series of schistosity-parallel, north-northwesterly trending ( $350^\circ$ ), shallowly easterly dipping quartz veins that crosscut steeply dipping,  $300^\circ$ -trending, porphyritic rhyolite. Grades ranged from 0.1 to 15.8 g/t Au in the main and parallel reefs, with 1–8 g/t Au reported from quartz stockwork in highly kaolinized tuff zones interbedded with the porphyritic rhyolite (Kimber, 1987). The mineralization style at Allens Find is unusual in that auriferous veins are hosted by felsic metavolcanic rocks of the c. 2733 Ma Marda Complex, whereas most of the gold in the region was mined from discordant quartz-vein systems hosted by BIF and mafic volcanic rocks of the lower greenstone succession. This suggests that different competency contrasts controlled gold precipitation in favourable sites, and that at least some of the gold mineralization postdates the deposition of the upper greenstone succession.

## Locality 8: Marda Complex fragmental ignimbrite west of Marda airstrip (MGA 720730E 6659080N)

by A. Riganti

*This locality is an area of low-lying bouldery outcrop on the northern side of a short track that runs west from the Bullfinch–Evanston road, near the Marda airstrip. It is about 400 m west of the main road.*

In this area (Fig. 17), the Marda Complex is dominated by rhyolitic ignimbrite sheets with subordinate rhyolitic lava flows and tuffaceous horizons that represent the volumetrically more conspicuous exposed volcanic phase of the complex (Hallberg et al., 1976).

At the excursion locality, the dominant rock type is a dark-grey, fragmental ignimbrite with a weakly developed igneous flow foliation, which includes crystal and lithic lapilli tuffs, as well as minor ash tuff and rare agglomerate. The ignimbrite is characterized by abundant angular to subrounded, mainly fine grained, lithic fragments, ranging from less than 1 cm to 10 cm, but typically only a few centimetres across (Fig. 19). These lapilli are typically set in a crystal-rich, fine-grained to aphanitic, largely quartzofeldspathic groundmass matrix, with abundant plagioclase and subordinate quartz phenocrysts up to 3 mm long. The plagioclase and quartz crystals are commonly resorbed, and rare mafic grains, now replaced by chlorite or actinolite, are either prismatic or diamond-shaped, and may originally have been pyroxene or hornblende phenocrysts.

Banding wraps around the lithic fragments locally, and is best observed on weathered surfaces where it is defined by dark-grey layers, a few millimetres thick, which alternate with less resistant, darker and thinner bands. Microscopically, the bands are defined by different proportions of quartz, feldspar, chlorite, and iron oxides. The highly variable



Figure 19. Rhyolitic ignimbrite near Marda, with centimetre-size fragments and abundant plagioclase phenocrysts. Pocket knife is 11 cm long

attitude of flow foliation observed in this area may be a primary feature, the result of later folding, or a combination of both. Some lapilli also display internal flow-banding textures, indicating fragmentation and incorporation from previously erupted volcanic units. Overall, the volcanic textures of the fragmental ignimbrite at this locality are consistent with subaerial deposition.

The lithic fragments are compositionally varied (Fig. 20a–d). Porphyritic, flow-banded, or fine-grained (devitrified) rhyolitic lapilli are dominant. Andesite fragments are characterized by feldspar microlites, in some instances flow-oriented, surrounded by a dark-brown, cloudy matrix; some fragments have a poorly preserved vesicular texture. There are also dacitic and cherty fragments, as well as dark vitric shards. Silicified areas with abundant poikilitic quartz grains within the fragmental ignimbrite may represent fiamme (collapsed pumice). Carbonate, sericite, and chlorite alteration range from minor to locally extensive. The overall geochemical composition of the fragmental ignimbrite is rhyolitic to rhyodacitic (Appendix 1).

A geochronology sample from this excursion locality yielded a SHRIMP U–Pb zircon igneous crystallization age of  $2732 \pm 3$  Ma (Nelson, 2001), confirming the previously determined conventional U–Pb zircon age of  $2735 \pm 2$  Ma (Pidgeon and Wilde, 1990).

## **Locality 9: Marda Complex rheoignimbrite (MGA 720500E 6664440N)**

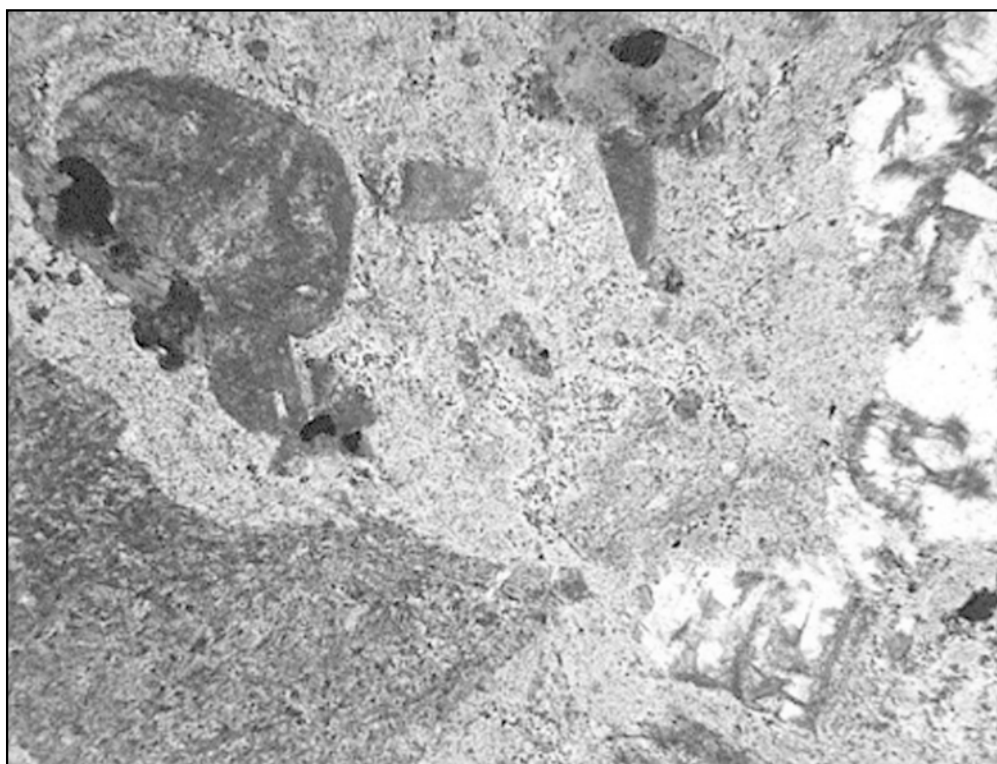
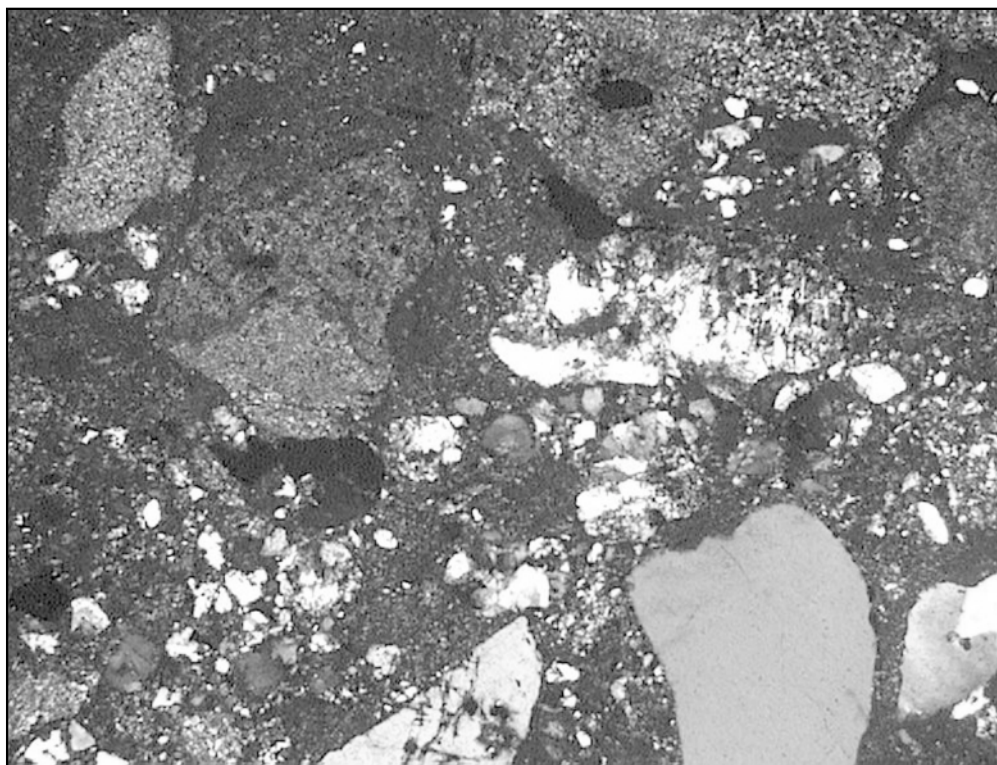
**by A. Riganti**

*This locality (Fig. 17) is about 3 km west of the Bullfinch–Evanston road, and about 1.2 km north along the track to Pigeon Rocks from the Diemals – Mount Jackson boundary fence. The fenceline crosses the Bullfinch–Evanston road about 5 km north of the Marda airstrip.*

The ignimbrite is typically a medium- to dark-grey rhyolite, characterized by a prominent igneous flow foliation that is commonly enhanced by weathering. Consistently subvertical banding on a millimetre scale defines a eutaxitic texture with alternating black to dark-grey, glassy layers and paler, greyish bands (Fig. 21a). Individual bands are typically continuous over a distance of up to a few centimetres only, and commonly tail off at the extremities. They probably represent fiamme that have stretched as a result of secondary mass flowage of the rock while it was still in a plastic state. The foliation wraps around sparse to locally abundant, idiomorphic and, in places, broken plagioclase phenocrysts which are up to 3 mm in length, and are typically parallel to, or lie at a low angle to, the flow foliation. In addition to plagioclase crystals, subordinate, fine-grained lithic fragments, mainly of rhyolitic composition, are also present. Silicification is common in the form of quartz-filled cavities that are elongate parallel to the flow foliation, and is likely to have been caused by percolation of aqueous and gaseous solutions.

In thin section, the darker bands are characterized by a central portion with granular, commonly sutured quartz, which grades into a fine-grained groundmass with devitrification textures (Fig. 21b). The paler bands have a perlitic texture, in which quartzofeldspathic spherules are surrounded by brown, cloudy, clay-rich patches. Idiomorphic to subidiomorphic opaques are ubiquitous accessory phases. Plagioclase phenocrysts have been extensively altered to sericite or saussurite.

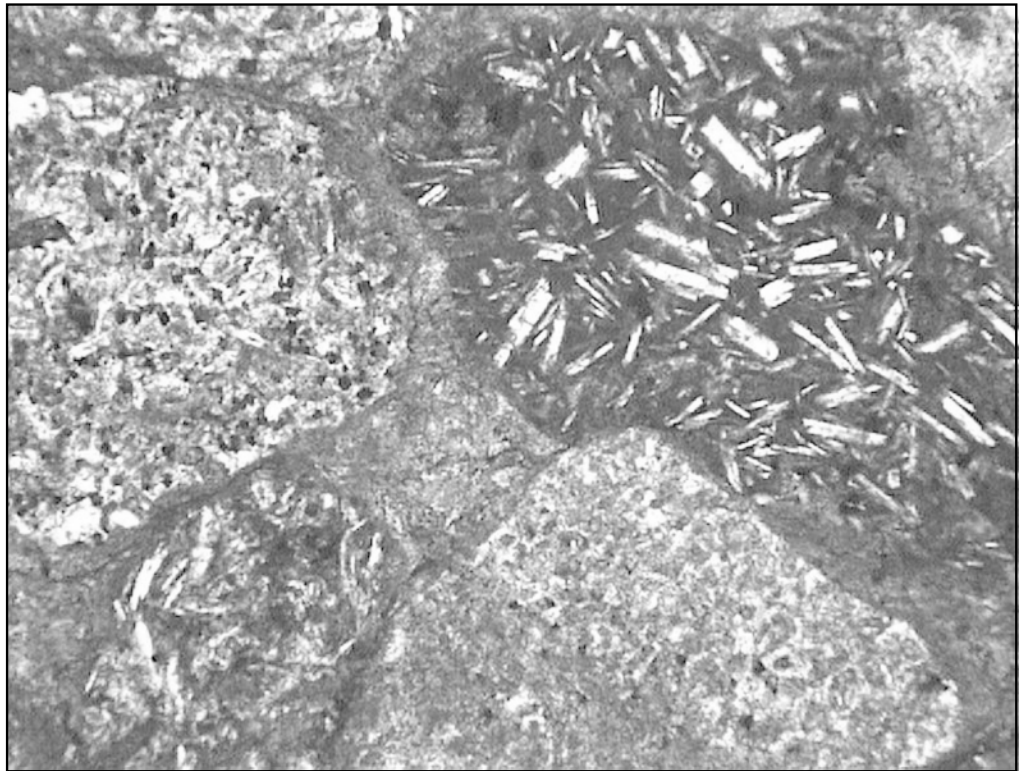
The rheoignimbrite from this locality has a SHRIMP U–Pb zircon age of  $2734 \pm 3$  Ma (Nelson, 2001).



4IAS SW29

06.07.01

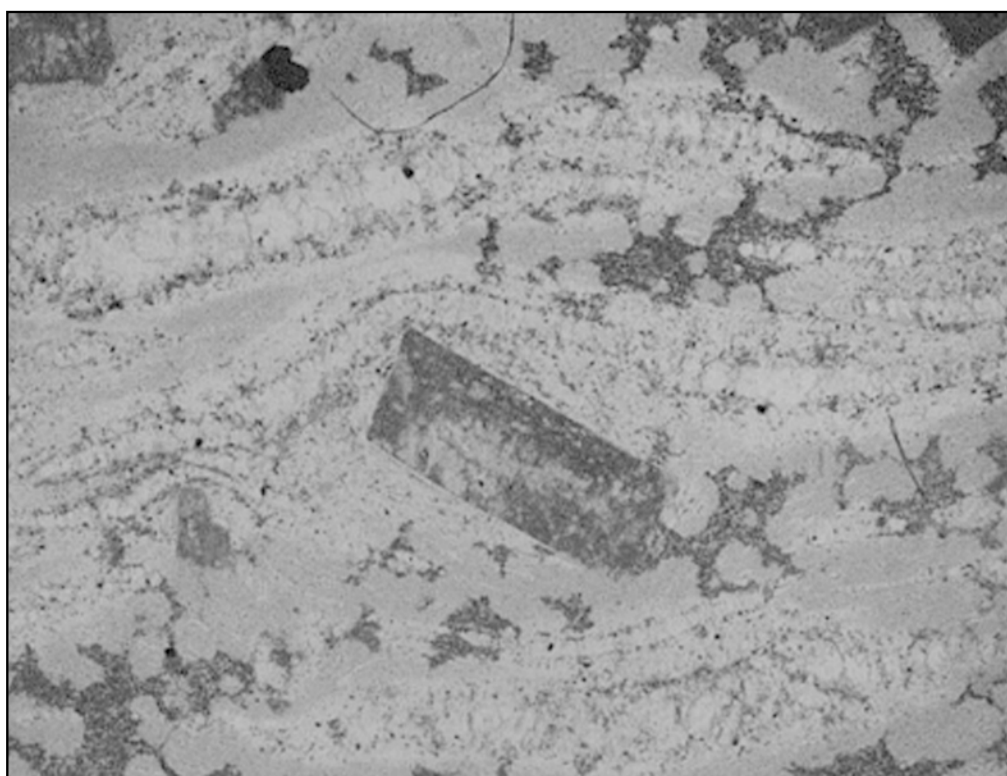
**Figure 20.** Photomicrographs of fragmental rhyolitic ignimbrite showing: a) rhyolitic and quartz fragments and possible chert clasts; sample GSWA 159337, crossed nicols, field of view is 4 mm; b) rhyolitic fragments and altered plagioclase and mafic (centre top) phenocrysts in a devitrified quartz–feldspar matrix; sample GSWA 159335, plane polarized light, field of view is 2.5 mm



4IAS SW30

06.07.01

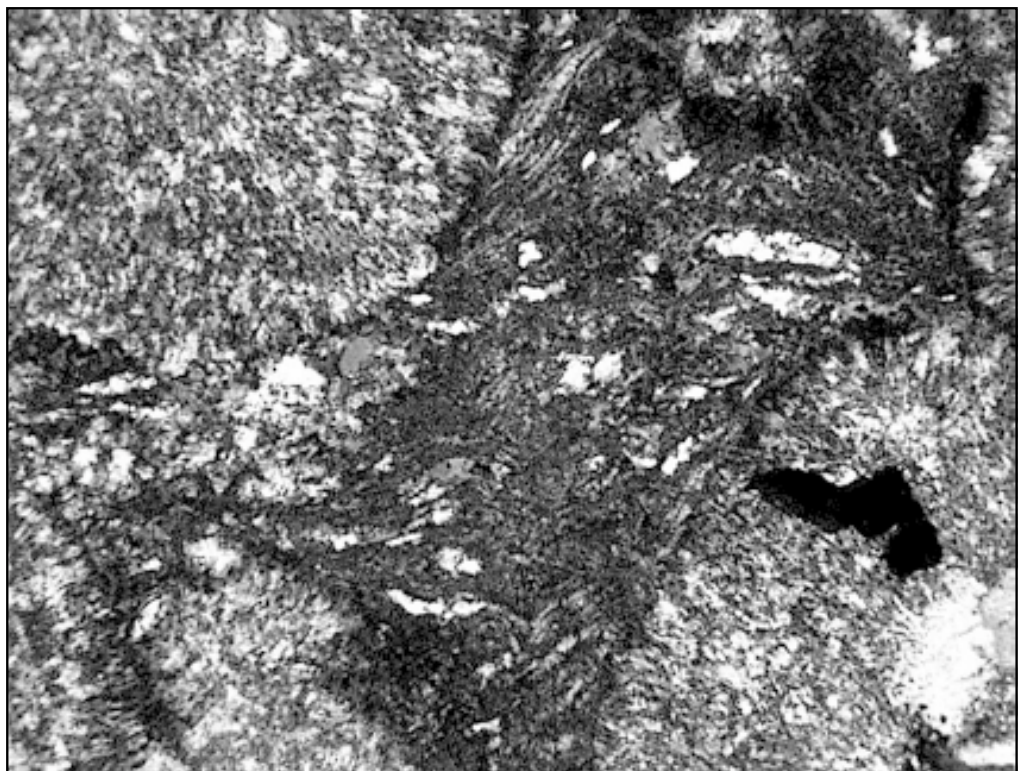
**Figure 20.** Photomicrographs of fragmental rhyolitic ignimbrite showing: c) andesitic fragments displaying a plagioclase microlithic texture; sample GSWA 159363, plane polarized light, field of view is 2.5 mm; d) plagioclase and resorbed quartz phenocrysts in a matrix of welded glass shards; sample GSWA 159360, crossed nicols, field of view is 4 mm



4IAS SW31

06.07.01

**Figure 21.** Flow foliation in rhyolitic ignimbrite: (a) alternating dark and pale grey bands with sparse white plagioclase phenocrysts; (b) photomicrograph showing banding wrapping around altered plagioclase phenocrysts; paler bands consist mainly of recrystallized granular quartz, and the darker bands are quartzofeldspathic. Sample GSWA 164840, plane polarized light; field of view is 4 mm



4IAS SW32

06.07.01

**Figure 22. Devitrification textures in spherulitic rhyolite: (a) flow foliation overprinted by spherulitic textures; sample GSWA 159345, plane polarized light, field of view is 4 mm; (b) crossed nicols view displaying radial textures within the spherulites**

The ignimbrite has been intruded by northeast-trending differentiated mafic sills which range from finely granular dolerite at the margins to medium-grained gabbro and diorite in the central portions. The sills are characterized by a granular assemblage of relict augite, largely chloritized or replaced by actinolitic amphibole, and smaller, extensively saussuritized plagioclase grains, with minor interstitial quartz. The mafic sills are best exposed to the southeast of the excursion locality, but dolerite debris can be found along the track just to the north of the geochronology sample site. The mafic sills have not been dated, but Hallberg et al. (1976) attributed doleritic to dioritic dykes from this area to the andesitic volcanic phase of the Marda Complex.

To the south of the excursion locality, immediately north of the Diemals – Mount Jackson boundary fence, a fine-grained, pale greenish-grey to black and dark-grey lithotype contains parallel laminations and possible graded bedding. The presence of feldspar microlites suggests that this might be an ash-fall deposit. Although lack of continuous outcrop prevents establishment of a younging direction, layering is concordant with the attitude of flow foliation in the adjacent ignimbrite.

## **Locality 10: Marda Complex volcanic rocks — igneous and tectonic fabrics (MGA 723820E 6664540N)**

**by A. Riganti**

*This locality lies west of the Bullfinch–Evanston road, about 1.2 km north of the Diemals – Mount Jackson boundary fence.*

At the start of the traverse, immediately to the west of the Bullfinch–Evanston road (Fig. 17), medium- to dark-grey rhyolitic ignimbrite is characterized by millimetre- to centimetre-scale flow foliation and variously abundant feldspar- and quartz-phenocrysts. Highly contorted foliation in many of the boulders at this locality is interpreted as a flow foliation, a syndepositional feature of these highly viscous flows. In places, the flow foliation wraps around large (up to 20 cm) clasts of felsic porphyry. Tectonic folding at this locality is evident in the form of steeply northeasterly plunging upright folds with wavelengths of approximately 50 cm. Axial-planar cleavage is locally preserved.

To the west, a northeasterly trending unit of rhyolitic composition is distinguished by a prominent spherulitic texture that gives the rock a knobbly appearance on weathered surfaces. The texture is defined by tightly packed, rounded spherulites set in a medium-grey, fine-grained, locally banded, groundmass. The spherulites form discrete individuals or may coalesce into larger masses, and range in shape from spherical to ellipsoidal and irregular, with no preferential orientation in the most elongate types. They range in size (diameter or length of apparent longest axis) from a few millimetres up to 2 cm, but spherulites up to 10 cm can be seen in outcrop about 1.5 km northwest of the excursion locality. Sparse, mostly euhedral, plagioclase, and minor K-feldspar and quartz phenocrysts, up to 3 mm, are both in the groundmass between the spherulites, and irregularly distributed within the spherulites. Locally preserved banding wraps around the spherulites and the phenocrysts in places. Many spherulites are characterized by dark-green, fine-grained, chlorite-rich or, less commonly, hollow centres of various sizes. The local presence of secondary quartz crystals in these voids suggests that the chlorite-rich portions may have been vesicles that were later infilled by low-temperature mineral phases.

The spherulites represent devitrified glass and are mainly quartzofeldspathic and fine grained with a distinctive radial texture that overprints the flow foliation (Fig. 22a,b). Poorly developed, irregular concentric zoning is locally preserved, and

consists of alternating grey, pale-green, and cream orbicules. No systematic variation in the orbicules' distribution has been noted, and petrographic examination indicates the zoning to be defined by layers of granular quartz, considerably coarser than the material that constitutes the rest of these bodies, and subordinate chlorite patches. The spherulites have a thin rind of dark-brown material.

The spherulitic rhyolite unit is about 30 m thick, and can be followed laterally for approximately 200 m. Contacts with the adjacent units are poorly exposed, but the presence of banding in the spherulitic rhyolite, similar to that observed in the ignimbrite to the east, might indicate a gradual transition between these two lithotypes. To the west, the spherulitic rhyolite is in sharp contact with a pale- to medium-grey, fine-grained, sparsely porphyritic rhyolite flow. This unit becomes more deformed farther to the west, grading into strongly deformed, weathered, felsic schist. A vertical tectonic foliation in the schist trends northeasterly, the same direction as the fold axes in the banded ignimbrites at the start of the traverse.

## **Locality 11: Butcher Bird Monzogranite (MGA 728500E 6665480N)**

**by A. Riganti**

*The excursion locality (Fig. 17) is on the western margin of the Butcher Bird Monzogranite, about 4.5 km to the east of the Bullfinch–Evanston road, along a poorly defined track that leaves the road about 2.2 km north of the Diemals – Mount Jackson boundary fence.*

The Butcher Bird Monzogranite is a pink-grey to red, massive, medium- to coarse-grained, plagioclase-phyric granophyre that intruded the eastern part of the c. 2733 Ma Marda Complex, and is interpreted to represent a high-level intrusion of the same magma that produced the more acid component of the Marda extrusive rocks (Hallberg et al., 1976; Riganti et al., 2000).

The outline of the Butcher Bird intrusion is evident on aeromagnetic images. The granite has a sharp western contact that appears to crosscut Marda Complex lithologies at different levels. Although the eastern contact is not exposed, aeromagnetic images suggest that here the Butcher Bird Monzogranite intruded mafic rocks of the lower greenstone succession. The aeromagnetic image further suggests that the Butcher Bird Monzogranite was intruded by the poorly outcropping Chatarie Well Granite in the north (Fig. 7; Riganti and Chen, 2000).

At the excursion locality, and in the surrounding area, the contact of the Butcher Bird Monzogranite is marked by the presence of numerous granitic veins and apophyses within flow banded rhyolites and ignimbrites of the Marda Complex, and by the finer grain size of the granophyre adjacent to these extrusive lithotypes. Petrographically, the Butcher Bird Monzogranite is distinguished by prominent plagioclase megacrysts up to 6 mm long that commonly contain incipient sericitization and clouding. Quartz phenocrysts, up to 2 mm long, are subordinate, and some preserve a resorbed bipyramidal or pseudo-hexagonal habit. Granophyric intergrowths radiate from the plagioclase and quartz grains (Fig. 23), and quartz phenocrysts are in optical continuity with the quartz in the granophyre. Interstitial spaces are filled by a finely granular assemblage of plagioclase and quartz. Accessory minerals include altered mafic grains (possibly pyroxene), magnetite, opaque oxides, apatite, and zircon; biotite, actinolitic amphibole, epidote, chlorite, and traces of carbonate are late magmatic phases, some of which partly fill sparse miarolitic cavities a few millimetres across. The ubiquitous distribution of granophyric intergrowths and the presence of resorbed, subhedral quartz

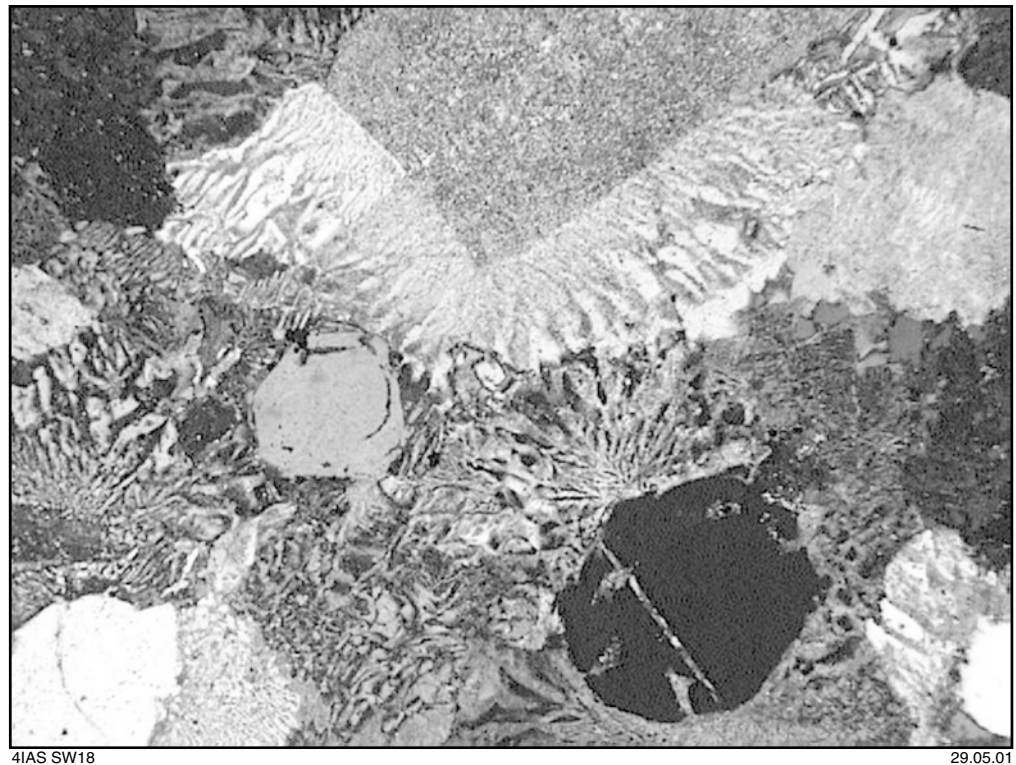


**Figure 23.** Textural characteristics of the Butcher Bird Monzogranite: granophyric intergrowths radiate from sericitized plagioclase megacrysts; euhedral quartz crystals show incipient resorption and are in optical continuity with the quartz in the granophyre. Sample GSWA 164833, crossed nicols; field of view is 2.5 mm

phenocrysts suggest that the Butcher Bird Monzogranite was emplaced at a high crustal level.

A granite sample from a locality about 11 km to the south-southeast (MGA 730250E 6654610N) yielded a SHRIMP U–Pb zircon age of  $2730 \pm 4$  Ma (Nelson, 2001), which is within error (95% confidence level) of the age of extrusive rocks of the Marda Complex ( $2732 \pm 3$  and  $2734 \pm 3$  Ma; cf. **Localities 8 and 9**). This result lends support to the interpretation (based on chemical similarity; Appendix 1) that the Butcher Bird Monzogranite represents a high-level intrusion of the magma that was the source of the Marda Complex rhyolitic rocks (Hallberg et al., 1976; Riganti et al., 2000).

## **Locality 12: Red Legs gold prospect (MGA 730210E 6687400N)**

**by S. Wyche**

*The locality is on the eastern side of the Die Hardy Range, and is marked by an extensive area of mineral-exploration grids and drillholes. It lies on the western side of a track that joins the Bullfinch–Evanston road 3 km to the southeast, about 2 km northeast of the gap in the range at Die Hardy.*

The Red Legs prospect (Fig. 24) is one of a number of gold prospects that were identified by Savage Resources Ltd (taken over by Pasminco Ltd in 1999) during an extensive soil-sampling program that was carried out during the late 1990s. Gold

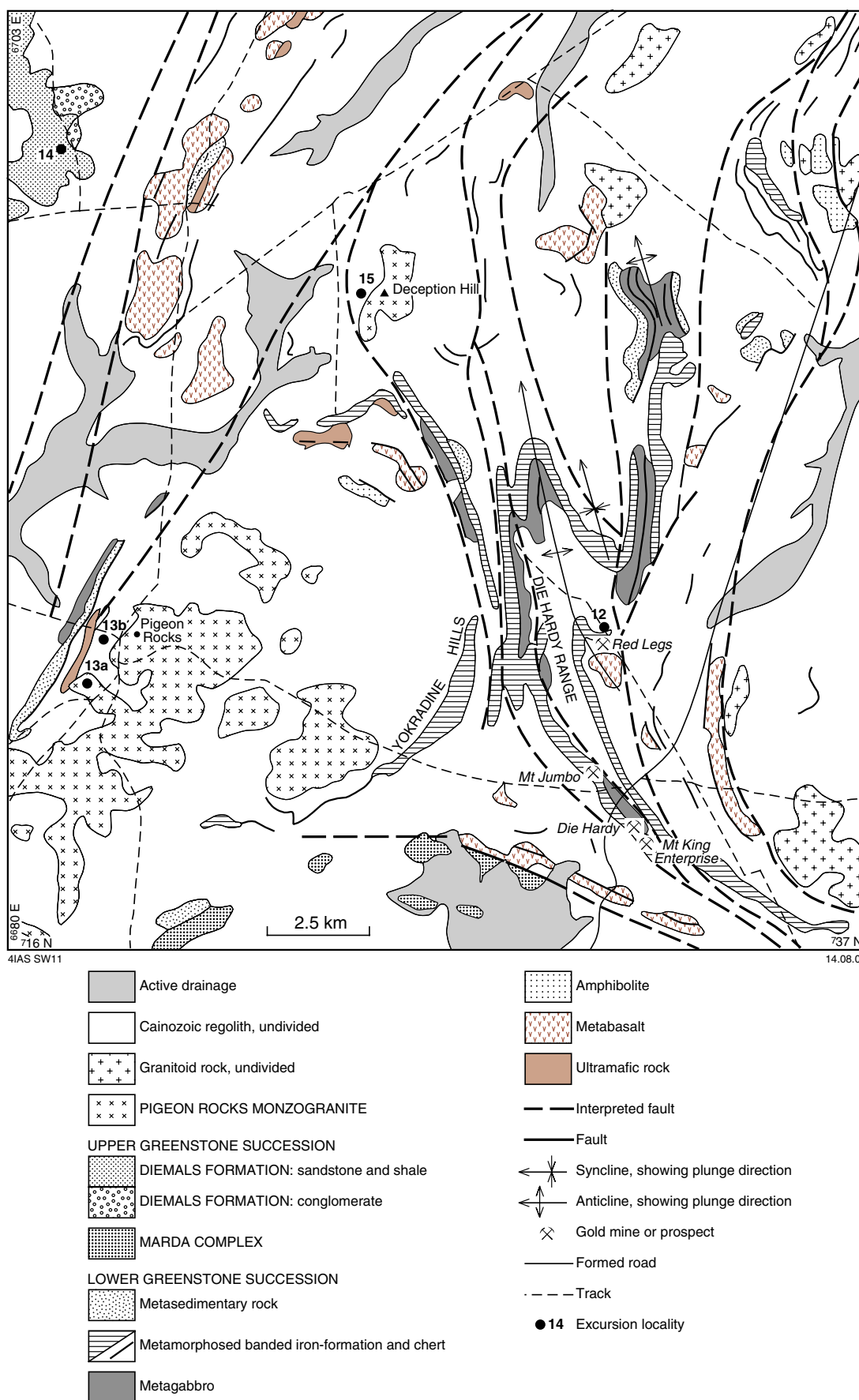


Figure 24. Die Hardy Range and Pigeon Rocks area, showing Localities 12-15

mineralization is probably similar in style to that at Evanston to the northeast (see **Locality 16**) and Die Hardy, about 4 km to the south, where mineralization is epigenetic, structurally controlled, and is hosted by quartz veins and shear zones along contacts between BIF and mafic and ultramafic rocks.

At Red Legs, RAB (rotary air-blast) and RC (reverse circulation) drilling have identified gold mineralization up to 15 m thick, over a strike length of about 300 m, to a maximum depth of 100 m. Mineralization is open along strike in both directions, and downdip. Drilling included one intersection of 7.2 g/t Au in sulfide mineralization over 7 m, suggesting that there is potential for gold mineralization below the weathering profile (Register of Australian Mining, 2000–2001).

Deformation in the Die Hardy Range area is characterized by intense folding and reverse faulting. North-trending macroscopic folds outlined by units of BIF have wavelengths of 0.5 – 2.5 km. These upright folds plunge gently (typically <25°) to either the north or south. Numerous small-scale folds and crenulation hinge lineations are parallel to the hinges of macroscopic folds. Folds are typically west verging, and east-dipping reverse faults are parallel to the axial traces of the folds, and truncate BIF units. A locally preserved, downdip lineation is defined by preferred alignment of hematite on bedding and fault surfaces. In amphibolite and foliated granitoid rocks adjacent to the eastern granite–greenstone contact, a steeply dipping foliation locally contains a steeply plunging mineral lineation.

The Red Legs prospect lies near the hinge of an asymmetric, west-verging, D<sub>2</sub>–D<sub>3</sub> anticline on the eastern side of the Die Hardy Range (Fig. 24), at the base of the major BIF-rich association that forms the middle part of the lower greenstone succession (see **Lower greenstone succession — Die Hardy Range area**). The anticline has a shallow (10–25°) northerly plunge, indicated by numerous minor folds, crenulations, and mineral lineations.

Folding was probably initiated during D<sub>2</sub> east–west compression, and tightened up and faulted during D<sub>3</sub> as younger granitoid bodies to the east impinged upon the greenstone succession during continued east–west compression to form the Evanston – Mount Dimer arcuate structure (Chen et al., 2001).

Monzogranite at Olby Rock (Appendix 1), 7 km to the southeast, has a SHRIMP U–Pb zircon crystallization age of 2697 ± 8 Ma, and contains a substantial population of xenocrystic zircons at 2738 ± 16 Ma (Nelson, 1999). These xenocrystic zircons are within error (95% confidence level) of the age of the Marda Complex and associated granitoid rocks (see **Localities 8, 9, 11, and 13**).

## **Locality 13: Pigeon Rocks Monzogranite (MGA 718600E 6687600N)**

**by S. Wyche**

*An unnamed well on the western side of Pigeon Rocks.*

The Pigeon Rocks Monzogranite is a variously deformed and recrystallized, even-grained biotite monzogranite that intrudes the lower greenstone succession, and outcrops over a lobate, northeasterly trending area of about 14 by 8 km maximum dimension (Fig. 24). It lies west of the Die Hardy Range and forms a distinct low-response area on aeromagnetic images as it is surrounded on 75% of its circumference by BIF. The monzogranite is heterogeneously deformed, with the strongest deformation closest to granite–greenstone contacts. Foliation is defined by the alignment of biotite grains and, where visible, typically parallel to granite–greenstone contacts. The dip of the foliation

appears to be mainly steep, but can be difficult to determine due to the lack of relief in many outcrops. The mode of emplacement of the Pigeon Rocks Monzogranite is not certain. However, the lobate shape of the intrusion, the contact-parallel foliation, the fact that greenstones dip away from the intrusion in every direction, and the local presence of downdip stretching lineations and slickenlines in adjacent greenstones suggest emplacement as a diapir or laccolith.

The Pigeon Rocks Monzogranite probably acted as a bulwark during east–west compression, causing tightening up of folds in the Die Hardy Range, reverse faulting, and wrapping of folds around the Pigeon Rocks pluton as the younger granitoid rocks impinged upon the lower greenstone succession.

The Pigeon Rocks Monzogranite has a SHRIMP U–Pb zircon age of  $2729 \pm 4$  Ma (Nelson, 1999). The sample site lies about 200 m south of the unnamed well at Locality 13. A chemical analysis of monzogranite from this locality is presented in Appendix 1. The age is within error (95% confidence level) of the ages determined for the Marda Complex to the south (see **Localities 8 and 9**), and the associated Butcher Bird Monzogranite (see **Locality 11**). Although similar in age and setting, the Pigeon Rocks Monzogranite is texturally and petrographically distinct from the Butcher Bird Monzogranite (e.g. the Butcher Bird Monzogranite has a characteristic granophyric texture). The first locality (**Locality 13a**; MGA 718200E 6686200N) is southwest of the main granitoid mass, on the track that leads southeast to the Mount Jackson Homestead. The granite–greenstone contact lies approximately 700 m to the northwest. A traverse across the fairly continuous suboutcrop of monzogranite between here and the contact shows that the monzogranite in this area is weakly foliated, with a probably steep dipping foliation that is defined by alignment of biotite and trends approximately parallel to the contact. Deformation intensity increases towards the contact. There is abundant quartz and pegmatite veining near the contact. Small-scale brittle faults, that cut the granitoid with apparent dextral offset, have a range of east- to northeast-trending orientations and overprint the foliation.

Farther north, beside a west-northwesterly trending track that extends from just north of an unnamed well (**Locality 13b**; MGA 718400E 6688000N), thin ridges of BIF, in a succession that includes strongly deformed tholeiitic and high-Mg basalt, preserve a downdip stretching lineation. The lineation is marked by fine hematite that has recrystallized on bedding surfaces, parallel to the direction of movement. This lineation has been observed at a number of localities on the northern and western sides of the pluton, and supports diapiric emplacement of the body.

## **Locality 14: Diemals Formation conglomerate (MGA 717500E 6699860E)**

**by A. Riganti**

*This locality is reached via a track that heads west from the main track between Pigeon Rocks and Diemals Homestead, about 10 km north of Pigeon Rocks, and 2.8 km north of the turnoff onto the Pigeon Rocks Road (i.e. the road to the northeast that joins the Bullfinch–Evanston road). Travel due west along this track for about 2.7 km, turn north onto another track, and drive a farther 1.8 km to reach the locality*

This locality (Fig. 24) is one of a number of places where lenses of metamorphosed polymictic conglomerate with subordinate sandstone are intercalated with silty argillite and pebbly sandstone in the lower part of the Diemals Formation.

At the locality, a poorly sorted, clast-supported conglomerate with a ferruginous and quartz-rich, sandy to silty matrix contains rounded to subangular clasts that range

in size from 1 to 40 cm. Clasts of reworked sandstone and argillite are dominant, and there are relatively abundant clasts of banded chert, BIF, and weathered mafic rocks. Other clast types include quartz, granitoid and felsic porphyry, and amygdaloidal rocks of mafic to intermediate composition. In general, the composition of clasts in the conglomerate is representative of the range of rock types exposed to the east. Some of the reworked sandstone clasts are composite, and contain lithic fragments of chert and sandstone.

The conglomerate is deformed, with sandstone and weathered mafic clasts typically the most flattened (Fig. 25a). Some chert and BIF boulders contain tight to isoclinal folds, indicating that the greenstones from which these clasts are derived were deformed prior to deposition of the Diemals Formation (Fig. 25b). To the west, a gradational contact with pelites is indicated by a progressive decrease in thickness of the conglomeratic lenses, a reduction in size of clasts within the beds, and the presence of increasingly thick, finer grained intercalations. Sedimentary structures in the latter are poorly developed, but include grading, parallel laminations, scour troughs, and local cross-bedding. Regional trends suggest overall younging to the west, but local younging to the east is observed on the limbs of mesoscale folds. One of these structures is visible at the top of the breakaway, where a thicker unit of silty argillite is folded into a mesoscale synform with a moderate to steep south-southwesterly plunge. This fold is one of the parasitic folds on the eastern limb of a major syncline, the ?D<sub>3</sub> Yarbu Syncline (Fig. 6), in the Diemals Formation.

## Locality 15: Deception Hill Porphyry (MGA 724920E 6695970N)

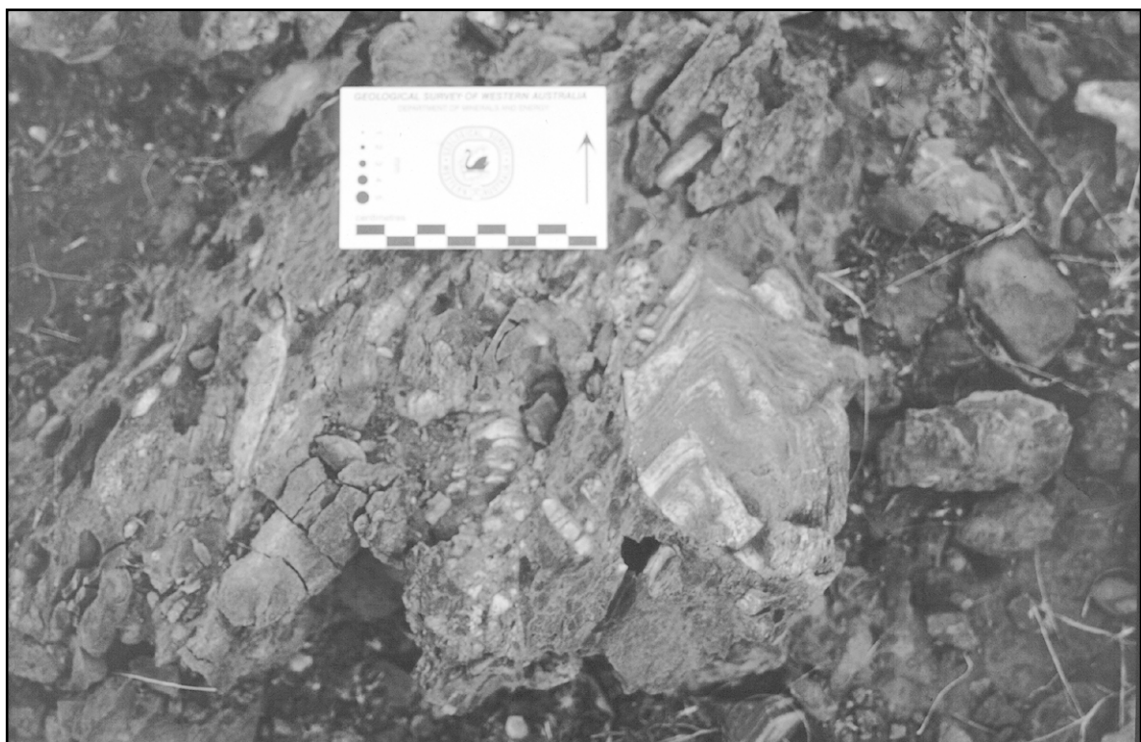
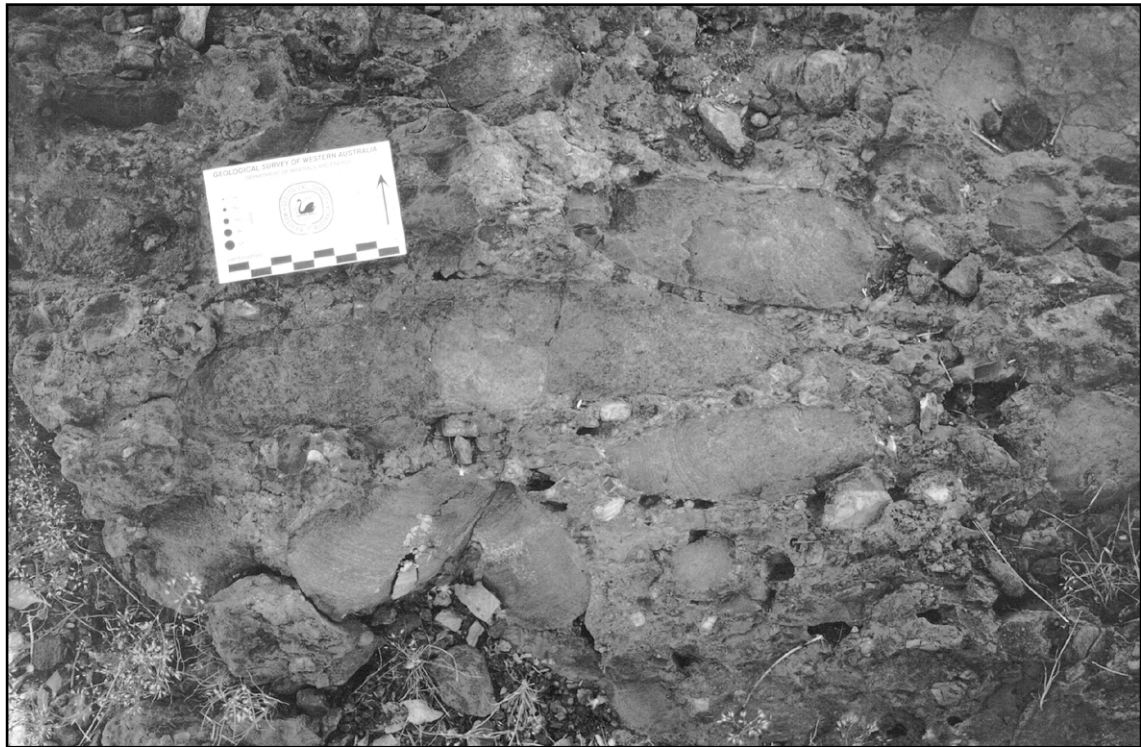
by S. Wyche

*The locality is a geochronology sample site at the eastern end of a gridline that runs east from a prominent southerly trending gridline, about 2.1 km south of the Pigeon Rocks Road.*

The Deception Hill Porphyry forms a prominent inselberg that lies north-northwest of the Die Hardy Range (Fig. 24). The rock is a leucocratic porphyry of dacitic composition (Appendix 1) that contains phenocrysts of plagioclase, quartz, and biotite in a fine-grained, recrystallized quartzofeldspathic groundmass (Fig. 26). Phenocrysts are locally up to 5 mm, but more typically less than 2 mm, and plagioclase phenocrysts are much more abundant than quartz. Both quartz and plagioclase phenocrysts are present as single grains, and as clusters of grains of either quartz or plagioclase. Accessory phases include opaque-oxide grains, apatite, and chlorite. Plagioclase phenocrysts have been altered to albite, and the rock contains secondary carbonate minerals. Biotite may have been a primary phase but also appears to have locally replaced a mafic mineral, probably amphibole. The porphyry is weakly deformed with a foliation that trends at about 160°, approximately parallel to the regional S<sub>2</sub> foliation.

The relationship between the Deception Hill Porphyry and the surrounding greenstones is obscured by deep weathering and lack of outcrop. No greenstone–porphyry contacts are exposed, and so the porphyry could be below, within, or intruding the lower greenstone succession.

The Deception Hill Porphyry has an interpreted SHRIMP U–Pb zircon age of  $3023 \pm 10$  Ma (Nelson, 1999). This age is reasonably well constrained, although the analysis did identify a small population of zircons with an age of  $2787 \pm 10$  Ma, attributed by Nelson (1999) to a post-crystallization disturbance event. A chemical analysis of porphyry from this locality is presented in Appendix 1. The c. 3023 Ma age is the oldest determined for any rock in the central Yilgarn Craton.



4IAS SW 16

29.05.01

**Figure 25. Polymictic conglomerate of the Diemals Formation: (a) strongly flattened sedimentary and mafic clasts in a ferruginous sandy matrix; (a) banded chert clast showing tight folding**

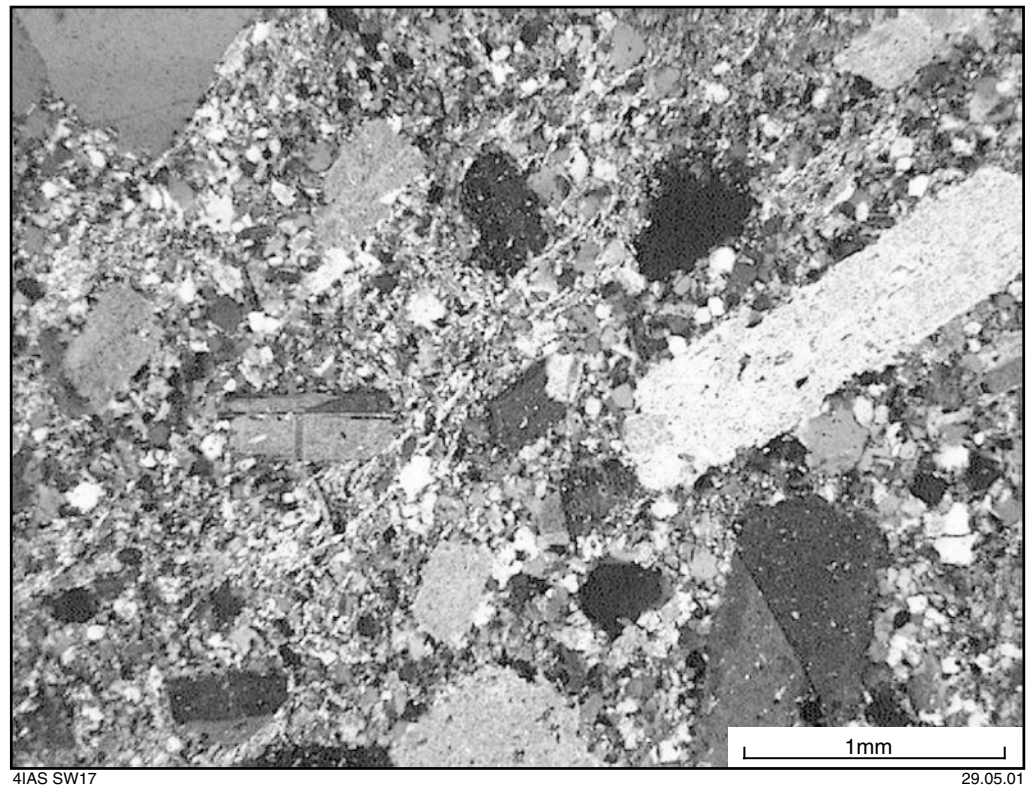


**Figure 26.** Deception Hill Porphyry under crossed nicols showing abundant albitized plagioclase phenocrysts, and subordinate quartz phenocrysts, in a microcrystalline quartzofeldspathic groundmass

## Locality 16: Refolded BIF, Evanston (MGA 740230E 6705770N)

by J. E. Greenfield

*The turnoff to this locality from the Bullfinch–Evanston road is about 7.5 km south of the major T-intersection between the Bullfinch–Evanston road and the Menzies–Evanston road, and about 1.3 km south of the intersection with the haul road for the Evanston mine. The stopping point is about 1 km east-northeast of the turnoff along a minor track. From the track, walk south for about 600 m, across a dry creekbed and a small BIF ridge. The locality is at the northern end of a large BIF ridge with a view of the Evanston mine to the north-northeast.*

This locality (Fig. 27) is within the northeasterly trending Evanston greenstones (Wyche et al., 2001; Greenfield, 2001) which contain BIF, strongly foliated amphibolite, and high-grade (amphibolite-facies) mafic and ultramafic schist. The northeasterly trending foliation is defined by peak metamorphic minerals such as tremolite–actinolite, hornblende, and biotite.

Evidence of all of the regional deformation events (see **Structural geology**) can be seen in the Evanston greenstones, and the locality is adjacent to the D<sub>3</sub> Evanston Shear Zone. Strongly foliated monzogranite in the Evanston Shear Zone (Fig. 3) has a SHRIMP U–Pb zircon age of  $2654 \pm 6$  Ma (see **Locality 17**; Nelson, 2001). This date is within statistical error (95% confidence level) of the  $2656 \pm 3$  Ma age obtained by Qiu et al. (1999) for an undeformed monzogranite that has intruded the D<sub>3</sub>

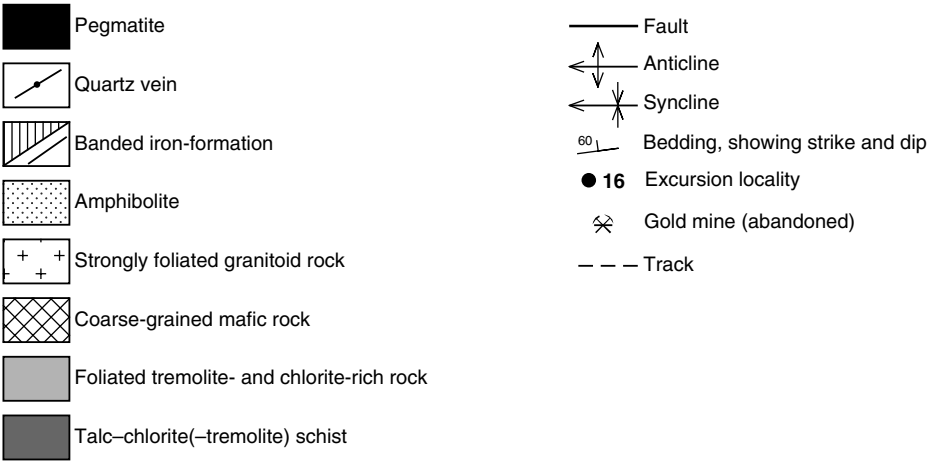
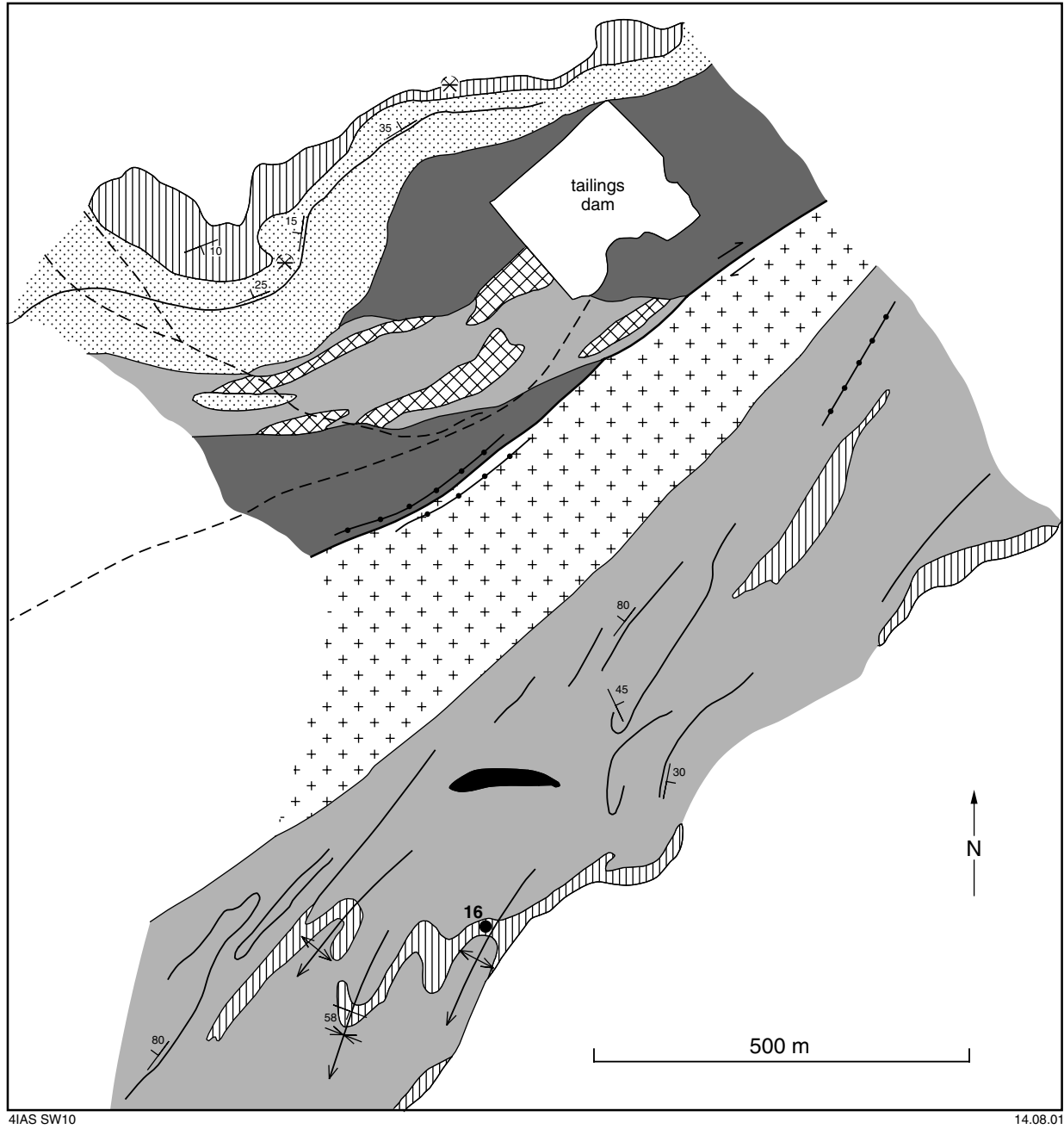


Figure 27. Interpreted geology of the Evanston area, showing Locality 16 and Evanston mining area

Koolyanobbing Shear Zone about 130 km to the south. If the deformation on the Evanston and Koolyanobbing Shear Zones represents the same deformation event ( $D_3$ ), then the minimum age for this deformation must be c. 2655 Ma.

At the locality, a BIF ridge preserves refolding of  $F_1$  folds by upright  $F_2$ – $F_3$  folds. The outcrop contains BIF with intercalated chert layers, underlain by tremolite–chlorite schist. At the base of the ridge on the northern side, early ( $F_1$ ) folds are isoclinal and were originally recumbent, but now have reclined fold hinges plunging steeply to the northwest and southeast due to superimposed, upright folding (Fig. 28). The superimposed folds ( $F_2$ – $F_3$ ) at the top of the ridge are open, and  $F_1$  fold hinges are subhorizontal to moderately plunging. Extreme  $D_1$  deformation has resulted in the local development of  $F_1$  sheath folds in the chert unit at the top of the ridge. Here, a curved fold-hinge, that is convex to the north, indicates a south to north shear component during folding. This is consistent with a northerly vergence determined from other  $F_1$  folds in the region.

At the top of the outcrop, open, upright  $F_2$ – $F_3$  folds plunge moderately to the southwest, and have a shallow-dipping enveloping surface. These folds have metre-scale wavelengths, and are interpreted to be subordinate M-folds in the hinge of a large antiform. This would account for the steepening of  $F_2$  fold limbs and  $F_1$  fold hinges on the flanks of the outcrop. The  $F_2$ – $F_3$  fold axes are parallel to the regional-scale Evanston Shear Zone at all scales. Southwesterly trending foliation in tremolite–chlorite schist at the base of the outcrop is also parallel to the Evanston Shear Zone.

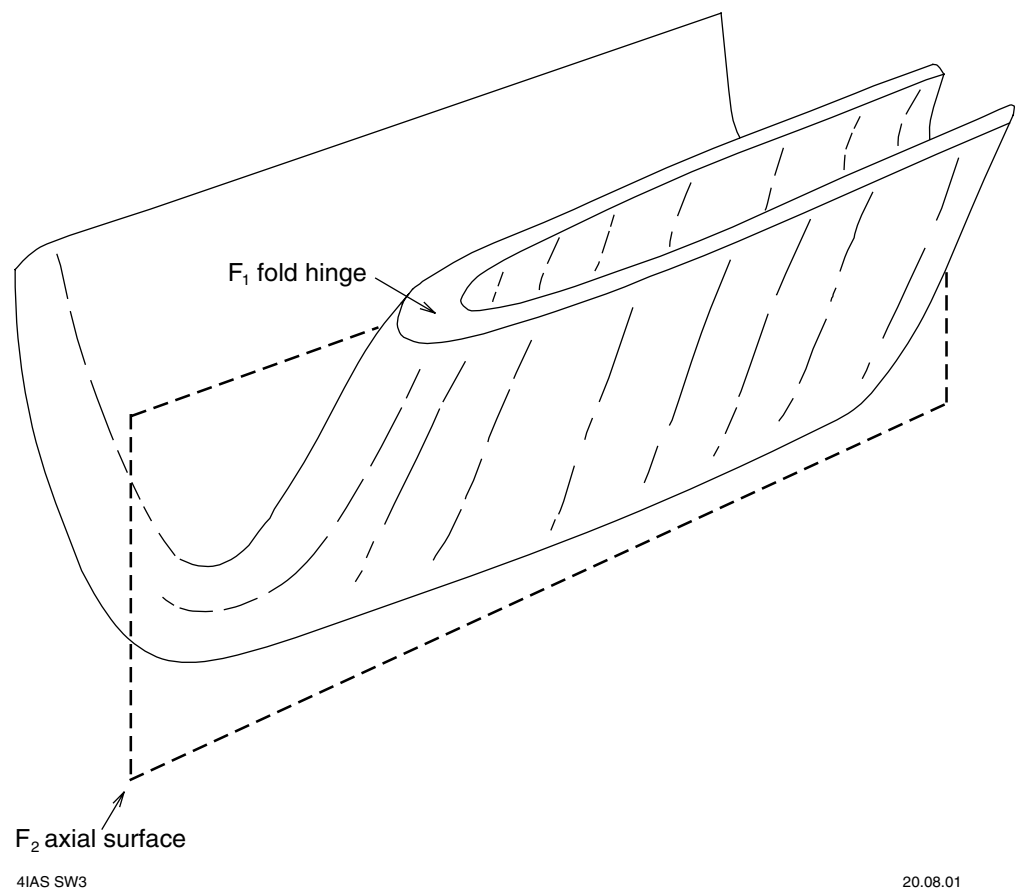


Figure 28. Schematic illustration of the refolding geometry seen at Locality 16

Gold mineralization at Evanston is concentrated on the northwestern side of the greenstones, near the granite–greenstone contact. Most mineralization is in quartz veins in subhorizontally bedded BIF. The Main lode is controlled by  $S_0$ – $S_3$  intersections, and is associated with strong sulfide–carbonate alteration (Matheson and Miles, 1947; Dalstra, 1995).

The Evanston mine produced 1141 kg of gold at an average grade of 18 g/t Au between 1938 and 1960 (Townsend et al., 2000). Silver has also been recovered from Evanston mine tailings, and 30 kg was produced between 1957 and 1960 (Walker and Blight, 1983). Mining recommenced in a small openpit over the old workings in 1998, and ore is processed at the nearby Gwendolyn mine.

## **Locality 17: Asymmetric feldspar porphyroclasts in the Evanston Shear Zone (MGA 742510E 6710230N)**

**by S. F. Chen**

*This locality is an area of rock pavement that lies about 2 km to the south of the Menzies–Evanston road, along a fenceline that crosses that road 500 m east of the major T-intersection with the Bullfinch–Evanston road.*

Locality 17 (Fig. 2) lies within the northeasterly trending Evanston Shear Zone (Fig. 3), a 1–3 km-wide high-strain zone. In its southwestern part, the shear zone consists of strongly foliated granitoid rocks, amphibolite, and mafic and ultramafic schists that contain a gently plunging to subhorizontal mineral lineation. Asymmetric feldspar porphyroclasts and Z-shaped asymmetric folds at the local scale, and the deflection patterns of the Mount Elvire and Mount Manning greenstone belts adjacent to the shear zone at the regional scale (Figs 3 and 7), indicate a dextral shear sense. The middle section of the shear zone comprises several prominent quartz veins in strongly foliated to mylonitic granitoid rocks. A number of north-trending faults or shear zones splay off the northeastern end of the shear zone (Fig. 9).

This locality is situated on the southeastern margin of an elongate granitoid body, the Rainy Rocks intrusion, that is approximately 50 km long and up to 5 km wide, with the long axis parallel to the Evanston Shear Zone. Dalstra (1995) described two phases in the Rainy Rocks intrusion, a dark biotite-rich phase, and a more leucocratic, medium- to coarse-grained, variously deformed phase with abundant microcline porphyroclasts. The southeastern margin of the intrusion near its southwestern end is strongly deformed, with a strong, northeasterly trending foliation and a gently ( $<20^\circ$ ) plunging mineral lineation. The granitoid is only weakly to moderately deformed at Rainy Rocks, about 7 km to the northeast.

At Locality 17, strongly foliated monzogranite forms part of the Evanston Shear Zone. A pervasive foliation within the monzogranite trends  $038$ – $042^\circ$ , parallel to the shear zone. It is subvertical or dips steeply to the northwest, with a locally prominent mineral lineation that plunges gently to the southwest. Numerous stretched, and some rotated, asymmetric porphyroclasts of feldspar and quartz have been identified according to their geometry and internal textures (Fig. 29). Most porphyroclasts indicate dextral strike-slip movement on the Evanston Shear Zone. The northeasterly trending foliation is locally truncated by semi-ductile to brittle fractures that trend north-northwest with sinistral offsets up to 20 cm.

A geochronological sample taken from the strongly foliated monzogranite at this locality has yielded a SHRIMP U–Pb zircon age of  $2654 \pm 6$  Ma (Nelson, 2001). This material is probably the leucocratic phase of Dalstra (1995). A SHRIMP U–Pb zircon age analysis by Dalstra (1995) on the dark, biotite-rich granitoid phase at Rainy Rocks

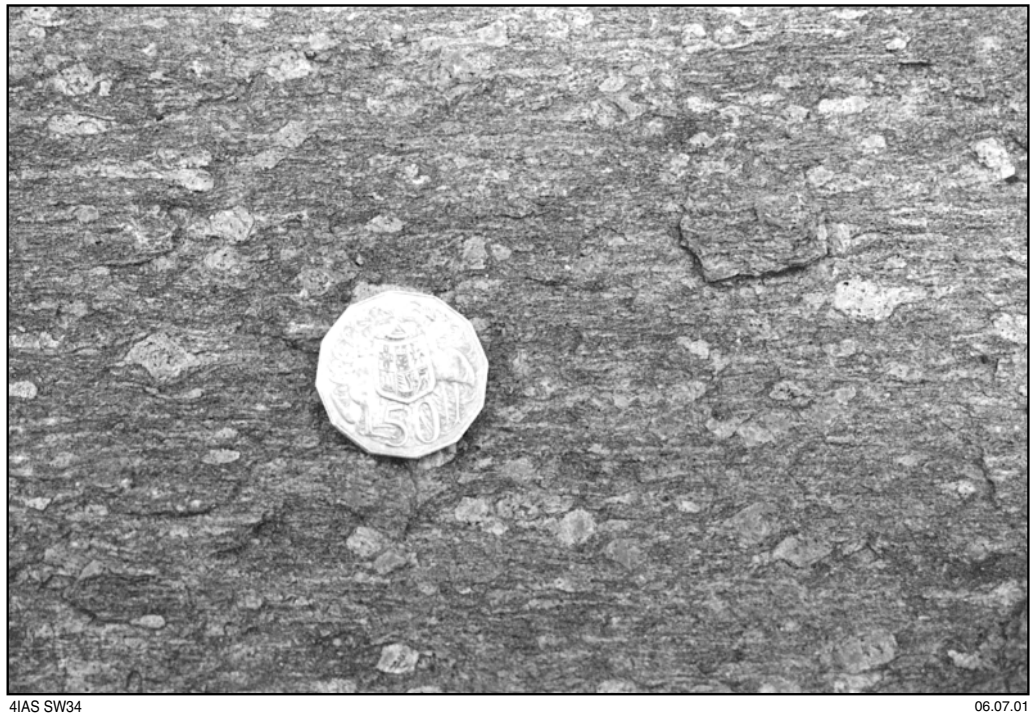


**Figure 29. Rotated and stretched asymmetric porphyroclasts of feldspar and quartz, showing a dextral shear sense on the Evanston Shear Zone at Locality 17**

produced a complex population of zircons that suggest a crystallization age of  $2678 \pm 14$  Ma. Although the latter age determination is not well constrained, it suggests that the different phases in this granitoid represent distinctly different intrusions.

### **Locality 18: Overprinting deformation and metamorphic relationships around a fold hinge (MGA 762930E 6722730N)**

**by J. E. Greenfield and S. F. Chen**

*This locality is reached via the Lake Barlee Road (to Mount Elvire Homestead) which heads north from the Menzies–Evanston road about 5 km east of the major T-intersection between that road and the Bullfinch–Evanston road. Follow this road for 15.6 km and, just before a large creek bed, turn right at an overgrown minor track heading east. After about 9.6 km, this track turns south, and the best access to the locality is about 1.3 km south of the bend. From here, walk about 300 m to the east, along a curving ridgeline.*

This locality (Fig. 1) lies within the South Elvire greenstone belt of Griffin (1990) that contains BIF, amphibolite, pelite, peridotite, and calc-silicate rocks metamorphosed to middle- to upper-amphibolite facies. A major  $F_2$  synform with a curved hinge line plunges moderately to the north, and is the most prominent structure in the area. The Evanston Shear Zone is adjacent to the northwest, and separates this area of greenstone from its possible northern extension (Fig. 3). Drag patterns of the greenstones against the shear zone, including the deflection of the  $F_2$  fold axis, indicate dextral strike-slip during  $D_3$ .

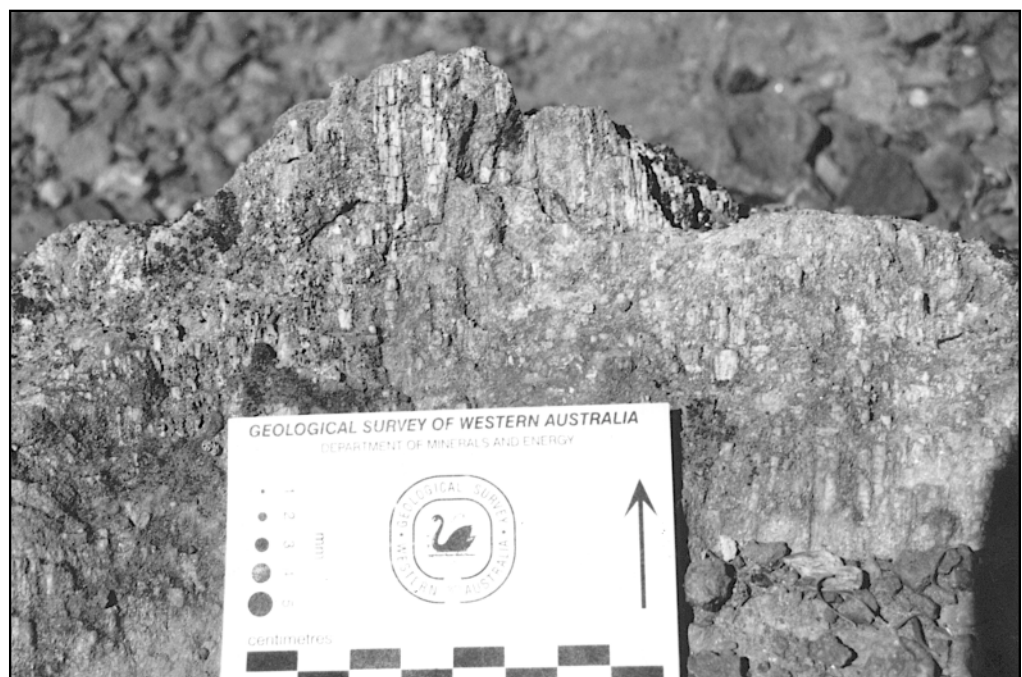
At Locality 18, amphibolite-facies calc-silicate, pelitic, and mafic rocks, and BIF outcrop in the hinge zone of the  $F_2$  synform. Muscovite schist preserves an  $S_1$  layer-parallel foliation that dips moderately to the north. The foliation has been crenulated and folded during  $D_2$ , with the crenulation hinge lineations plunging moderately to the north, parallel to the  $F_2$  synformal fold hinge. Garnet porphyroblasts in the schist commonly overprint the muscovite foliation, although there is some suggestion of muscovite wrapping around the porphyroblasts. Peak-metamorphic sillimanite porphyroblasts overprint the foliation and define a mineral lineation (Fig. 30) that is also parallel to the  $F_2$  fold hinge. Thus peak metamorphism in this belt must have been broadly synchronous with  $D_2$ .

Calc-silicate rocks in the region contain hornblende, grossular, plagioclase, quartz, epidote, and diopside, and most have a hornfelsic appearance. However, they are of limited areal extent, being confined to the eastern edge of the Mount Manning and South Elvire greenstone belts. The calc-silicate rocks are interpreted to be of metasomatic origin, with fluids derived from adjacent monzogranites (Greenfield, 2001; Dalstra et al., 1999).

### **Locality 19: Unconformity at the base of the Diemals Formation south of Kim Bore (around MGA 710600E 6713000N)**

by S. F. Chen and S. Wyche

*This locality is adjacent to a breakaway, about 4.5 km south-southeast along a track from the intersection, near Kim Bore, of this track and the track from Diemals Homestead, about 13.5 km to the east.*



4IAS SW33

06.07.01

**Figure 30. Sillimanite porphyroblasts on the  $S_1$  surface are parallel to  $F_2$  fold hinges at Locality 18 (scale-bar shown is in centimetres)**

The unconformity between the Diemals Formation and the mafic-dominated lower greenstone succession is marked by a moderately southerly to southwesterly dipping basal conglomerate and pebbly sandstone, within the Diemals Formation, that overlies steeply west-southwesterly dipping black shale and mafic rocks of the lower greenstone succession (Fig. 31). At this locality, there is a discontinuous basal conglomerate to the Diemals Formation, and post-depositional deformation along the unconformity and within the Diemals Formation (Fig. 31).

Here, the lower greenstone succession consists of medium- to coarse-grained gabbro, fine-grained high-Mg basalt with pyroxene-spinifex texture, and a thin unit of black shale. Chert and BIF are exposed farther to the east. The gabbro and high-Mg basalt are typically massive to weakly foliated. The black shale is locally ferruginized and hosts traces of copper mineralization (Marston, 1979). Bedding in the black shale trends 335–345° and dips steeply, mainly to the west-southwest, but locally to the east-northeast, subparallel to an  $S_2$  foliation. An easterly trending crenulation cleavage and small-scale open folds are superimposed on the bedding and  $S_2$  foliation.

Clasts in the basal conglomerate, 3–20 cm in size, are angular to subrounded and poorly sorted, in a ferruginized, sandy matrix. They are mainly composed of reddish-brown, deeply weathered rocks, probably derived from mafic rocks (Fig. 32), but include some black shale, jaspilite, and chert clasts. The composition of these clasts reflects that of the underlying lower greenstone succession. Some chert boulders contain folds that indicate deformation prior to erosion and redeposition in the conglomerate.

Above the basal conglomerate, the Diemals Formation consists of sandstone and pebbly sandstone in which pebbles, 1–5 cm in size, are dominated by vein-quartz clasts. The matrix to the sandstone is locally mafic (i.e. it consists of coarse-grained quartz in a fine-grained, grey, mafic matrix). Sandstones adjacent to the unconformity are strongly deformed. An early foliation ( $S_2$ ) that trends north to north-northwest is truncated by a later, steep foliation ( $S_3$ ) that trends northwest. Locally preserved asymmetric quartz grains, aligned with  $S_3$ , indicate a sinistral shear sense. These observations suggest that strain was partitioned into the unconformity during  $D_3$  sinistral strike-slip shearing.

Away from the unconformity to the south, the pebbly sandstone and sandstone are deformed in a large-scale, upright anticline. Bedding dips moderately to the southwest on the western limb, and to the southeast on the eastern limb. The hinge of the anticline plunges 30° to the south (Fig. 31), with an axial-planar foliation that is subvertical or dips steeply to the east.

## **Locality 20: Mafic tuff south of Diemals Homestead (MGA 722941E 6714450N)**

**by S. F. Chen and S. Wyche**

*This locality is on the track between Diemals Homestead and Pigeon Rocks, about 1.2 km south of the homestead. The traverse involves a walk of about 600 m to the south, on the eastern side of the track.*

At this locality, several thin units of mafic tuff lie within thick tholeiitic basalt flows to the south of Diemals Homestead (Fig. 31). The tuffaceous rocks are pale grey, fine grained, well bedded, and laminated to thin bedded (typically millimetre- to centimetre-scale bedding), whereas the tholeiitic basalt flows with vesicles and amygdalae are darker grey, and massive to weakly foliated. Individual mafic tuff units range from 5 to 30 m in thickness. Locally preserved graded bedding and cross-bedding indicate southward younging.

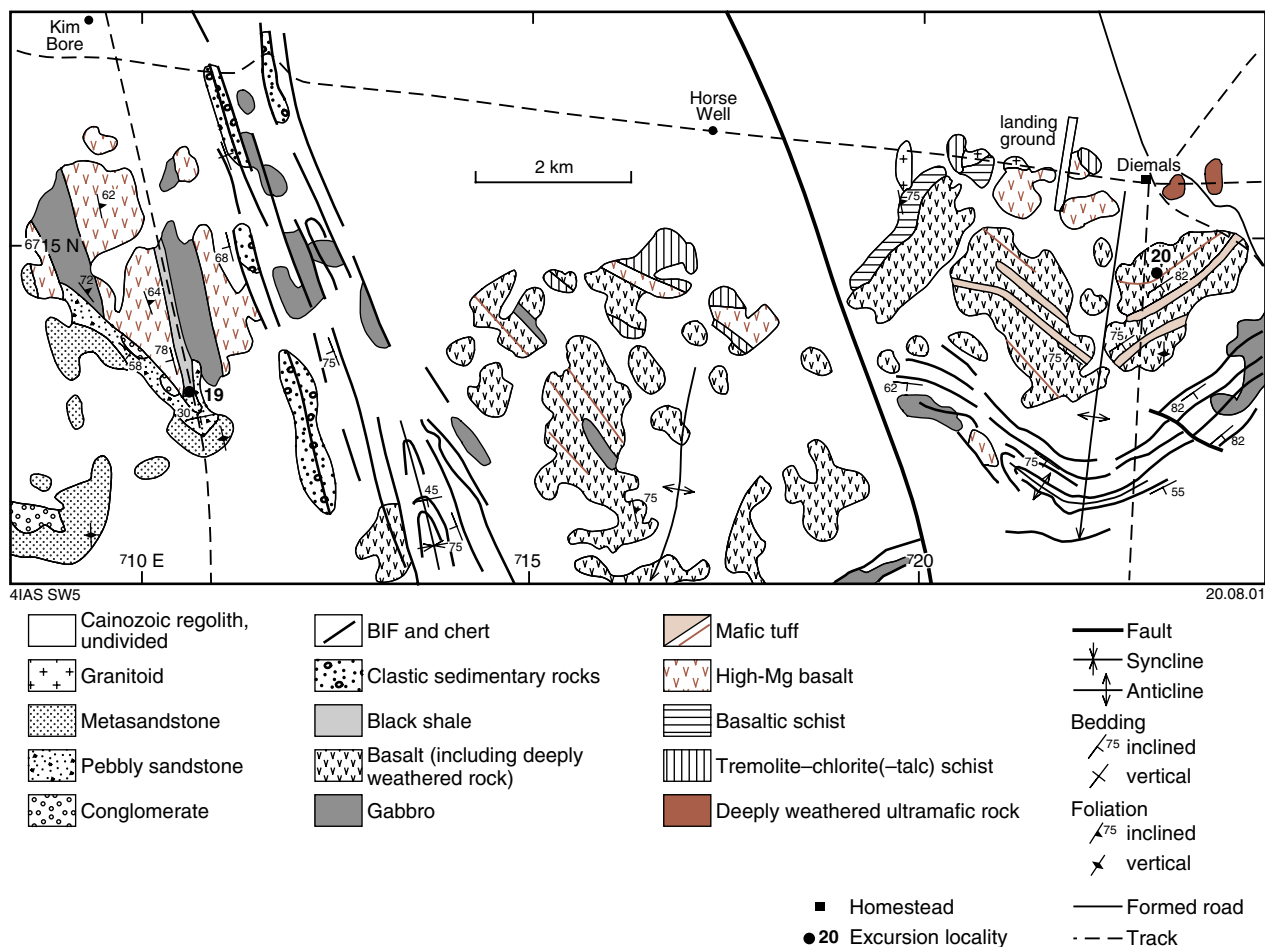


Figure 31. Geology of the Diemals - Kim Bore area, showing the unconformity between the Diemals Formation and lower greenstone succession (Locality 19), and the mafic tuffs (Locality 20)

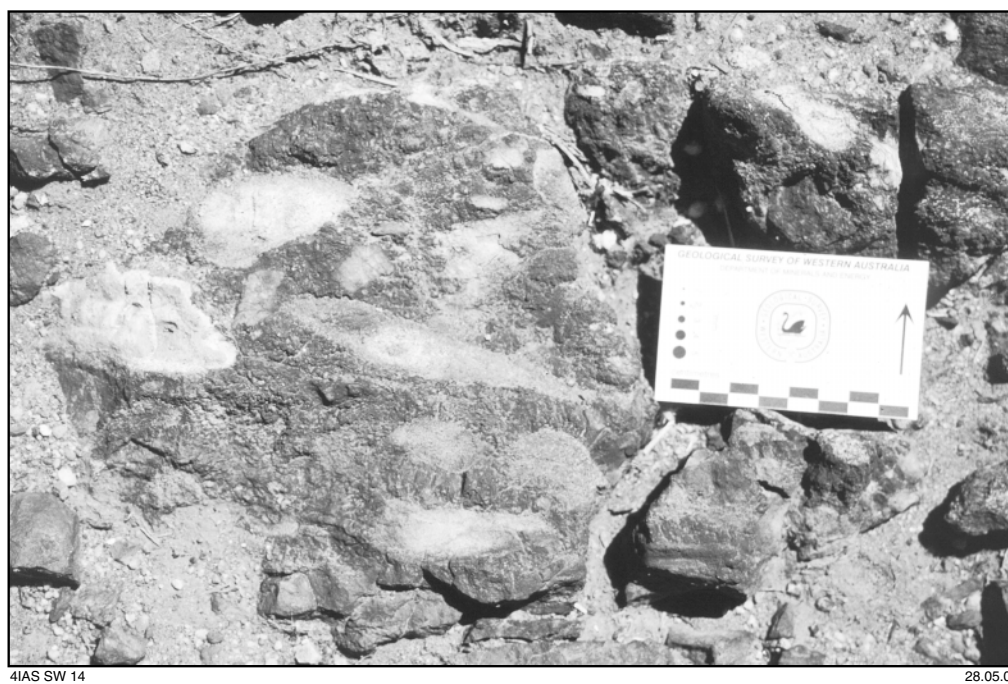


Figure 32. Deeply weathered basal conglomerate in the Diemals Formation (Locality 19)

The tuffaceous material consists of cryptocrystalline chlorite, feldspar, clinozoisite, and fibrous actinolite. Secondary carbonate is locally abundant. Some mafic tuff outcrops contain angular clasts (up to 1 cm long) of similar material. Abundant subspherical voids, up to 5 mm across and locally filled with carbonate, cut across bedding features and may represent either devitrification textures or later alteration. Chemical analyses of the tuffaceous rocks indicate compositions in the range from basalt to basaltic andesite (Appendix 1; Wyche et al., 2001).

## **Locality 21: Altered volcanic rocks at Pincher Well (MGA 675300E 6821650N)**

**by S. Wyche**

*This locality is about 1 km southwest of Pincher Well, which is about 3 km west of the Lake Barlee – Youanmi road, and about 15 km south of its intersection with the Paynes Find – Sandstone road.*

At Pincher Well (Fig. 9), a strongly altered felsic volcanic and sedimentary rock association forms an extensive area of outcrop across Pincher Hill, about 3 km west of the Youanmi Shear Zone. There are abundant outcrops of the Youanmi layered mafic intrusion to the north and west (Stewart et al., 1983).

At Locality 21, abundant rubbly outcrop of deformed, fine-grained, dark green–grey, chlorite–sericite–biotite–quartz–hematite rock has been interpreted as an altered dacite (Stewart et al., 1983). Some outcrops contain abundant irregular, leucocratic ovoids up to 1 cm long that are sericite rich and biotite poor. These ovoids were interpreted by Stewart et al. (1983) as possible lapilli, but are more likely to be secondary features. A SHRIMP U–Pb zircon age of  $2814 \pm 14$  Ma has been obtained for a sample from this locality (Nelson, in prep.).

The stratigraphic setting of the felsic rocks at Pincher Well is unknown, but felsic volcanic rocks that appear to stratigraphically overlie the Windimurra Intrusion about 40 km to the northwest, the Kantie Murdana Volcanics (see **Locality 24**), have a SHRIMP U–Pb zircon age of  $2813 \pm 3$  Ma (Nelson, 2001).

About 1.5 km northwest of Locality 21, sulfide mineralization is hosted by a silica–sulfide(–magnetite) unit within a unit of metamorphosed BIF and chert. The metasedimentary rocks are draped around a dome of felsic volcanic and volcanoclastic rocks that comprises the greater part of the outcrop in the area. This prospect has an inferred resource estimated at 20 Mt at 2% Zn (Ferguson, 1999). Another prospect with a similar setting, about 12 km to the west-southwest (Freddie Well), contains an inferred resource estimated at 680 000 t at 7.6% Zn and 0.2% Cu (Ferguson, 1999; Register of Australian Mining, 2000–2001).

## **Locality 22: Yuinmery Shear Zone near Yuinmery Homestead**

**by S. F. Chen**

The northwesterly trending Yuinmery Shear Zone (Fig. 9; Yuinmery Fault of Stewart et al., 1983 and Eisenlohr et al., 1993) is defined by strongly foliated to mylonitic and gneissic granitoid rocks, and locally contains ultramafic and mafic schists adjacent to the contact with the Youanmi greenstone belt. Its northwestern section is a 2–3 km-wide, high-strain zone. From east to west, a pervasive foliation changes from

northwesterly to northerly trending, and contains a well-developed mineral lineation that changes gradually from subhorizontal to steeply plunging (Eisenlohr et al., 1993). In the middle section of the shear zone, strongly foliated and poorly exposed monzogranite in a wide high-strain zone contains a steep foliation that dips predominantly to the northeast. Farther south, the shear zone lies within banded granitoid gneiss that is intruded by less deformed to undeformed monzogranite. Well-developed S–C fabrics (Fig. 33a), asymmetric porphyroclasts, and eye structures, together with a prominent, gently southeasterly plunging mineral lineation, consistently indicate a sinistral movement sense. Within the shear zone, the S-fabric, defined by a northerly trending gneissic banding or foliation, is sinistrally displaced by a northwest-trending foliation (C-fabric). In granitoid gneiss away from the shear zone, the northwesterly trending foliation is commonly absent.

Locality 22 comprises two stops in the northwestern part of the Yuinmery Shear Zone, to the west and southwest of Yuinmery Homestead (Fig. 9). We will start from the strongly foliated granitoid in the east, about 2 km away from the granite–greenstone contact, and move towards the contact to see the gradual change in the orientations of the main foliation and the plunge angles of a pronounced mineral lineation.

### **Locality 22a: Eastern part of the Yuinmery Shear Zone (MGA 695930E 6838030N)**

*The turnoff to Yuinmery Homestead is about 10 km east-northeast of the Youanmi mine, on the Youanmi–Sandstone road. Take the road to Yuinmery Homestead for about 9 km. This locality is near a north-trending fenceline that crosses the road to the west of the homestead.*

Moderately to strongly foliated monzogranite in the eastern part of the Yuinmery Shear Zone is intruded to the northeast by less deformed granitoid. The foliation trends 325–335° and dips steeply to the northeast, away from the greenstones. Here, a mineral lineation plunges 2–10° to both the northwest and the southeast, suggesting a dominant strike-slip movement. About 400 m to the west, dark-grey, medium-grained granitoid rock, mapped by Stewart et al. (1983) as tonalitic gneiss, also contains a pervasive foliation that dips steeply to the northeast and contains a gentle (2–10°) mineral lineation that plunges both northwest and southeast. This rock has a SHRIMP U–Pb zircon age of  $2701 \pm 8$  Ma (Nelson, in prep.).

### **Locality 22b: Western part of the Yuinmery Shear Zone (MGA 695880E 6834390N)**

*From Locality 22a, drive about 3.8 km along the fence to the south.*

Strongly foliated to mylonitic monzogranite at this stop contains an intense L–S tectonite fabric (Eisenlohr et al., 1993). At the base of the hill, a pervasive foliation trends 325–330°, and dips steeply, mainly to the southwest. It contains a pronounced mineral lineation that plunges moderately (20–35°) to the northwest. A typical small-scale restraining jog, bound by two northwest-trending, right-stepping, discrete shear zones, contains foliations that splay off the boundary shear zones at moderate angles (Fig. 33b). The curvature of these foliations against the boundary shear zones clearly indicates a sinistral shear sense. S–C fabrics that are locally preserved in strongly foliated granitoid rocks, about 1.2 km to the north, also indicate a sinistral shear sense in the Yuinmery Shear Zone.



4IAS SW35

06.07.01

**Figure 33.** Shear sense indicators from the Yuinmery Shear Zone: (a) S–C fabrics with a north-trending S-plane sinistrally truncated by a northwest-trending C-plane (AMG 723830E 6796940N); (b) a small-scale restraining jog defined by northwest-trending, right-stepping, sinistral shear zones in mylonitic granitoid at Locality 22B

To the west, towards the granite–greenstone contact, the strike of the main foliation gradually changes from  $330^{\circ}$  to nearly due north. The foliation dips steeply, mainly to the southwest, but locally to the northeast. A prominent mineral lineation is defined by elongate feldspar and quartz grains, and grain aggregates. It plunges moderately to the northwest within granitic mylonite in the east, and becomes steeply plunging to downdip in mafic schist and amphibolite in the west, corresponding to the change in foliation strike. Farther west, a dominantly northerly trending foliation in the Youanmi greenstone belt is axial planar to a macroscopic syncline (Fig. 9) that was interpreted by Stewart et al. (1983).

Eisenlohr et al. (1993) reported a reverse movement sense (west-block up) in areas of steeply plunging mineral lineation, as inferred from asymmetric porphyroclasts. They suggested that the reverse movement postdated sinistral shearing. An alternative interpretation is that the steep mineral lineation with associated north-trending foliation in greenstones was caused by either  $D_2$  east–west shortening or by  $D_3$  impingement of granitoid blocks, or by the combination of both deformations.

## **Locality 23: Youanmi Shear Zone in the Bell Chambers Well area**

**by S. F. Chen**

The northeasterly trending Youanmi Shear Zone (Fig. 9; Youanmi Fault of Stewart et al., 1983 and Eisenlohr et al., 1993) forms the eastern boundary of an extensive region containing large layered mafic intrusions. The shear zone changes in width, orientation, and strain state along strike (Libby, 1992; Eisenlohr et al., 1993). In the northeast, it forms a wide, high-strain zone in strongly foliated and mylonitic granitoid rocks. Well-developed S–C fabrics and asymmetric porphyroclasts indicate a dextral shear sense. Shear bands and Z-shaped asymmetric folds in mafic schist also indicate a dextral shear sense in the middle segment of the shear zone. In this area, the shear zone contains a number of ridge-forming quartz veins. Farther south, the Youanmi Shear Zone follows the northerly trending granite–greenstone contact (Eisenlohr et al., 1993). Here, symmetric and flattened porphyroclasts of feldspar and quartz, and locally preserved downdip slickenlines, indicate intense contraction and dip-slip movement.

At this locality, in the Bell Chambers Well area, we will traverse a high-strain zone of strongly deformed granitoid rocks within the northeastern part of the Youanmi Shear Zone (Fig. 9). The centre of the shear zone is composed of granitic mylonite and is flanked by strongly foliated to gneissic granitoid rocks to both the northwest and the southeast. We will first examine the deformation characteristics in the centre of the shear zone, and then compare them to the strongly foliated granitoid rocks to the east.

### **Locality 23a: Centre of the Youanmi Shear Zone (MGA 707760E 6888410N)**

*To reach this locality, travel west along a track that crosses the Sandstone–Youanmi road about 15 km southwest of Sandstone, following the route of an abandoned telephone line for 8.8 km to a sharp bend, and travel a farther 3.3 km to the southwest to Locality 23a.*

The centre of the Youanmi Shear Zone is marked by mylonitic granitoid rocks, approximately 2 km to the west of the contact of granitoid rocks with the Sandstone greenstone belt. A pervasive mylonitic foliation trends  $025\text{--}035^{\circ}$ , and dips steeply to the northwest, away from the greenstones. Most feldspar and quartz grains are strongly stretched and aligned along the main foliation, but many asymmetric porphyroclasts

that indicate dextral shear have also been preserved. A prominent mineral lineation, defined by preferred alignment of stretched feldspar and quartz, plunges gently (2–15°) to the southwest. There are no S–C fabrics in the centre of the shear zone.

To the east, well-developed compositional banding is defined by alternating leucocratic and mesocratic granitoid bands up to 1 m in width. These include pegmatite veins that are mainly parallel to the northeast-trending gneissic banding and foliation. However, some are tightly folded. A northerly trending brittle fracture filled with vein quartz truncates a pegmatite vein, with a sinistral offset of 25 cm. Another set of easterly trending brittle fractures shows a dextral displacement. These brittle fractures are probably conjugate structures developed during a later deformation event.

A SHRIMP U–Pb zircon age of  $2667 \pm 8$  Ma has been obtained for a sample of foliated granitoid rock from this locality (Nelson, in prep.).

### **Locality 23b: Eastern part of the Youanmi Shear Zone (MGA 709811E 6889268N)**

*From Locality 23a, travel 1.4 km back along the track to a fenceline. Turn right and drive 1 km to Locality 23b.*

The eastern part of the Youanmi Shear Zone contains strongly foliated to gneissic granitoid rocks. It is characterized by well-developed S–C fabrics, numerous asymmetric porphyroclasts, and a gently plunging mineral lineation. The S-fabric, defined by preferred alignment of feldspar, quartz and mica, trends 020–025° and is mainly parallel to the gneissic banding, along which some pegmatite veins are boudinaged. The C-fabric trends 035–042° and dextrally displaces the S-fabric. The curvature of the S-fabric against the C-fabric also indicates a dextral shear sense. Both the S- and C-fabrics are subvertical or dip steeply to the northwest, away from the greenstones.

Asymmetric porphyroclasts of feldspar and quartz are very common within the shear zone. Most are stretched porphyroclasts with asymmetric tails indicating dextral shear (Fig. 34), with some feldspar in strongly attenuated aggregates. A gently plunging mineral lineation that plunges 2–5° to the southwest also indicates a dominant strike-slip movement on the Youanmi Shear Zone.

Other structures that have been noted at this stop include a zonal cleavage (2–4 cm apart) trending 020° that is parallel to the gneissic compositional banding, and a small-scale, semi-ductile, sinistral shear zone that trends 312°.

Farther east, a strong foliation within granitoid rocks adjacent to the granite–greenstone contact trends 015–030° and dips steeply to the southeast, towards the greenstones. A weak mineral lineation plunges 5–20° to the southwest. Tholeiitic basalt near the contact is strongly deformed and metamorphosed into mafic schist or amphibolite, with a steep foliation that commonly dips to the southeast. In the greenstones, the deformation intensity decreases from west to east, and the strike of foliation gradually changes from north-northeasterly to nearly due north.

### **Locality 23c: Eastern part of the Youanmi Shear Zone (MGA 710007E 6890204)**

*From Locality 23a, travel 2.8 km back towards the northeast. Locality 23c is located on the eastern side of the abandoned telephone line.*



4IAS SW36

06.07.01

**Figure 34. Asymmetric porphyroclasts of feldspar showing a dextral shear sense on the Youanmi Shear Zone at Stop 23B**

This stop examines a large area of well-exposed, strongly foliated to gneissic, granitoid rocks within the eastern part of the Youanmi Shear Zone. As at Locality 23b, a dextral shear sense is indicated by S–C fabrics and numerous asymmetric porphyroclasts. The S-plane is defined by preferred alignment of feldspar, quartz, and mica grains. It trends 022–028°, and dips steeply to the west-northwest, away from the Sandstone greenstone belt which is exposed about 1 km to the east. The S-plane is dextrally truncated by a subvertical C-fabric that trends 035–040°. Well-developed asymmetric porphyroclasts of feldspar and quartz consistently indicate a dextral shear sense on the Youanmi Shear Zone. A prominent, gently plunging mineral lineation also indicates a dominant strike-slip movement.

Other structures include a locally preserved zonal cleavage subparallel to the gneissic compositional banding, and small-scale, brittle fractures that trend 004°, and have a sinistral movement sense.

## **Locality 24: Windimurra vanadium mine (MGA 650270E 6868700)**

**by J. Withall**

*From Sandstone, travel about 106 km along the Sandstone – Mount Magnet road (i.e. about 45 km east of Mount Magnet) and then turn south onto the road to Youanmi. The Windimurra Vanadium Project access road (to the south) is 22 km along this road. Mine administration is 7 km along this road (past the village). The access road is built on the lateritic ridge that forms the surface expression of the vanadium deposit. Outcrops on both sides of the road consist of vanadium-enriched titano-magnetite bands.*

The Windimurra vanadium deposit is hosted within the Shephards Discordant Zone of

the Windimurra Complex, a differentiated and moderately fractionated, layered gabbroic intrusion. The complex is situated in the eastern part of the Murchison Terrane of the Yilgarn Craton (Figs 1 and 2). This Archaean layered igneous complex is separated from adjacent, younger granitoid rocks by shear zones (Fig. 35).

## Regional geology

The Windimurra Complex (Ahmat, 1990) has an elliptical outcrop ( $85 \times 37$  km, about  $2345 \text{ km}^2$ ) and is the largest single body of gabbroid rocks in the Yilgarn Craton. The overall composition of the Windimurra Complex is that of high-alumina tholeiitic basalt. The exposed portion consists mainly of a layered succession of leucogabbro, leucogabbro, leucotroctolite, and olivine gabbro (much of which is leucocratic) cumulates. The complex shows a broad upward trend from dunite, through leucogabbros, to ferrogabbro.

Olivine and pyroxenes typically become more iron rich, and plagioclase more sodic, higher in the stratigraphy. Rhythmic layering and cryptic layering are widespread, and have developed at all scales. Vanadiferous titanomagnetite (VTM) layers and lenses (up to 10 m thick) are found in the upper portions of the complex, and minor chromite segregations (up to several centimetres thick) near the bottom. This pattern is similar to the Bushveld Complex and many other large layered mafic–ultramafic intrusions. Figure 36 shows the overall stratigraphy of the complex, and the position of the Shephards Discordant Zone (SDZ).

Major shear zones, up to 1.5 km wide, which grade outwards into foliated granitoid, surround the complex. A Sm–Nd two-point whole-rock isochron indicated that the age of the Windimurra Complex is  $3.05 \pm 0.25$  Ga. The surrounding granitoid rocks and the oldest set of dykes intruding the complex have Rb–Sr whole-rock isochron ages of 2.6 Ga and 2.7 Ga respectively (Ahmat and de Laeter, 1982).

The Windimurra Complex is tectonically, or unconformably, overlain by the weakly deformed and low-metamorphic grade rocks of the Kantie Murdana Volcanics, consisting of felsic volcanics, chert, BIF, and dolerite. The Kantie Murdana Volcanics have a SHRIMP U–Pb zircon age of  $2813 \pm 3$  Ma (Nelson, 2001).

## Windimurra vanadium deposit and the Shephards Discordant Zone (SDZ)

### Geological summary

The SDZ, characterized by magnetitites and magnetite-bearing gabbros, is a transgressive sill-like body that extends over a strike length of 45 km and has a thickness ranging from 500 to 600 m. Its surface expression is up to 1 km wide, and the central portion is characterized by abundant magnetite scree. The ‘magnetitite’ is actually titanomagnetite containing 10 to 20%  $\text{TiO}_2$  in the form of ilmenite.

The current vanadium resource is located in the north of the SDZ (Fig. 35). Ahmat (1986b) and Habteselassie (1994) have studied the overall stratigraphic succession in the SDZ, which shows progressive fractionation upwards. The main part is 400 m thick, and consists of anorthositic magnetite gabbro, and numerous magnetite layers and lenses from 5 cm to 2 m wide. The lower 150 m of this succession contains the vanadium resource.

Much of the SDZ has been altered, metamorphosed, sheared, and deeply weathered to a depth of approximately 50 m. It commonly stands out as a prominent laterite ridge (e.g. Shephards Hill). The unusually deep weathering is believed to be due to acid

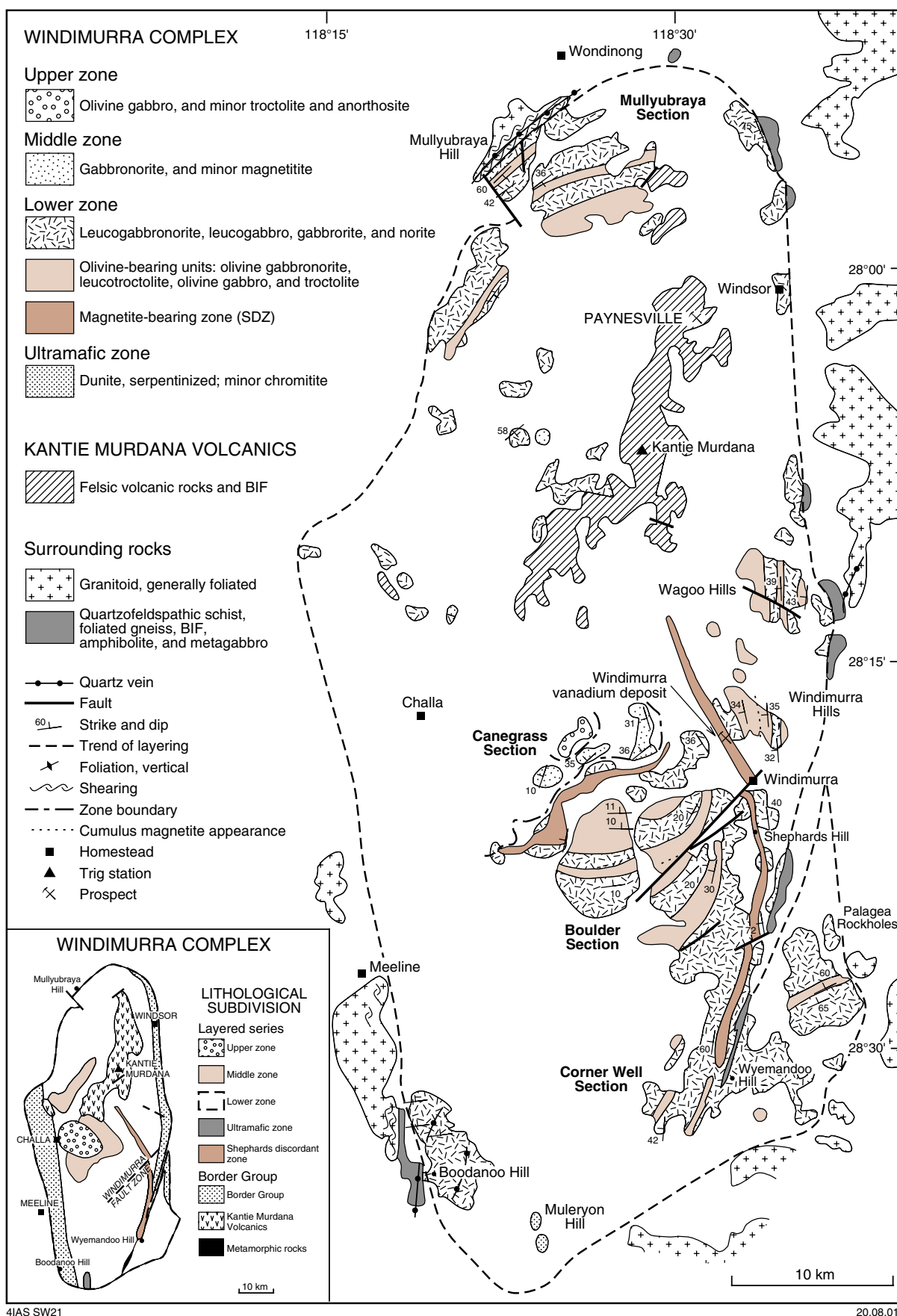
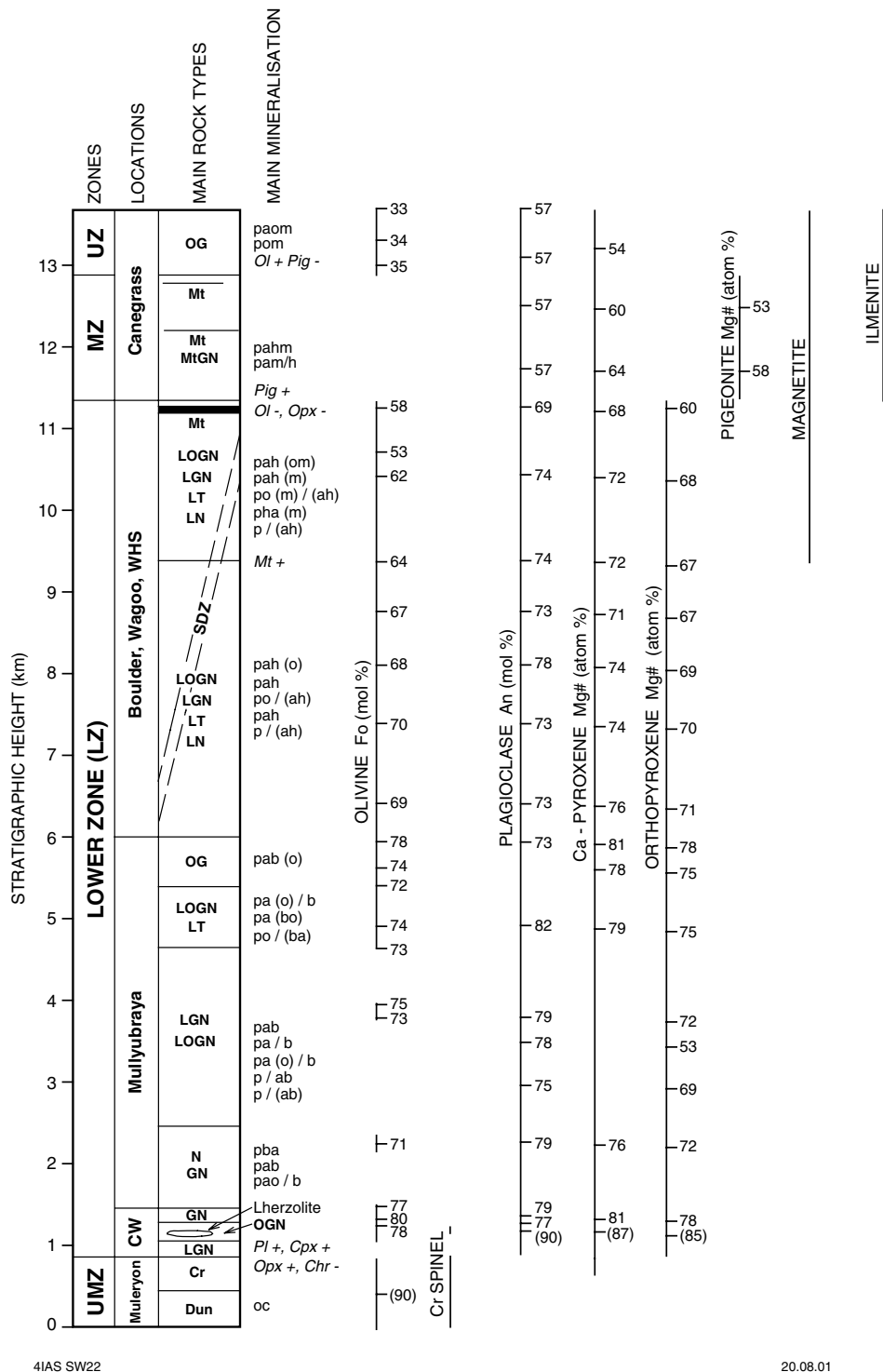


Figure 35. Geological map of the Windimurra Complex showing the main areas of outcrop (after Ahmat, 1990)



**Figure 36.** Schematic section, and range and composition of the cumulus minerals of the Layered Series of the Windimurra Complex. Locations: CW — Corner Well; WHS — Windimurra Hills section; SDZ — Shephards Discordant Zone; UMZ — ultramafic zone. Main rock types: Dun — dunite; Cr — chromitite; LGN — leucogabbro-norite; GN — gabbro-norite; N — norite; LN — leuconorite; LOGN — leuco olivine-gabbro-norite; OG — olivine-gabbro-norite; LT — leucotroctolite; Mt — magnetite. Mineralogy: p — plagioclase; a — augite; o — olivine; b — bronzite; h — hypersthene; m — magnetite; c — chromite. Minerals succeeding the / symbol represent postcumulus phases and minerals in parentheses represent minor components. Cumulus phase changes: + indicates stratigraphic level of important cumulus phase; - indicates disappearance of important cumulus phase. Pl — plagioclase; Ol — olivine; Opx — orthopyroxene; Cpx — clinopyroxene; Pig — pigeonite; Chr — chromite; Mt — magnetite; Mg = 100 Mg/(Mg + Fe<sup>2+</sup>) atom %. Figure after Ahmat (1990)

solutions emanating from the oxidation of primary sulfides, at and above the water table. The resource is largely contained within this saprolitic weathered material. In parts of the upper lateritized magnetitite, there are nodules and veins of goethite–limonite (low in  $V_2O_5$  and  $TiO_2$ ), typically with fibrous and radiating crystal forms. This depth of weathering is not a feature of other vanadiferous titano-magnetite deposits such as the Bushveld of South Africa and Panzhihua of central China. Because of its resistance to weathering, the magnetitite scree is enriched relative to the magnetite content in fresh gabbro.

The majority of the SDZ dips at 35–45° to the west, and is recognized as a strong regional magnetic feature. The zone also produces a positive gravity anomaly. The zone consists of a basal unit containing magnetite–olivine gabbro, magnetite troctolite, and an upper unit of thick, alternating layers of magnetite leucogabbro and magnetitite (magnetite content over 90%).

The basal unit consists of distinctive, laterally persistent magnetite troctolite and olivine gabbro, up to 40 m thick. Olivine content ranges from 1–3% at the base to 40% near the top. Magnetite content is up to 15%. There are two leucogabbro–gabbro subunits within the upper unit. The lower subunit is characterized by podiform magnetite, and the upper subunit by more stratiform magnetite. Magnetite constitutes approximately 10% (by volume) of the two subunits, and mapping in the Shephards Hill area indicates a minimum of about 18 lenses (>20 cm thickness) in the lower unit, and a minimum of 15 lenses in the upper unit. Up to 50 separate magnetite horizons have been intersected in drilling.

### **Mineralization**

The bulk of mineralization is within magnetite (titano-magnetite) bearing gabbro and leucogabbro, in a broadly continuous layered sequence ranging in thickness from 20 to 80 m. Locally, the relative proportions of plagioclase, clinopyroxene (augite), and magnetite may vary considerably, and the composition ranges from anorthosite (plagioclase >90%) to magnetitite (magnetite >90%). Layers in the sequence have sharp basal contacts due to accumulation of magnetite as a cumulus phase, and upper gradational contacts. The sharp basal contact of individual magnetitites is believed to be due to rapid changes in oxygen fugacity and composition of the magma during fractionation. Magnetite is also present as disseminated blebs in the gabbro, with blebs up to 8 mm across.

The basal contact of each layer consists of a narrow, chlorite-rich band, 2 to 20 cm in thickness. A layer of cumulate VTM containing up to 90% opaque minerals overlies this band and is the richest vanadium accumulation. Farther up the sequence, cumulate plagioclase becomes more common and VTM content decreases. Individual layers may grade upwards into a leucogabbro or anorthosite. The VTM concentration in a given layer may range from 90% to less than 10%.

Vanadium replaces some of the ferric ion ( $Fe^{3+}$ ) in the vanadiferous titano-magnetite as  $FeV_2O_5$ . Most of the vanadium is within the magnetite portion of the titano-magnetite or in the weathered form, titano-martite. The magnetite grains in the weathered zone are granular and highly fractured, cumulus to interstitial in magnetite, and mostly interstitial and disseminated in magnetite gabbros. In most exposed rocks the magnetite has been martitized.

The VTM forms large, granular aggregates, up to 5 mm wide, interspersed with lenticular bodies of silicate minerals of similar dimensions. Approximately 90% of the VTM has a grain size exceeding 0.4 mm. The VTM is mainly composed of magnetite that can contain up to 30% by volume of ilmenite intergrowths derived from exsolution.

The ilmenite forms fine-grained lamellae within fresh magnetite, with up to 10% as coarser, blebby intergrowths (<2 mm diameter) in weathered magnetite. The relative grain size of the magnetite and ilmenite varies considerably, but most is in the order of 5 to 10 microns.

The vanadium content within the magnetite has been analysed by SEM (scanning electron microscope) spot analysis (<2.4 µm diameter), which measures the host magnetite between the secondary ilmenite lamellae, giving an average grade of 1.7% V<sub>2</sub>O<sub>5</sub>. Grain-size or ‘broad-beam’ analysis (120–267 µm diameter) includes most of the secondary ilmenite, and approximates the original whole-grain composition, as most magnetites are homogeneous at this scale. The V<sub>2</sub>O<sub>5</sub> content then ranges from 0.8 to 1.4%. Mine processing has shown this to be a true reflection of the grade, with an average magnetite concentrate of 1.2% V<sub>2</sub>O<sub>5</sub> achieved to date. The V<sub>2</sub>O<sub>5</sub> content in rocks is a function of dilution of the atomic level vanadium in ‘pure’ magnetite at all scales as the magnetite composition varies with host rock and with stratigraphic position. The vanadium content in hematite is comparable to that in unweathered magnetite, implying that it appears to be relatively immobile during weathering (Habteselassie et al., 1996).

Habteselassie (1994) found that the bulk vanadium content in magnetites decreased slightly with stratigraphic height, while TiO<sub>2</sub> increased. The variation is dependent on the proportions of magnetite present. The ratio of V<sub>2</sub>O<sub>5</sub> to TiO<sub>2</sub> in core analysis decreases upwards with stratigraphic height, but there is no clear stratigraphic correlation with samples selected from magnetite and magnetite gabbro.

Low V<sub>2</sub>O<sub>5</sub> contents are found in iron-bearing minerals other than magnetite. The ilmenite phases may contain up to 0.5% V<sub>2</sub>O<sub>5</sub>, and some of the pyrite contains up to 0.1% V<sub>2</sub>O<sub>5</sub>. Pyrite makes up to 1% of the volume of the fresh rock, and is disseminated throughout as anhedral grains up to 0.44 mm in diameter. Other minor sulfides present are pentlandite, pyrrhotite, chalcopyrite, and violarite. Clays contain on average 0.18% V<sub>2</sub>O<sub>5</sub>, whilst chlorite contains about 0.30% V<sub>2</sub>O<sub>5</sub>. The effects of weathering on vanadium distribution in the SDZ have been described by Habteselassie et al. (1996).

The gangue minerals consist of plagioclase (often clinozoisitized or saussuritized) and clinopyroxene. With the possible exception of clinopyroxene, the gangue does not contain appreciable vanadium.

## Mine production

Mining commenced in July 1999 with production of approximately 2.5 Mt per year at an average grade of 0.52% V<sub>2</sub>O<sub>5</sub>. After stripping up to 3.5 m of caprock, all the ore is fed into the process plant. Material is blended in the openpit on a 25° working face that is perpendicular to the strike of the geology. The openpit is designed to extract a blend of ore that provides maximum recovery of the vanadiferous titaniferous magnetite through the use of both low-intensity wet-drum magnetite separators, and rare-earth wet-drum magnetite separators.

The mine has a planned life of more than 16 years, with the extensions of the orebody, to both the north and south, yet to be drilled to resource status. The present indicated resource is estimated as more than 100 Mt, and it is likely that this orebody will support mining for the foreseeable future.

## References

- AHMAT, A. L., 1986a, Metamorphic patterns in the greenstone belts of the Southern Cross Terrane, Western Australia: Western Australia Geological Survey, Report 19, p. 1–21.
- AHMAT, A. L., 1986b, Petrology, structure, regional geology and age of the Windimurra Complex, Western Australia: University of Western Australia, PhD thesis (unpublished).
- AHMAT, A. L., 1990, Windimurra Complex, *in* Geology and mineral resources of Western Australia: Western Australia Geological Survey, Memoir 3, p. 120–124.
- AHMAT, A. L., and de LAETER, J. R., 1982, Rb–Sr isotopic evidence for Archaean–Proterozoic crustal evolution of part of the central Yilgarn Block, Western Australia — constraints on the age and source of the anorthositic Windimurra Gabbroid: Geological Society of Australia, Journal, v. 29, p. 177–190.
- BARLEY, M. E., EISENLOHR, B. N., GROVES, D. I., PERRING, C. S., and VEARNCOMBE, J. R., 1989, Late Archaean convergent margin tectonics and gold mineralization: A new look at the Norseman–Wiluna Belt, Western Australia: Geology, v. 17, p. 826–829.
- BARLEY, M. E., and GROVES, D. I., 1990, Deciphering the tectonic evolution of Archaean greenstone belts: the importance of contrasting histories to the distribution of mineralization in the Yilgarn Craton, Western Australia: Precambrian Research, v. 46, p. 3–20.
- BLOEM, E. J. M., DALSTRA, H. J., GROVES, D. I., and RIDLEY, J. R., 1994, Metamorphic and structural setting of Archaean amphibolite-hosted gold deposits near Southern Cross, Southern Cross Terrane, Yilgarn Block, Western Australia: Ore Geology Reviews, v. 9, p. 183–208.
- BLOEM, E. J. M., DALSTRA, H. J., RIDLEY, J. R., and GROVES, D. I., 1997, Granitoid diapirism during protracted tectonism in an Archaean granitoid–greenstone belt, Yilgarn Block, Western Australia: Precambrian Research, v. 85, p. 147–171.
- BUSBY, C. J., and INGERSOLL, R. V., (editors), 1995, Tectonics of sedimentary basins: Blackwell Science Inc., 579p.
- CHAMPION, D. C., and SHERATON, J. W., 1997, Geochemistry and Sm–Nd isotope systematics of Archaean granitoids of the Eastern Goldfields Terrane, Yilgarn Craton, Australia: constraints on crustal growth: Precambrian Research, v. 83, p. 109–132.
- CHAPPELL, B. W., and WHITE, A. J. R., 1974, Two contrasting granite types: Pacific Geology, v. 8, p. 173–174.
- CHEN, S. F., WILSON, C. J. L., LUO, Z. L., and DENG, Q. D., 1994, The evolution of the Western Sichuan Foreland Basin, southwestern China: Journal of Southeast Asian Earth Sciences, v. 10, p. 159–168.
- CHEN, S. F., and WILSON, C. J. L., 1996, Emplacement of the Longmen Shan Thrust-Nappe Belt along the eastern margin of the Tibetan Plateau: Journal of Structural Geology, v. 18, p. 413–430.
- CHEN, S. F., LIBBY, J. W., GREENFIELD, J. E., WYCHE, S., and RIGANTI, A., 2001, Geometry and kinematics of large arcuate structures formed by impingement of rigid granitoids into greenstone belts during progressive shortening: Geology, v. 29, p. 283–286.
- CHEN, S. F., and WYCHE, S., 2001, Bungalbin, W.A. Sheet 2837: Western Australia Geological Survey, 1:100 000 Geological Series.
- CHIN, R. J., and SMITH, R. A., 1983, Jackson, W.A.: Western Australia Geological Survey, 1:250 000 Geological Series Explanatory Notes, 30p.
- CORFU, F., and DAVIS, D. W., 1991, A U–Pb geochronological framework for the Western Superior Terrane, Ontario, *in* Geology of Ontario edited by P. C. THURSTON, H. R. WILLIAMS, R. H. SUTCLIFFE, and G. M. STOTT: Ontario Geological Survey, Special Volume 4, p. 1335–1346.
- DALSTRA, H. J., 1995, Metamorphic and structural evolution of the greenstone belts of the Southern Cross – Diemals region of the Yilgarn Block, Western Australia, and its relationship to the gold mineralisation: University of Western Australia, PhD thesis (unpublished).
- DALSTRA, H. J., BLOEM, E. J. M., RIDLEY, J. R., and GROVES, D. I., 1998, Diapirism synchronous with regional deformation and gold mineralisation, a new concept for granitoid emplacement in the Southern Cross Terrane, Western Australia: Geologie en Mijnbouw, v. 76, p. 321–338.
- DALSTRA, H. J., RIDLEY, J. R., BLOEM, E. J. M., and GROVES, D. I., 1999, Metamorphic evolution of the central Southern Cross Terrane, Yilgarn Craton, Western Australia: Australian Journal of Earth Sciences, v. 46, p. 765–784.
- EILU P. K., MATHISON, C. I., GROVES, D. I., and ALLARDYCE, W. J., 1999, Atlas of alteration assemblages, styles and zoning in orogenic lode-gold deposits in a variety of host rock and metamorphic settings: Geology Department (Centre for Strategic Mineral Deposits) and University Extension, University of Western Australia, Publication 30, 50p.
- EISENLOHR, B. N., GROVES, D. I., LIBBY, J., and VEARNCOMBE, J. R., 1993, The nature of large-scale shear zones and their relevance to gold mineralization, Yilgarn Block: Minerals and Energy Research Institute of Western Australia, Report no. 122, 161p.
- FERGUSON, K. M., 1999, Lead, zinc and silver deposits of Western Australia: Western Australia Geological Survey, Mineral Resources Bulletin 15, 314p.

- FLETCHER, I. R., ROSMAN, K. J. R., WILLIAMS, I. R., HICKMAN, A. H., and BAXTER, J. L., 1984, Sm–Nd geochronology of greenstone belts in the Yilgarn Block, Western Australia: *Precambrian Research*, v. 26, p. 333–361.
- FROUDE, D. O., COMPSTON, W., and WILLIAMS, I. S., 1983, Early Archaean zircon analyses from the central Yilgarn Block: Australian National University, Canberra, Research School of Earth Sciences (RSES), Annual Report 1983, p. 124–126.
- GEE, R. D., 1982, Southern Cross, W.A.: Western Australia Geological Survey, 1:250 000 Geological Series Explanatory Notes, 25p.
- GEE, R. D., BAXTER, J. L., WILDE, S. A., and WILLIAMS, I. R., 1981, Crustal development in the Yilgarn Block, in *Archaean Geology* edited by J. E. GLOVER and D. I. GROVES: International Archaean Symposium, 2nd, Perth, W.A., 1980, Proceedings: Western Australia Geological Society of Australia, Special Publication, no. 7, p. 43–56.
- GREENFIELD, J. E., 2001, Geology of the Lake Giles 1:100 000 sheet: Western Australia Geological Survey, 1:100 000 Geological Series Explanatory Notes, 19p.
- GREENFIELD, J. E., and CHEN, S. F., 1999, Structural evolution of the Marda–Diemals area, Southern Cross Terrane: Western Australia Geological Survey, Annual Review 1998–99, p. 68–73.
- GRIFFIN, T. J., 1990, Southern Cross Terrane, in *Geology and mineral resources of Western Australia*: Western Australia Geological Survey, Memoir 3, p. 60–77.
- GROVES, D. I., KNOX-ROBINSON, C. M., HO, S. E., and ROCK, N. M. S., 1990, An overview of Archaean lode-gold deposits: Geology Department (Key Centre) and University Extension, University of Western Australia, Publication 20, p. 2–18.
- HABTESELASSIE, M. M., 1994, Vanadium distribution in the Shephards Discordant Zone, Windimurra Complex, Western Australia: Minerals and Energy Research Institute of Western Australia, Report 123, 162p.
- HABTESELASSIE, M. M., MATHISON, C. I., and GILKES, R. J., 1996, Vanadium in magnetite gabbros and its behaviour during lateritic weathering, Windimurra Complex, Western Australia: *Australian Journal of Earth Sciences*, v. 43, p. 555–566.
- HALLBERG, J. A., JOHNSTON, C., and BYE, S. M., 1976, The Archaean Marda igneous complex, Western Australia: *Precambrian Research*, v. 3, p. 111–136.
- KIMBER, P. B., 1987, 1986 Annual Report, Allens Find gold prospect, MC Mining NL: Western Australia Geological Survey, Statutory mineral exploration report, Item 5231 A19427 (unpublished).
- LIBBY, J. W., 1992, Reply to Discussion: The nature and tectonic significance of the crustal-scale Koolyanobbing shear zone, Yilgarn Craton, Western Australia: *Australian Journal of Earth Sciences*, v. 39, p. 563–565.
- LIBBY, J., GROVES, D. I., and VEARNCOMBE, J. R., 1991, The nature and tectonic significance of the crustal-scale Koolyanobbing shear zone, Yilgarn Craton, Western Australia: *Australian Journal of Earth Sciences*, v. 38, p. 229–245.
- MARSTON, R. J., 1979, Copper mineralization in Western Australia: Western Australia Geological Survey, Mineral Resources Bulletin 13, p. 128.
- MARSTON, R. J., 1984, Nickel mineralization in Western Australia: Western Australia Geological Survey, Mineral Resources Bulletin 14, 271p.
- MATHESON, R. S., and MILES, K. R., 1947, The mining groups of the Yilgarn Goldfield north of the Great Eastern Railway: Western Australia Geological Survey, Bulletin 101, 242p.
- MYERS, J. S., 1990, Precambrian tectonic evolution of part of Gondwana, southwestern Australia: *Geology*, v. 18, p. 537–540.
- MYERS, J. S., 1997, Preface: Archaean geology of the Eastern Goldfields of Western Australia — regional overview: *Precambrian Research*, v. 83, p. 1–10.
- MYERS, J. S., and HOCKING, R. M., 1998, Geological map of Western Australia, 1:2 500 000 (13th edition): Western Australia Geological Survey.
- NELSON, D. R., 1997, Evolution of the Archaean granite–greenstone terrain of the Eastern Goldfields, Western Australia — SHRIMP U–Pb zircon constraints: *Precambrian Research*, v. 83, p. 57–81.
- NELSON, D. R., 1999, Compilation of geochronology data, 1998: Western Australia Geological Survey, Record 1999/2, 222p.
- NELSON, D. R., 2000, Compilation of geochronology data, 1999: Western Australia Geological Survey, Record 2000/2, 251p.
- NELSON, D. R., 2001, Compilation of geochronology data, 2000: Western Australia Geological Survey, Record 2001/2, 205p.
- NELSON, D. R., in prep., Compilation of geochronology data 2001, Western Australia Geological Survey, Record.
- PIDGGEON, R. T., and HALLBERG, J. A., 2000, Age relationships in supracrustal sequences in the northern part of the Murchison Terrane, Archaean Yilgarn Craton, Western Australia: a combined field and zircon U–Pb study: *Australian Journal of Earth Sciences*, v. 47, p. 153–165.
- PIDGGEON, R. T., and WILDE, S. A., 1990, The distribution of 3.0 Ga and 2.7 Ga volcanic episodes in the Yilgarn Craton of Western Australia: *Precambrian Research*, v. 48, p. 309–325.

- QIU, Y. M., McNAUGHTON, N. J., GROVES, D. I., and DALSTRA, H. J., 1999, Ages of internal granitoids in the Southern Cross region, Yilgarn Craton, Western Australia, and their crustal evolution and tectonic implications: *Australian Journal of Earth Sciences*, v. 46, p. 971–981.
- REGISTER OF AUSTRALIAN MINING, 2000–2001: Perth, Western Australia, Resource Information Unit, 672p.
- RIGANTI, A., 2001, Barlee, W.A. Sheet 2739: Western Australia Geological Survey, 1:100 000 Geological Series.
- RIGANTI, A., and CHEN, S. F., 2000, Jackson, W.A. Sheet 2737: Western Australia Geological Survey, 1:100 000 Geological Series.
- RIGANTI, A., CHEN, S. F., WYCHE, S., and GREENFIELD, J. E., 2000, Late Archean volcanism and sedimentation in the central Yilgarn Craton, *in* GSWA 2000 Extended Abstracts: Western Australia Geological Survey, Record 2000/8, p. 4–6.
- ROLLEY, P. J., and BAXTER, J. L., 1990, Marvel Loch gold deposit, *in* *Geology of the Mineral Deposits of Australia and Papua New Guinea, Volume 1* edited by F. E. HUGHES: Australasian Institute of Mining and Metallurgy, Monograph 14, p. 297–300.
- STEWART, A. J., WILLIAMS, I. R., and ELIAS, M., 1983, Youanmi, W.A.: Australia BMR, 1:250 000 Geological Series Explanatory Notes, 58p.
- TAYLOR, S. R., and HALLBERG, J. A., 1977, Rare-earth elements in the Marda calc-alkaline suite: an Archean geochemical analogue of Andean-type volcanism: *Geochimica et Cosmochimica Acta*, v. 41, p. 1125–1129.
- TOWNSEND, D. B., GAO MAI, and MORGAN, W. R., 2000, Mines and mineral deposits of Western Australia: digital extract from MINEDEX — an explanatory note: Western Australia Geological Survey, Record 2000/13, 28p.
- TYLER, I. M., and HOCKING, R. M., 2001, Tectonic units of Western Australia (scale 1:2 500 000): Western Australia Geological Survey.
- WATKINS, K. P., and HICKMAN, A. H., 1990, Geological evolution and mineralization of the Murchison Terrane Western Australia: Western Australia Geological Survey, Bulletin 137, 267p.
- WALKER, I. W., and BLIGHT, D. F., 1983, Barlee, W.A.: Western Australia Geological Survey, 1:250 000 Geological Series Explanatory Notes, 22p.
- WANG, Q., SCHIOTTE, L., and CAMPBELL, I. H., 1996, Geochronological constraints on the age of komatiites and nickel mineralisation in the Lake Johnston greenstone belt, Yilgarn Craton, Western Australia: *Australian Journal of Earth Sciences*, v. 43, p. 381–385.
- WATKINS, K. P., and HICKMAN, A. H., 1990, Geological evolution and mineralization of the Murchison Terrane Western Australia: Western Australia Geological Survey, Bulletin 137, 267p.
- WILLIAMS, I. R., 1974, Structural subdivision of the Eastern Goldfields Terrane, Yilgarn Block: Western Australia Department of Mines Annual Report 1973, p. 53–59.
- WITT, W. K., and DAVY, R., 1997, Geology and geochemistry of granitoid rocks in the southwest Eastern Goldfields Terrane: Western Australia Geological Survey, Report 49, 137p.
- WITT, W. K., and SWAGER, C. P., 1989, Structural setting and geochemistry of Archean I-type granites in the Bardoc–Coolgardie area of the Norseman Wiluna belt, Western Australia: *Precambrian Research*, v. 44, p. 323–351.
- WYBORN, L. A. I., 1993, Constraints on interpretations of lower crustal structure, tectonic setting and metallogeny of the Eastern Goldfields and Southern Cross Terranes provided by granite geochemistry: *Ore Geology Reviews*, v. 8, p. 125–140.
- WYCHE, S., 1999, Geology of the Mulline and Riverina 1:100 000 sheets: Western Australia Geological Survey, 1:100 000 Geological Series Explanatory Notes, 28p.
- WYCHE, S., CHEN, S. F., GREENFIELD, J. E., and RIGANTI, A., 2001, Geology of the Johnston Range 1:100 000 sheet: Western Australia Geological Survey, 1:100 000 Geological Series Explanatory Notes, 31p.

## Appendix 1

### Selected whole-rock geochemical data

GSWA No.	159393 <sup>(a)</sup>	159335 <sup>(a)</sup>	159392 <sup>(a)</sup>	168959 <sup>(b)</sup>	142919 <sup>(b)</sup>	142920 <sup>(b)</sup>	142915 <sup>(b)</sup>	143289 <sup>(a)</sup>	143371 <sup>(a)</sup>	143285 <sup>(a)</sup>
Rock type	Andesite	Rhyodacite	Rhyolite	Monzo-granite	Monzo-granite	Porphyry	Monzo-granite	High-Mg basalt	Basalt	Mafic tuff
Locality	Marda Complex	Marda Complex	Marda Complex	Butcher Bird mine E	Pigeon Rocks	Deception Hill	Olby Rock	Deception Hill N	Watch Bore N	Diemals Homestead
Easting	716288	720294	720958	730253	718691	725061	736171	722941	705338	723285
Northing	6663906	6659737	6665113	6654610	6687180	6696120	6683210	6703138	6732550	6714120

	Percentage									
SiO <sub>2</sub>	59.04	69.07	75.61	74.79	74.97	72.16	72.87	52.26	54.18	50.57
TiO <sub>2</sub>	0.95	0.52	0.20	0.24	0.12	0.23	0.18	0.50	0.80	0.47
Al <sub>2</sub> O <sub>3</sub>	15.28	13.95	12.54	12.43	13.10	14.62	13.26	9.34	13.70	14.69
Fe <sub>2</sub> O <sub>3</sub>	1.79	1.41	0.51	2.44	1.11	1.58	1.55	1.29	1.32	1.71
FeO	5.81	2.91	1.72	0.84	0.44	0.92	0.80	8.39	6.78	8.47
MnO	0.10	0.07	0.04	0.06	0.04	0.03	0.04	0.19	0.17	0.18
MgO	3.43	0.87	0.24	0.15	0.18	0.54	0.28	13.58	7.81	8.44
CaO	5.82	2.67	0.62	0.83	0.87	1.39	1.13	10.89	10.82	10.66
Na <sub>2</sub> O	3.55	4.08	4.25	4.42	4.00	5.40	3.58	0.86	3.32	2.16
K <sub>2</sub> O	1.93	2.87	3.49	3.67	4.30	2.74	4.60	0.07	0.11	0.32
P <sub>2</sub> O <sub>5</sub>	0.28	0.12	0.01	0.03	0.04	0.08	0.05	0.04	0.01	0.04
LOI	2.08	1.36	0.87	0.71	1.13	1.08	2.27	3.47	1.30	2.72
<b>Total</b>	<b>100.03</b>	<b>99.90</b>	<b>99.98</b>	<b>100.63</b>	<b>100.31</b>	<b>100.77</b>	<b>100.62</b>	<b>100.89</b>	<b>100.32</b>	<b>100.43</b>

	Parts per million									
Ba	752	892	1 101	1 087	482	712	933	28	30	62
Cr	22	13	2.1	<2	<2	8	<2	1 583	278	306
Cu	28	7.0	6.9	6	16	11	8	63	1.2	83.4
Ga	18	15.1	15	15	18	20	18	8.6	15	12
Hf	3.9	10	8.0	8.1	5.0	3.5	4.8	3.3	4.9	2.7
Nb	9.0	11	15	12.6	15.1	4.6	15	2.0	3.0	1.7
Ni	26	8.5	0.2	10	2.4	5.9	4	264	65	148
Pb	9.6	37	34	24	45	38	51	1.5	3.3	1.5
Rb	52	89	106	129	268	88	237	1.6	0.8	9.5
Sc	19	11	6.0	6	4	2	4	52	48	46
Sr	338	184	74	82	70	229	103	39	80	114
Ta	<2	–	1.1	1.3	4.3	0.7	1.9	–	–	–
Th	8.4	18	23	19	23	10	32	0.3	2.0	0.2
U	1.0	3.1	4.0	4.4	12	2.7	7.4	0.3	0.7	0.1
V	124	28	1.4	<3	6	16	10	189	291	197
Y	21	28	38	31	18	4	23	16	26	17
Zn	70	82	65	50	25	18	35	69	75	78
Zr	213	271	347	303	94	137	172	29	68	27

La	38	49	74	54.37	24.51	28.32	53.53	2.10	3.68	1.67
Ce	72	90	135	102	48.55	44.68	99.07	5.09	8.72	3.84
Pr	8	9.8	14	10.24	4.43	4.06	9.55	0.78	1.36	0.56
Nd	30	34	49	36.97	14.78	13.2	31.36	3.62	6.36	2.62
Sm	5.2	6.2	8.4	6.53	2.5	1.76	5.24	1.16	2.23	0.95
Eu	1.4	1.35	1.45	1 006	374	472	726	0.44	0.62	0.39
Gd	4.4	5	7	6.21	2.19	1.18	4.62	1.61	3.06	1.53
Tb	0.62	0.76	1.02	1.06	0.38	0.13	0.74	0.31	0.58	0.31
Dy	4	5	6.8	–	–	–	–	2.27	4.11	2.41
Ho	0.74	1	1.25	5.48	2.22	0.64	3.7	0.53	0.90	0.57
Er	2.15	3	3.8	1.13	0.54	0.11	0.78	1.60	2.61	1.78
Tm	0	0.42	0.52	3.36	1.68	0.28	2.22	0.25	0.39	0.29
Yb	2	2.75	3.5	3.36	2.26	0.25	2.07	1.66	2.46	1.88
Lu	0.29	0.42	0.52	0.53	0.37	0.04	0.34	0.26	0.37	0.30

**NOTES:** (a) Analysed at the Australian National University. All major- and trace-element analyses were carried out by X-ray fluorescence (XRF); all rare-earth element analyses were carried out at the University of Queensland by inductively coupled plasma spectrometry (ICP)  
(b) Analysed by AGSO. For these samples, all major-element analyses and analyses for Ba, Cr, Cu, Rb, Sc, Sr, U, Zn, and Zr were carried out by AGSO using XRF; the remaining trace- and the rare-earth elements were analysed by ICP. The techniques are discussed in Morris (2000)

## Reference

MORRIS, P. A., 2000, Composition of Geological Survey of Western Australia geochemical reference materials: Western Australia Geological Survey, Record 2000/11, 33p.